Silicon Nanowires for Bioadhesion and Drug Delivery

by

Kathleen Elizabeth Fischer

A dissertation submitted in partial satisfaction of the
requirements for the degree of
Joint Doctor of Philosophy
with the University of California, San Francisco

in

Bioengineering
and the Designated Emphasis
in
Nanoscale Science and Engineering

in the

Graduate Division

of the

University of California, Berkeley

Committee in charge:

Professor Tejal A. Desai, Chair
Professor Dorian Liepmann
Professor Liwei Lin

Fall 2010

Abstract

Silicon Nanowires for Bioadhesion and Drug Delivery

by

Kathleen Elizabeth Fischer

Joint Doctor of Philosophy in Bioengineering
with the University of California, San Francisco,

Designated Emphasis in Nanoscale Science and Engineering

University of California, Berkeley

Professor Tejal Desai, Chair

Mucosal tissues have great potential for delivery of therapeutic macromolecules, but drug absorption is often thwarted by chemical and physical barriers, such as the mucus layer. Although mucoadhesive technologies increase gastrointestinal residence time, many macromolecules are subjected to degradation or clearance within the mucus layer. Recent advances in nanotechnology have allowed for the fabrication of silicon nanowires on microparticles in a conformal three-dimensional coating. These nanowire coatings have been shown to be robust in acid and to degrade on the scale of weeks in physiological solutions.

Nanowire-coated microparticles interact with nanoscale cellular features, such as microvilli, allowing of increased surface area of contact. These devices adhere strongly under harsh physiological conditions, such as shear of over 100 dynes/cm^2, a model mucus layer, and various insults to the cellular cytoskeleton. Because they adhere by geometry-dependent mechanisms and interact directly with the epithelial cells, they are retained better than mucoadhesives and adhere well to several types of tissue. Under tensile force, the nanowire-coated devices adhere up to 1000-fold stronger than the equivalent uncoated devices. Overall, charge and nanowire geometry are most influential in nanowire-related adhesion, indicating that surface area dependent forces are involved. The in vitro adhesion results have been validated in two separate animal models: the mouse and the dog. In beagles, nanowire-coated stainless steel particles were retained in the stomach at least ten times longer than similar controls. In mice, nanowire-coated microspheres remained in the stomach until at least 5 hours after dosing.

Furthermore, the nanowire coating on these devices offers a convenient reservoir, where macromolecules may be loaded. Because the therapeutics eventually encase all of the nanowires, a trade-off is made between loading capacity and adhesion. However, by loading controlled pore glass particles, adhesion may be retained and/or enhanced. In addition to the initial surface area adhesion, nanowire coatings induce cellular remodeling, though they are not internalized. Overall, these nanowires show low toxicity in Caco-2 cells and do not induce inflammation in vitro.

Thus, nanowire coatings show promise for resolving some of the most difficult oral delivery barriers, such as penetrating the mucus layer, adhering directly to cells, and increasing residence time in close proximity to the gastrointestinal epithelial cells. In vitro adhesion studies have been validated in vivo, and nanowires have been demonstrated to be biocompatible in vitro. By integrating nano- and microscale functionalities, nanowire-coated devices reap the benefits of both size scales, and show promise for application to a variety of therapeutic systems.

This manuscript is dedicated to my parents, Kathleen and Robert Fischer, to my brothers, Will Fischer and Kelly Skipper, and to my husband, Ryan Olf. Without you all, the sun would not shine nearly as brightly. As my mother would sing,

So let the sun shine in,
Face it with a grin.
Smilers never lose,
And frowners never win.

Table of Contents

Figures

Symbols and Abbreviations

3T3 – an immortalized swiss mouse fibroblast cell line
AFM – atomic force microscope
APTES – 3-aminopropyltriethoxysilane
BAEC – bovine aortic endothelial cell; an immortalized bovine endothelial cell line
BCA - bicinchoninic acid; a assay reagent to determine protein concentration
BSA – bovine serum albumin; a small protein
Caco-2 – an immortalized human colon carcinoma cell line
CPG – controlled pore glass particles
FITC – fluorescein isothiocyanate; a fluorescent agent
GI - gastrointestinal
IgG – immunoglobulin G; an antibody
MP – MicroParticle; a non-nanowire-coated microsphere
MTT - (3-[4,5- dimethylthiazol-2-yl]-2,5-diphenyl tetrazolium bromide); an assay to determine mitochondrial activity
NEMP – Nano-Engineered MicroParticle; a nanowire-coated microsphere
nm – nanometers
NW - nanowire
PBS – phosphate buffered solution; a saline solution with pH and osmolarity similar to that in vivo
PEG – polyethylene glycol; a hydrophilic, non-fouling molecule
RPMI-2650 – an immortalized human nasal carcinoma cell line
SEM – scanning electron microscope
TEM – transmission electron microscope
μm - micrometers

Terminology

The terms "devices," "particles," "beads," "spheres," "NEMPs," etc are used often and may cause confusion. In general, beads, control spheres, MPs, and microspheres refer to the uncoated control particles, which are 30-50 μm in diameter and typically spherical (giving them a bead shape), except in the case of the controlled pore glass (CPG). NEMPs, nanowire-coated spheres, and nanowire particles refer to the test particles that have nanowires grown on the surface. "Devices," "microparticles," and "particles" are used as an umbrella term, encompassing both the nanowire-coated particles and control particles, and in some contexts other systems that are not investigated here.

Acknowledgements

I would like to acknowledge the extraordinary help that I have received from my mentors, colleagues, and students. In particular, thanks to my advisor, Tejal Desai, and post-doctoral mentors, Sarah Tao and Kristy Ainslie. I cannot thank my labmates, both past and present, enough for all their help in lab and in life. Also, thanks to my Qualifying Exam committee, Professors Liepmann, Lin, Li, Lee, Cullander, and Majumdar, and thanks to my Dissertation committee, Professors Desai, Liepmann, and Lin. Numerous students and volunteers helped me make this project what it is, and I would like to acknowledge Laura, Yushan, Cheryl, Parminder, Ganesh, Aishwarya, Matt, and Mark. Furthermore, my collaborators have assisted with all aspects of this project, from fabrication to in vivo testing; thank you to Hugh, Esther, Veeral, Olivia, Benji, and Verne. Special thanks to those who helped me learn how to use new equipment, particularly Kurt, Vuk, Guangwei, and Reena, and to our administrators SarahJane and Rebecca, who kept me out of numerous potentially unpleasant situations.

I would also like to thank those who have supported my graduate career, including the NSF, through a Graduate Research Fellowship, the NIH, through a training grant, an R01, and an R21, Nanosys, Inc. and the University of California, through the UC Discovery Grant, the Sandler Family Foundation, and the Rogers Foundation. Without your support, this work would not have been possible.

Chapter 1: Introduction

Oral Drug Delivery

The oral route is one of the oldest and most prevalent ways of delivering therapeutics. Patients generally consider taking pills to be easy and painless. Healthcare professionals do not have to administer doses, making the peroral route less expensive. Furthermore, patients typically exhibit high rates of compliance, and thus high therapeutic efficacy is achieved when taking medications orally. In addition to healthcare providers and patients, pharmaceutical companies are able to extend the period of exclusivity of their intellectual property and thereby differentiate themselves from generic competitors by using drug delivery technologies to improve therapy. As a result, the oral drug delivery market was estimated to be $43.0 billion in 2008, and is expected to reach $71.3 billion by 2013. The delivery devices, themselves, account for roughly $3.5 billion in sales in 2008[2].

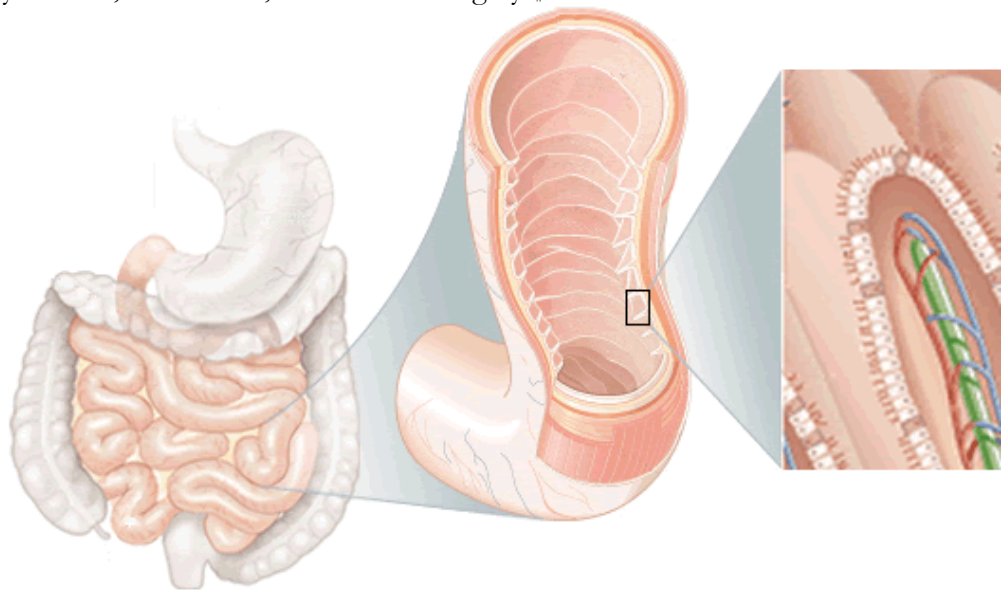

Figure 1: Scales of Intestinal Barriers[3]

Although the oral mucous membranes (mucosae) present a large and highly vascularized surface area for therapeutic absorption, they are also protected by significant barriers to drug permeation ranging from macroscale peristaltic contractions to molecular scale tight junctions (Figure 1)[4]. Wavelike peristaltic muscular contractions propel food, pathogens, and other intestinal contents through the digestive tract at the macroscale, creating an intestinal shear that typically ranges from approximately 0.01 to 10 dynes/cm^2, and can increase to 1000 dynes/cm^2 in diarrheal disease[5]. Chemical barriers in the lumen of the gastrointestinal tract include harsh degradative enzymes and a highly variable pH, which can range from 2.0 in the highly acidic regions of the stomach to 7.5 in the distal regions of the large intestine[6]. On the microscale, a 1-450 μm thick motile layer of gel-like mucus covers most of the gastrointestinal tract[7]. Chyme transits from the stomach through the human small intestine in a matter of approximately 150-240 minutes, and mucus has a

turnover time of 50-270 minutes in rats[8,9,10,11]. Thus, without adhesion to the underlying epithelium, therapeutics and devices are cleared from the small intestine in a matter of hours.

The mucus layer is composed of O-linked glycoproteins forming a mesh structure which interacts with molecules through hydrogen-bonding, hydrophobic interactions, electrostatic interactions and lectin/sugar recognition[12]. Aside from chemical interactions, branched and unbranched mucin chains form a block copolymer with an equivalent pore size of roughly 100-400 nm[13]. The mucus layer is made up of two sub-layers: a luminal motile layer and a membrane-bound adherant layer called the glycocalyx. In addition to trapping microparticles and macromolecules, the mucus layer carries dead cells, captured pathogens, bacteria, and numerous degrading enzymes that may inactivate sensitive peptides and macromolecules (Figure 2).

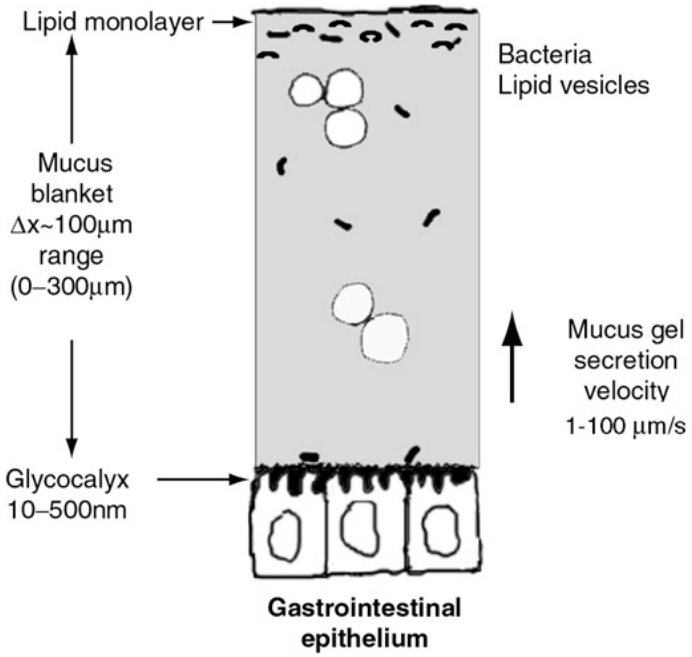

Figure 2: Characteristics of the Mucus Layer[13]

While the diffusion of some smaller proteins (15-950 kDa) is not reduced by cervical mucus[14], other in vitro experiments show that mucus decreases apparent permability coefficients by 50% or more[15]. Thus, larger proteins, nanoparticles, and microparticles may be trapped in the mucus layer[16].

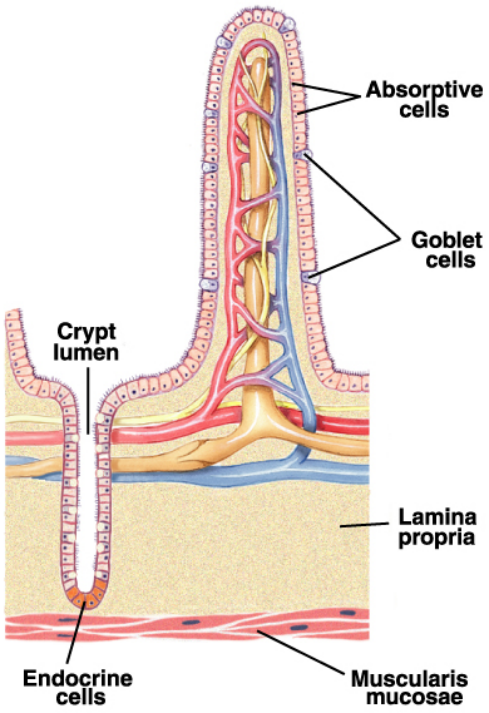

Figure 3: Intestinal Villus Anatomy[17]

Within the mucosae, absorptive cells are arranged on villi, protrusions into the small intestine to increase absorptive surface area (Figure 3). Goblet cells interspersed within the absorptive cells produce and secrete mucins, the proteins that constitute the majority of the mucus layer. Basal stem cells in the crypts between villi constantly produce new epithelial cells, which migrate to the tips of the villi and then detach. This process takes roughly 2-3 days in total[18].

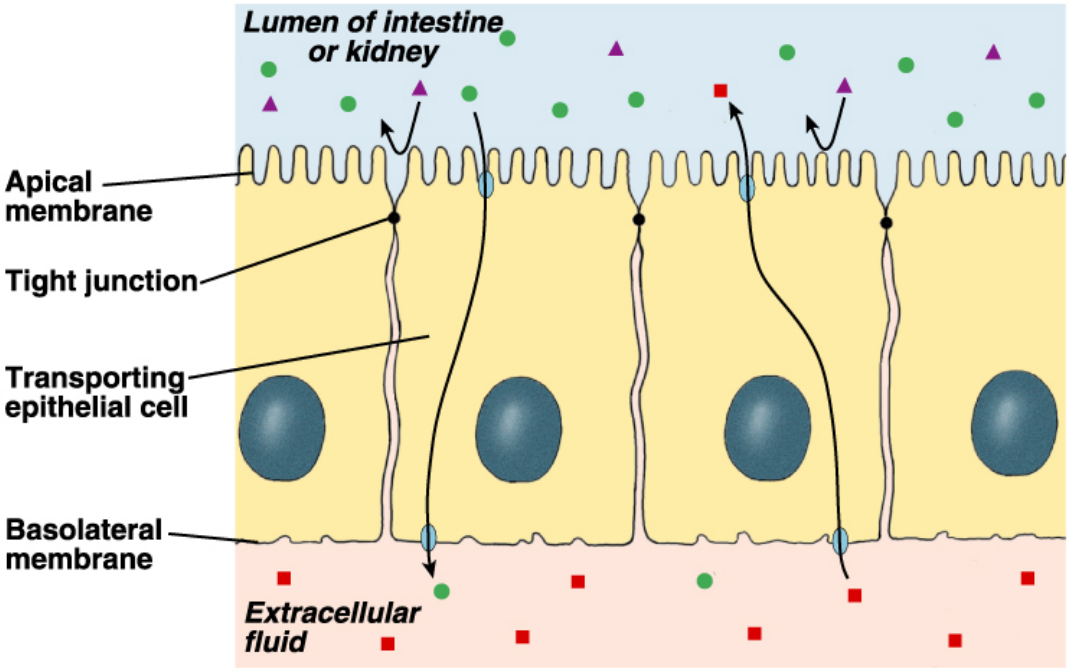

Figure 4: Epithelial Cell Membrane Anatomy[17]

After diffusing through the mucus layer, therapeutic molecules must pass through the layer of epithelial cells to reach the bloodstream (Figure 4). Molecules may transit via four potential pathways: through the cell, or transcellular; between the cells, or paracellular; by binding to specific carriers, or carrier-mediated; or through endocytosis and subsequent exocytosis, or transcytosis[19]. Without targeting specific surface proteins, macromolecules are essentially limited to the paracellular route[11]. Throughout the digestive tract, tight junctions composed of multiple layers of transmembrane protein complexes bind epithelial cells together at their apical surface (Figure 5). These junctions prevent unwanted macromolecules and organisms from entering the body via the paracellular route[20]. The tight junctions are most permeable in the proximal section of the small intestine, the duodenum, and become progressively tighter in the distal direction until reaching the colon. Thus, the proximal small intestine is considered to be the optimal target for oral delivery of macromolecular therapeutics.

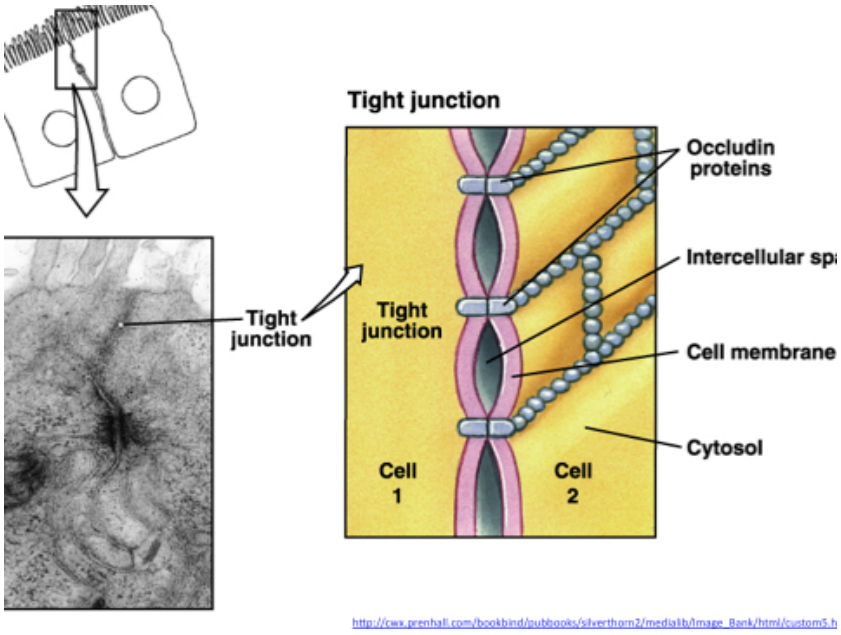

Figure 5: Tight Junction Anatomy[17]

Goals for Oral Delivery

Given the myriad barriers in the gastrointestinal tract, devices seeking to effectively deliver therapeutics should obtain the following objectives (Table 1).

Table 1: Goals for Oral Drug Delivery

Type	Objective
Intestinal Location:	Duodenum
Protection:	Reduce enzymatic and pH degradation
Absorption:	Increase residence time (eg: increase device retention on or in cells)
Concentration gradient:	Increase in close proximity to cells
Volume:	Loading capacity high enough to obtain therapeutic efficacy in 1-3 pills (up to about 4.5 mL[21]) per day
Efficacy:	Demonstrated in vivo
Toxicity:	Nontoxic and noninflammatory

As discussed in the Oral Drug Delivery section, tight junctions are the least obtrusive in the duodenum. Additionally, the pH begins to be neutralized in the duodenum with the introduction of enzymes and salts from the pancreas and gallbladder, reducing the likelihood

of pH-related macromolecular dissociation. Nonetheless, the duodenum has a rich blood supply and a large surface area. Thus, the duodenum is typically considered the optimal target for oral drug delivery.

Because a therapeutic must pass through the stomach and be delivered to the small intestine in an active form, any drug delivery device must at least protect from the low pH in the stomach. Enteric capsules, which degrade in response to a specific pH found along the length of the intestine, can protect molecules so that they bypass the stomach. Once in the duodenum, the pH rises to above pH 5.5, and enzymatic degradation replaces acidic degradation of proteins. Thus, an additional delivery device, such as a controlled release microsphere or a micropatch that only elutes therapeutics toward the mucosal cells would be optimal for additional protection of sensitive therapeutics.

Furthermore, because macromolecules have difficulty penetrating both the mucus layer and the cell layers in the mucosa, increasing the concentration gradient immediately in contact with cells increases the statistical likelihood of absorption, and thus bioavailability[22,23,24]. If therapeutics are eluted directly into the lumen of the intestine, they are removed rapidly with the chyme or mucus before they even encounter cells.

In order to adequately increase local concentration gradients and deliver enough drug to be therapeutic, any delivery device must be able to carry a large volume of drug in comparison to the volume of the delivery device. That is, in order to fit a large enough volume of therapeutic into a pill, the volume taken up by the delivery device must be small.

Lastly, any delivery device must be shown to be therapeutic in vivo, since many devices that were promising in vitro do not continue to be effective when exposed to the entire biological milieu. Similarly, any drug delivery device must be non-toxic and non-inflammatory in order to be appropriate for therapeutic purposes.

Micro- and Nanoparticles

Microparticles

Microparticles of varying shapes and sizes have been investigated for protection and retention of therapeutics. Numerous methods have been employed for creation of microspheres, but size and morphology depend on processing conditions and can vary widely[25]. Additionally, micropatches of a specified, flat shape may be fabricated repeatably through microfabrication processes and modified asymmetrically[23,24,26]. Both microspheres and micropatches offer potential for controlled release rates and physically protect therapeutics from enzymatic attack. However, flat devices may be conjugated with cytoadhesive molecules, like tomato lectin, on the same side that molecules are released, thereby increasing the concentration gradient directly at the cell surface (Figure 6). These flat devices also decrease the profile of the devices under flow conditions, thereby reducing the effects of fluid flow and shear and increasing device retention[25].

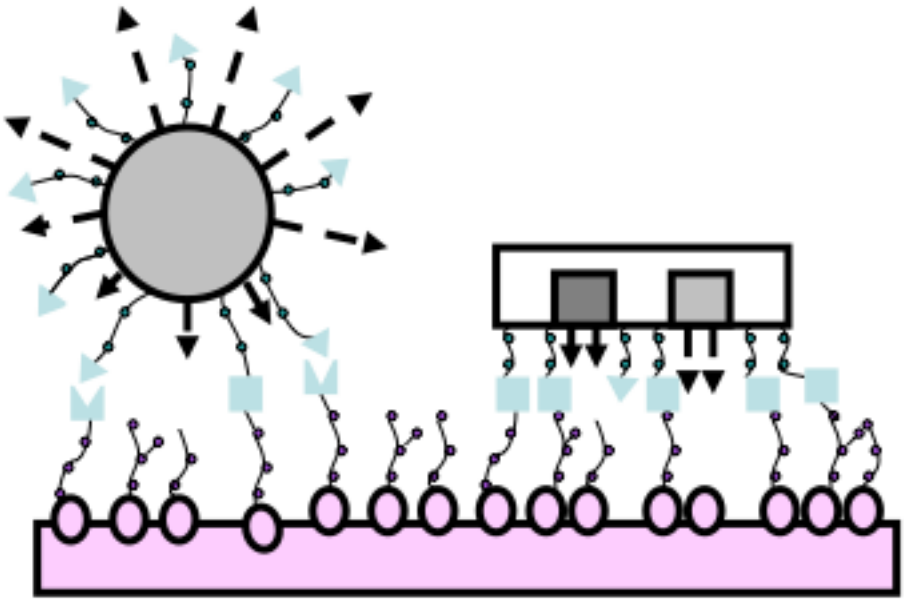

Figure 6: Spherical versus flat microparticle drug delivery devices[25]

Nonetheless, because of the chemical and mesh structure of the mucus layer, microparticles, whether spherical or flat have a difficult time traversing through the mucus and contacting cells (Figure 7). Most microparticles, whether intentionally or not, are entangled in the mucus layer and removed within a matter of hours[10]. Thus, although microparticles offer protection from degradation and improve the concentration gradient at the cell surface, they do not improve the residence time beyond that of the mucus layer.

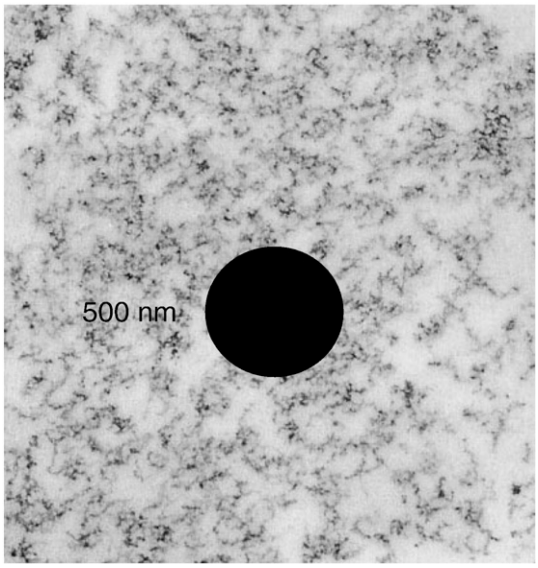

Figure 7: Depiction of a 500 nm particle over a TEM image of the mucus mesh[13]

Nanoparticles

Because of their nanoscale dimensions, nanoparticles can potentially penetrate the physical structure of the mucus layer (pore size of 100 nm[13]). With appropriate muco-inert surface chemistry, such as that exhibited by some viruses, nanoparticles can also avoid chemical entanglement[14,16]. However, nanoparticles suffer from significantly lower loading

capacity compared to microparticles[27,28], possible cellular toxicity, and potentially harmful accumulations in the liver, kidneys, and spleen[29,30]. Methods for evaluating toxicity of nanoparticles are still being developed, and as such, toxicological studies are ongoing and not yet conclusive. Thus, while nanoparticles seem promising for many aspects of gastrointestinal drug delivery, such as protection from degradation and improved drug absorption, questions about loading capacity and toxicity are still prohibiting widespread human use.

Bioadhesion

Numerous techniques for adhesion have been developed to prolong the residence time of microparticles in the intestine. Such adhesives can be categorized in two ways: mucoadhesives, which adhere primarily to the proteins in the mucus layer, and cytoadhesives, which adhere to the underlying cells in the mucosae. Chemical bioadhesives are the most highly investigated, though physical forms of adhesion are increasingly being shown to be relevant.

Chemical Bioadhesives

Originally, mucoadhesives were developed in order to increase device retention and improve the device proximity to mucosal cells. However, mucoadhesives are constrained by the mucin turnover time (50-270 minutes[10]), whereas devices which directly bind to cells are only constrained by the cell turnover time (2-3 days[31]). Thus, specific epithelial targeting agents, such as lectins, were utilized to adhere to glycosaminoglycans on the cell surface. Because these sugars are found in the mucous layer as well, competition between the mucous layer and cell surface for binding to mucoadhesives reduces the amount of direct device-cell binding to that of non-adhesive controls, particularly *in vivo*[32,33]. Thus, for robust mucosal adhesion, a micro- or nanodevice must penetrate the mucous layer and adhere directly to the epithelium.

Physical Adhesives

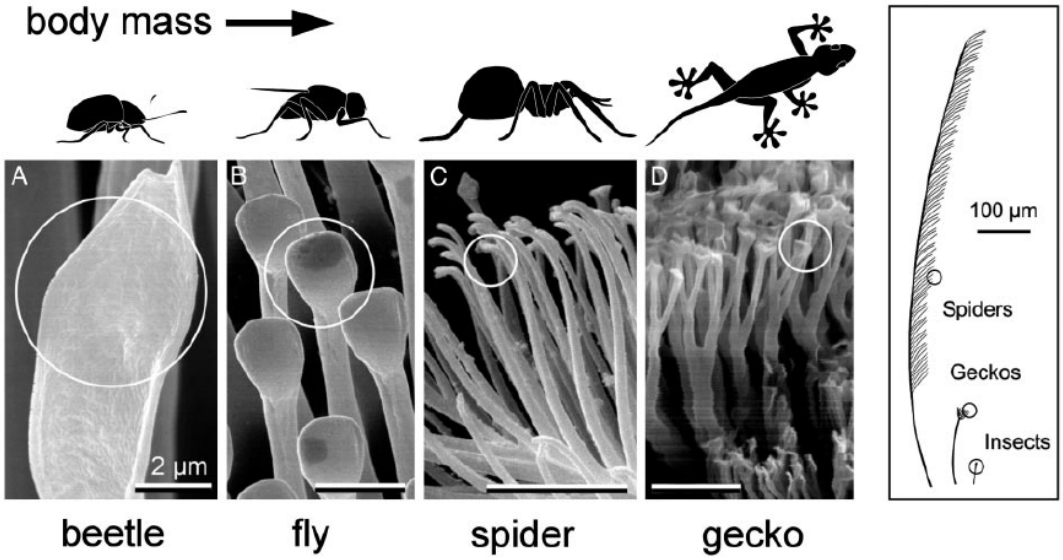

Figure 8: Biological examples of micro and nanoscale features in adhesion[34]

The hundreds-fold increase in surface area created by micro- and nanostructured gastrointestinal surfaces allows for significantly increased adhesion due to geometry alone (without chemical adhesives). One particularly promising class of geometric adhesives is gecko-inspired. Micro- and nano-structured surfaces naturally occur in a variety of insects and lizards, and have been shown to rely primarily on van der Waals forces for adhesion[35,36,37,38]. While numerous experiments have shown biomimetic nanowires and nanotubes to adhere with forces ranging from 0.04 times[39,40] to 30 times[41] the adhesive strength of geckos (reported to be 500 kPa[38]) in dry environments[42,43], only two groups have looked at submicron structures in aqueous conditions (elements of diameter 0.4 μm for Lee *et al.*[44] and 0.1 to 1 μm for Mahdavi *et al.*[45]). Despite using micro-structured surfaces, in a wet environment, chemical modification was necessary to bolster adhesion.

Under nanoadhesive conditions, as the number of adhesive elements per surface area increases (ie: diameter of individual elements decreases), the surface area to volume ratio increases and van der Waals adhesion is predicted to increase (Figure 8)[46,47]. Furthermore, because mucosal epithelia exhibit nano-structured microvilli, available surface area contact is considerably increased on the cell surface(Figure 9)[48,49,50,51]. Thus, by decreasing the diameter of the elements on the device surface to the nano-scale and targeting a microvilliated surface, it may be possible to generate strong bioadhesive forces due to geometric features alone.

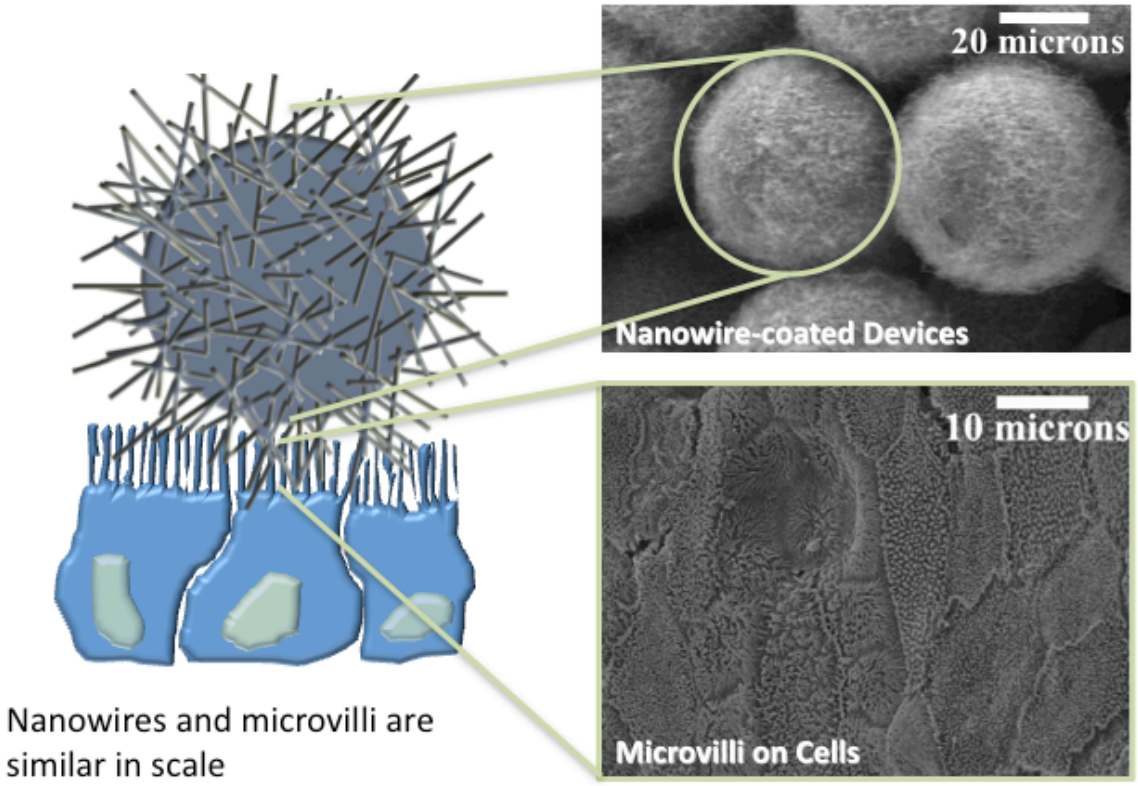

Nano-Engineered MicroParticles

By engineering nanostructures on the surface of microparticles, devices benefit from both the microscale and nanoscale: Nano-Engineered MicroParticles (NEMPs) have the loading capacity and biocompatibility of microparticles combined with the mucus penetration and enhanced adhesion of nanoparticles (Figure 10)[52,53,54,55,56,57].

Recent advances in nanofabrication now allow growth of relatively homogeneous nanowires as a three dimensional, conformal coating, so we have chosen to grow silicon nanowires onto silica microspheres. Because they may be integrated onto micro-scale devices, such as microspheres or flat micropatches, nanowires present a nano-engineered surface on a highly loaded microparticle. Furthermore, attaching nanowires to a microscale device prevents their internalization and subsequent cellular toxicity or systemic accumulation. A nanowire-based adhesion system offers additional features, such as a reservoir between the nanowires at their base and a template for spatially patterning chemical modifications[58].

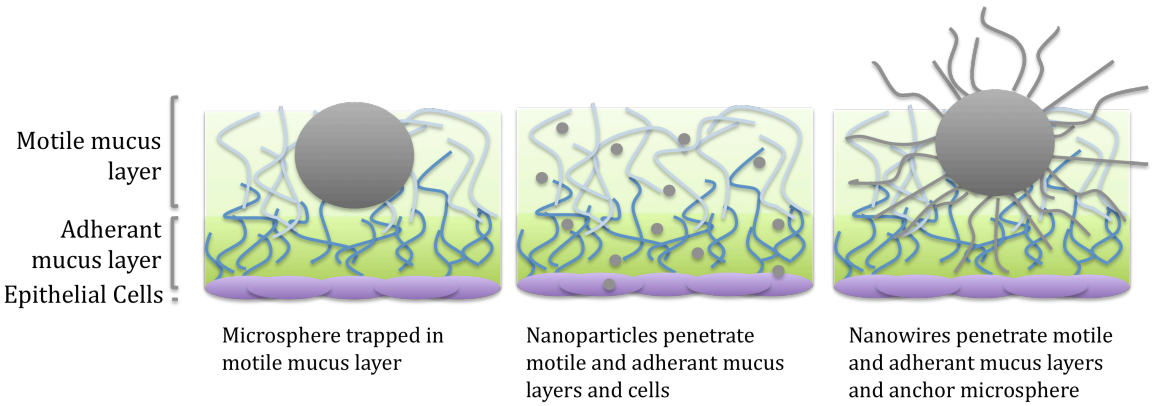

Figure 10: Schematic of mucus penetration differences with different micro and nanotechnologies

Silicon nanochanneled and nanoporous surfaces have been shown to be nontoxic and non-inflammatory *in vitro*[59]. Furthermore, silicon nanowires show a decrease in inflammatory response compared to flat glass, as indicated by monocyte activation, cytokine release, and reactive oxygen species[60].

As a result of the combination of nano- and microscale features, NEMPs offer the possibility to protect therapeutics against degradation, improve residence time at the mucosal surface, and increase concentration gradients in close proximity to cells while maintaining a high loading volume and without causing toxicity or inflammatory responses.

Chapter 2: Fabrication and characterization

Particle Fabrication

In this study, a surface deposited gold colloid of defined diameter was used as the growth catalyst for a Vapor-Liquid-Solid (VLS) based method to fabricate silicon nanowires (Si NW, Figure 11)[61,62]. This method of growing Si NW is very flexible and allows control of multiple growth parameters such as length, diameter and density as well as being adaptable to a variety of substrates including silicon, glass, ceramics, and metals. For this study, 60 nm gold colloid (British Biocell Int, Cardiff, UK) was deposited onto poly-l-lysine (Sigma-Aldrich, St Louis, MO) coated silica beads of 30-50 micron diameter (Polysciences, Warrington, PA). Poly-l-lysine provided a positively charged surface that enhanced colloid adhesion. After removing solvents and organic residue, the glass beads were placed in a growth furnace to grow silicon nanowires. Silicon tetrahydride (SiH_4), a silane, was used as the growing gas at a temperature of 480 ºC. The silane decomposed on the gold particles and the resulting silicon precipitated from the molten eutectic to form a silicon nanowire, the diameter of which was defined by the initial colloid diameter. The length of the wire was controlled by the length of time the reaction was allowed to continue. The nanowire density could be controlled by varying the density of catalyst deposited on the growth surface.

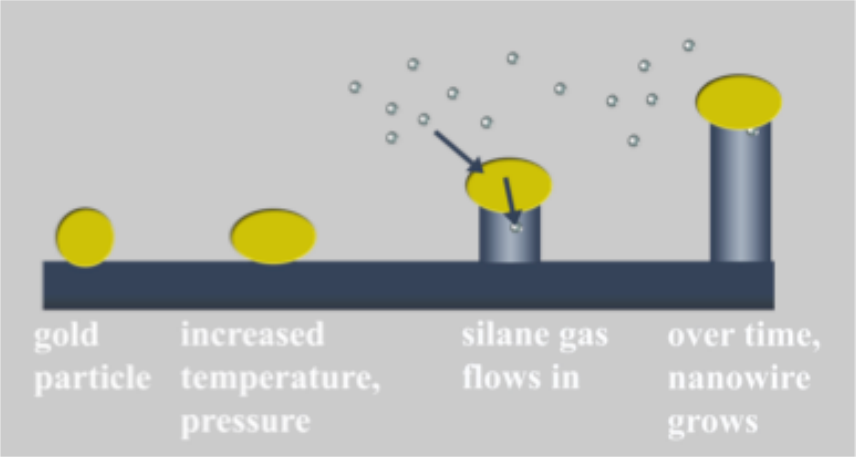

Figure 11: Nanowire growth schematic

Using this technique, nanowires were grown between 1 and 40 μm in length and 20-60 nm in diameter (Figure 12). Nanowire-coated devices often clustered together, due to van der Waals interactions.

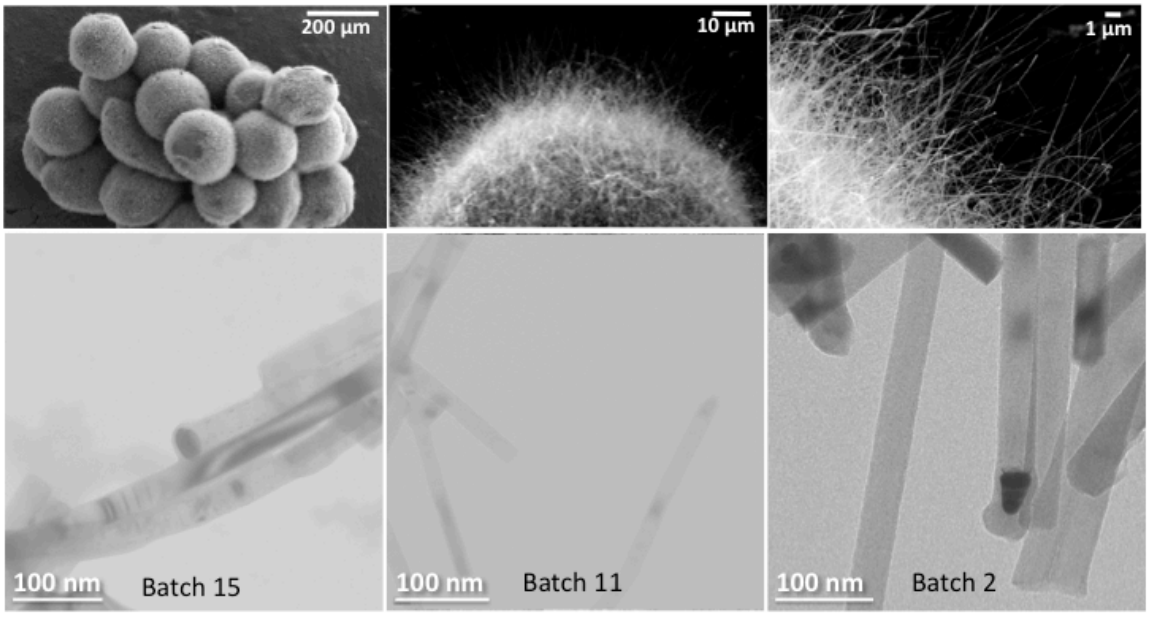

Figure 12: Nanowire batches from different magnifications (top) and with different diameters (bottom). SEM images reproduced with the permission of Nanosys, Inc.

Controlled Pore Glass Devices

To facilitate loading molecules into devices and to provide an alternate microscale geometry, nanowires were grown onto controlled pore glass particles (CPG, 30-70 µm width) with 200 nm pore size (Sigma Aldrich) using a process similar to that used for microspheres (Figure 13).

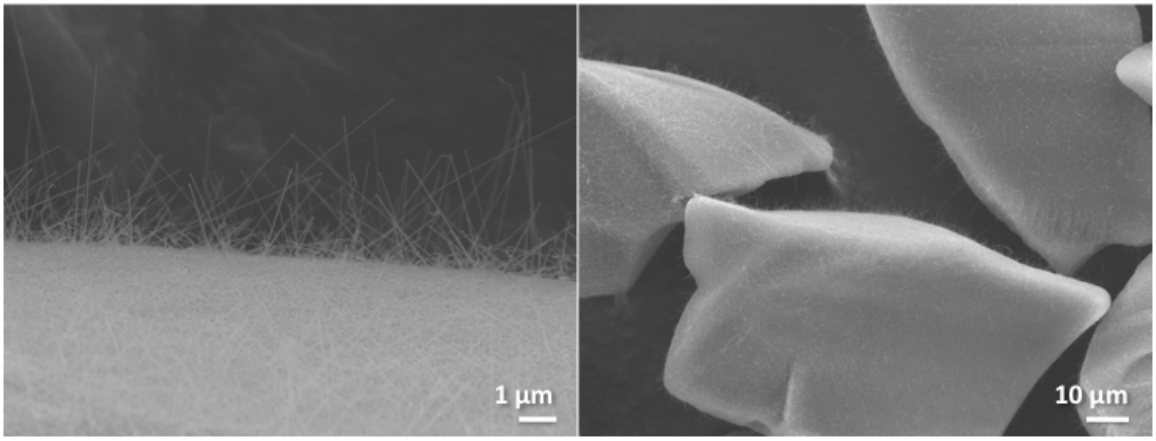

Figure 13: Controlled Pore Glass devices with nanowires. Reproduced with permission from Nanosys, Inc.

Stainless Steel Devices

Because silicon-based devices are not visible under x-ray, we grew nanowires on stainless steel spheres (McMaster-Carr, Elmhurst, IL). The stainless steel devices appear opaque under x-ray. Scanning electron microscopy indicated that the nanowire coating was high density and their approximate diameter was 210 µm (Figure 14).

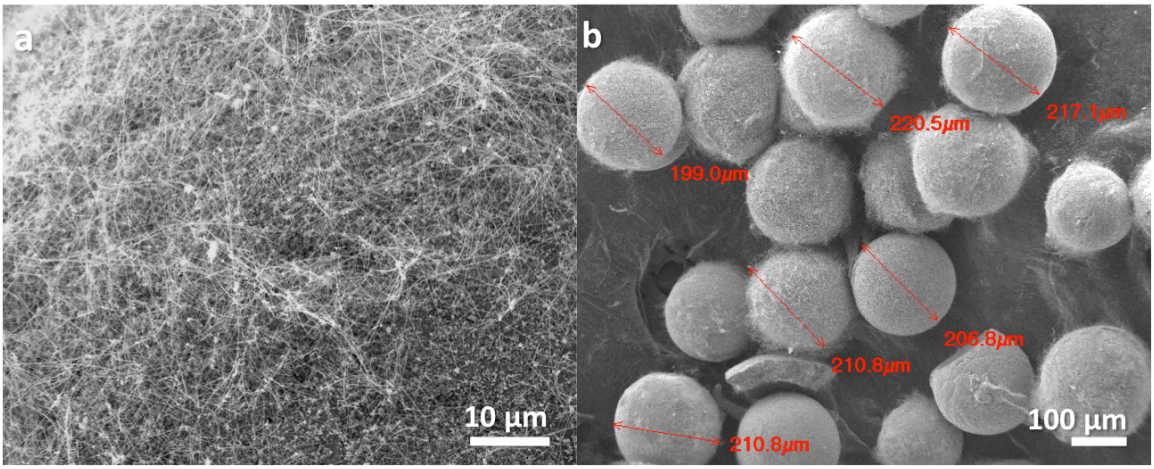

Figure 14: Nanowires grown on stainless steel devices.

Surface Area and Geometric Calculations

Geometric modeling was used to estimate the number of nanowires per device and the increase in surface area due to nanowires. Assuming the microsphere beads are spherical, they have a surface area, SA_b, of

$$SA_b = 4\pi R_b^{\,2}.$$

Where R_b = the radius of the bead (approximately 24 µm, based on measurements). Nanowires are approximated as cylinders with R_{nw} defined as the average nanowire radius (as measured by SEM and TEM), and l_{nw} defined as the average nanowire length. Thus, the surface area per nanowire, SA_{nw}, is

$$SA_{1NW} = 2\pi R_{NW}\ell.$$

The number of nanowires per bead can be calculated based on an assumed percent of surface area covered by nanowires, $SA_{assumed}$ (variable by bead batch). This gives the number of nanowires, N_{nw}, as

$$N_{NW} = \frac{SA_{assumed}SA_b}{\pi R_{NW}^{\,2}} = SA_{assumed}\frac{4R_b^{\,2}}{R_{NW}^{\,2}}.$$

Thus, the increase in surface area per device due to the nanowires is

$$\frac{SA_{NW}+SA_b}{SA_b} = \frac{N_{NW}SA_{1NW}+SA_b}{SA_b} = \frac{2SA_{assumed}\ell}{R_{NW}} + 1,$$

assuming that the surface area of the tips of the nanowires is the same as that taken up by their bases. Using data from SEM and TEM measurements, the increase in surface area can be calculated as a function of the assumed surface area covered by nanowires (% Nanowire

coverage of bead) and the nanowire length, given a nanowire radius (assumed 30 nm, in Figure 15).

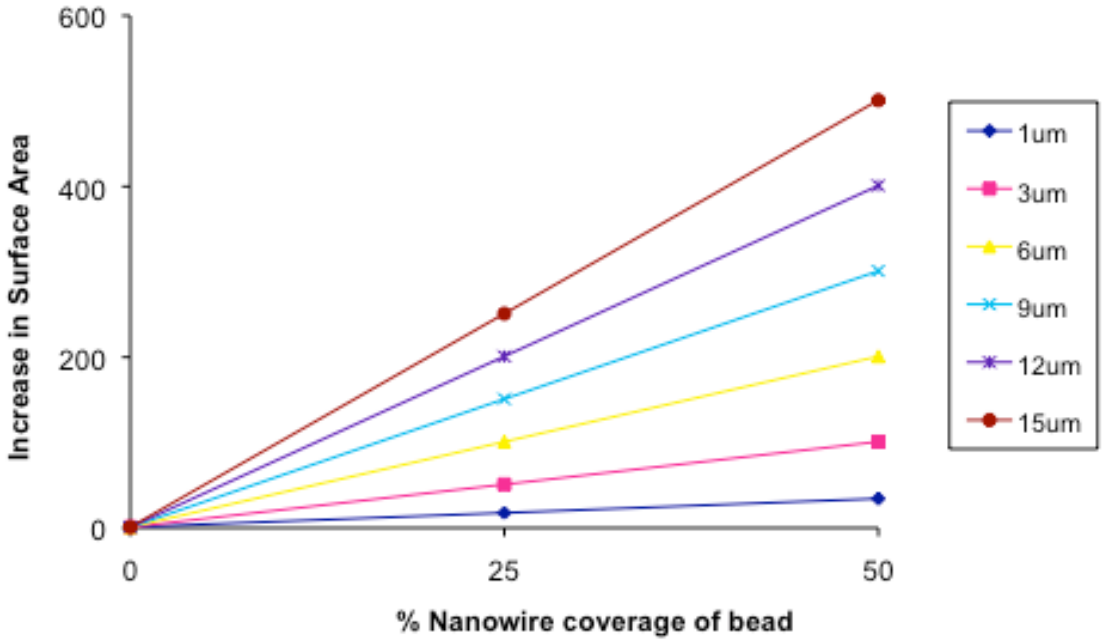

Figure 15: Theoretical Surface Area Increases from Nanowire Coating

The surface areas of three batches were measured using a multipoint surface area analysis using Krypton gas (Micromeritics Analytical Services, Norcross, GA). Control beads with no nanowires had a measured surface area of 0.0654 m^2/g; long nanowires (approximately 12.1 μm length) had a measured surface area of 0.5919 m^2/g, whereas shorter nanowires (approximately 1.4 μm length) had a measured surface area of 0.0817 m^2/g. Device weights were calculated in order to determine the increase in surface area per device (Figure 16). Assuming that nanowire lengths were constant, based on the above model, nanowire coverage for the devices was about 0.6 % for the shorter nanowires and about 1.5 % for the longer nanowires. Given 1% surface coverage, roughly 26,000 nanowires cover the surface of a device. For 5% and 10% coverage, the number of nanowires per device is 130,000 and 260,000. The assumption that nanowire lengths are constant is not necessarily accurate because measurements were taken from SEM images, which only show surface information. Thus, the path of longer nanowires may have been obscured and shorter nanowires may not have been visible at all. Nonetheless, the increase in surface area does seem to scale linearly with the length of the nanowires as predicted.

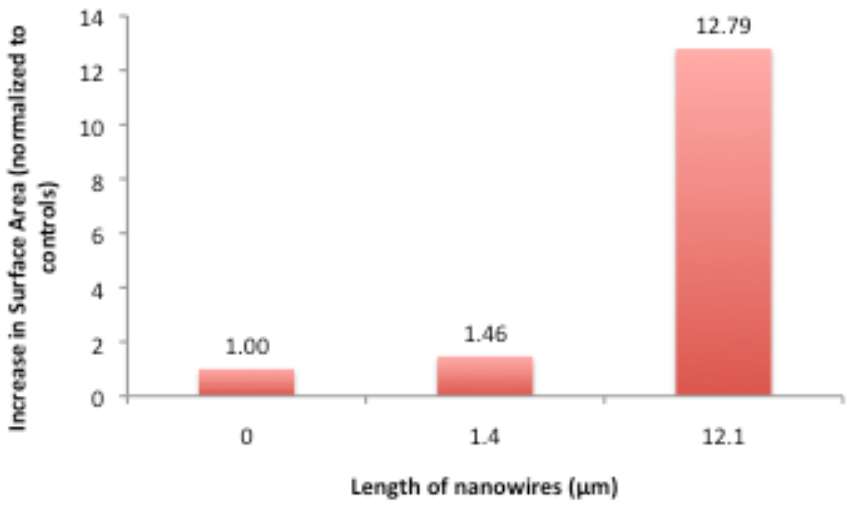

Figure 16: Measured Increase in Surface Area from Nanowire Coating

Additionally, because the nanowires change the packing characteristics of nanowire-coated beads as compared to uncoated beads, the mass per volume of devices (ie: the packing density of devices) was determined for several batches of different geometric proportions (Table 2).

Table 2: Device packing volume

Nanowire Device Fabrication Batch	Weight of 100 µL of devices (g)
S1	47.7
S2	124.9
S3	98.9
S4	114.0
0 – no nanowires control	133.1

Chemical modifications

Tomato Lectin Modification

Lectin modification of the nanowire-coated and control beads was achieved using silane chemistry. Surfaces were first hydroxylated by heating at 80 ºC in a 1:1:5 solution of ammonia (25% ammonium hydroxide in water): hydrogen peroxide (30% in water): water for 5 minutes. After three washes with water, devices were suspended in a 1:1:6 hydrochloric acid (50% in water): hydrogen peroxide (30% in water): water solution at 80 ºC for 5 minutes. After three additional water rinses, samples were resuspended in 5 ml of isopropanol and 0.1 ml of 3-aminopropyltriethoxysilane (APTES) for 90 minutes at room temperature. Samples were then moved to a vacuum filtration unit overnight. Avidin was attached after the method of Sultzbaugh and Speaker[63], by placing dry particles in a solution of 0.06 M 1-ethyl-3-(3-dimethylaminopropyl) carbodiimide hydrochloride (EDC), 0.04 M *N*-hydroxysuccinimide (NHS), and 1.5 uM avidin (Calbiochem, San Diego, CA) in water on a shaker overnight at room temperature. To conjugate lectin, after three water rinses, samples were exposed to 200 ug of biotin-labeled tomato lectin (Vector Laboratories, Burlingame,

CA) in 6 ml of water at room temperature for at least three hours. After lectin modification, samples were refrigerated at 4 ºC and used within 1 day or dried via vacuum filter for later use.

FITC and PEG Modifications

Surface modifications were done following the protocol described above with the following modifications made to attach FITC (Figure 17). After hydroxylation using either 30 seconds of oxygen plasma treatment or a five minute incubation in 1:1:5 solution of ammonia, hydrogen peroxide, and water at 80°C and a five minute incubation in 1:1:6 solution of hydrochloric acid: hydrogen peroxide: water at 80°C, samples were resuspended in 5 mL of isopropanol and 0.1 mL of 3-aminopropyltriethoxysilane (APTES) for 90 minutes. After vacuum filtration drying, devices were incubated in a solution of fluorescein isothiocyanate (FITC) – roughly 50 μg in 4 mL water – overnight at room temperature. By varying the amount of FITC added, we were able to obtain several different surface charges. Modifications with polyethylene glycol (PEG) followed [64], exposing plasma-cleaned devices to an 1.5% solution of PEG-silane (2-[Methoxy(polyethyleneoxy)propyl]trimethoxysilane, Gelest) in toluene for 2 hours, then rinsing in toluene, ethanol, and water prior to filtration and drying.

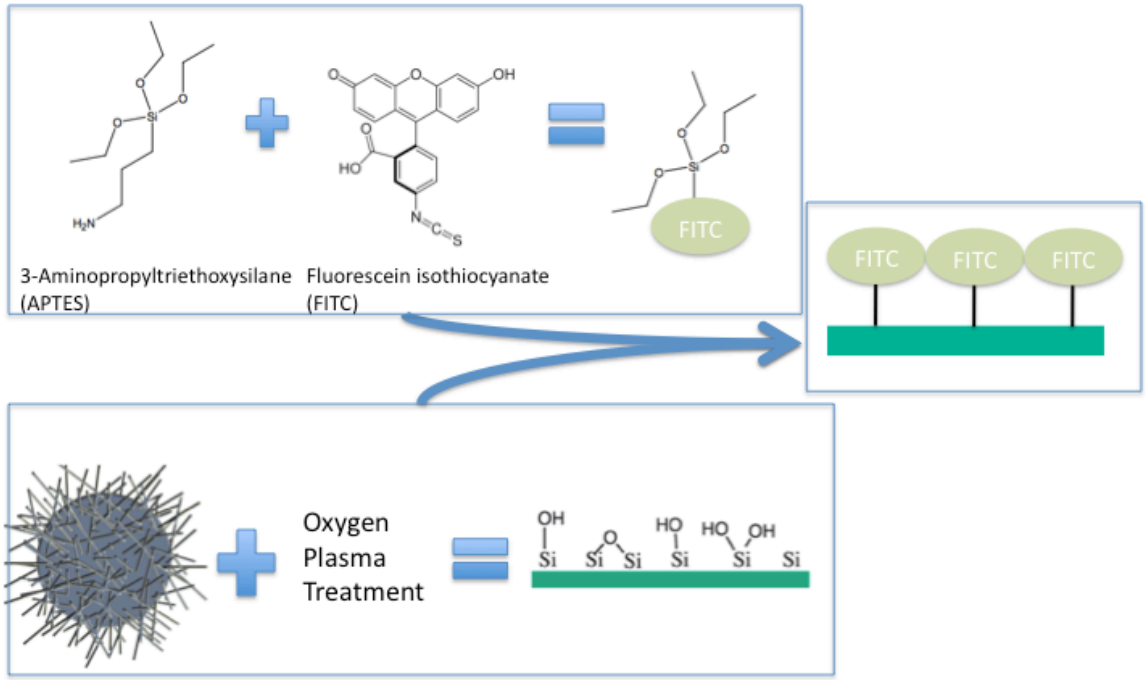

Figure 17: Schematic of a typical surface modification with fluorescein

Modifications with AlexaFluor 680 succinimidyl ester (Invitrogen, aliquoted at 10 mg/ml in anhydrous DMF) were similar to above. AlexaFluor 680 succinimidyl ester was mixed with APTES in isopropyl alcohol and incubated on a shaker plate at room temperature at least 3 hours. Devices were then exposed to 30 seconds of oxygen plasma and immediately added to the solution and incubated for at least 3 hours. Devices were transferred to a filter flask and washed with isopropyl alcohol and dried. After drying, devices were either heated to 110°C for 10 minutes of left in a vacuum oven overnight.

Particle characterization

Zeta Potential Measurements

Measurement of zeta potential assumes that objects are suspended and spherical. Particles as large and dense as the ones used for this project (greater than 10 μm) fall out of solution within 30 seconds, making accurate zeta potential measurements of an entire device impossible. Nanowires may be removed from the devices using sonication for 30 minutes, and provide a relatively accurate image of the surface with which the cells interact. However, because of their elongated shape, nanowires may be measured inaccurately. With these considerations in mind, along with the batch variation in surface modifications, we used several different techniques to characterize surface potential of the nanowires. Initially, we tried modifying silica nanoparticles (diameter 900 nm) with the same chemistry as the nanowire-coated devices. However, due to concerns about nanoscale geometry affecting the geometry and measurement of surface chemistry, we ultimately chose to measure nanowires directly (Figure 18; unmodified nanowires - black diamond, positively modified group - gray square, negatively modified group - white triangle).

Modified and unmodified nanowires were suspended in deionized water and their zeta potential was measured at varying pH (with the addition of hydrochloric acid and potassium hydroxide to alter pH) using a Malvern Zetasizer Nano. Zeta potential measurements can be found in the Supporting Information.

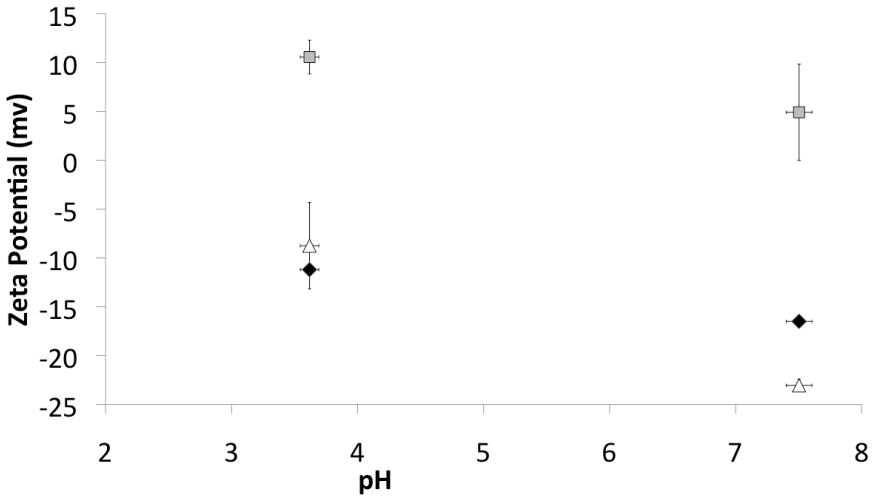

Figure 18: Zeta potential measurements of modified nanowires

Geometric Variations

By varying the properties of the gold catalyst and other properties of the vapor-liquid-solid fabrication process (eg: length of oven time), it is possible to generate numerous different varieties of nanowires with different lengths, diameters, and coating densities. Each particular group was kept separately and given a batch number to prevent mixing between different geometries. Using SEM, TEM, and image analysis software (ImageJ), we quantified the different geometric variations available (a sample is visible in Figure 19).

Nanowire Length	12 um	1 um	8 um	20 um	4 um
Nanowire Diameter	40 nm	40 nm	40 nm	60 nm	20 nm
Nanowire Coating Density	High	Medium	Low	Lowest	Low
Images (not all the same magnification – scale bar is 1 micron)	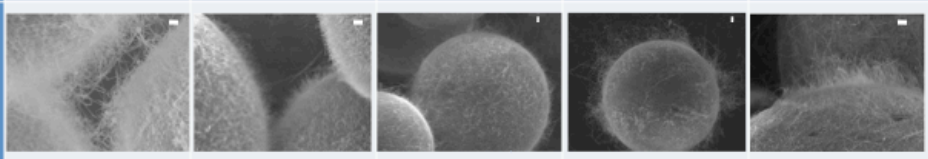				

Figure 19: Nanowire geometric variations

Exposure to acid

To ensure that the nanowires would be stable under a variety of physiological pH conditions, devices were exposed to solutions ranging from pH 2 to pH 6.5 for 2 hours. After removal from solution, devices were imaged with a SEM, and lengths were analyzed using ImageJ (Figure 20). Acidic conditions were found to make no significant difference in nanowire length.

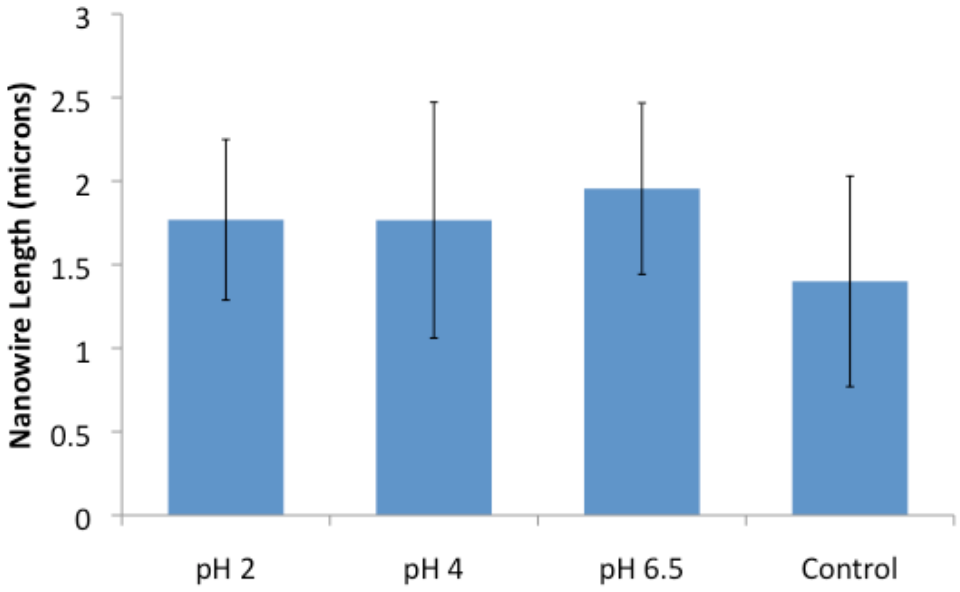

Figure 20: Effect of acid on nanowire length

Degradation

Although nanowires are expected to be removed from the gastrointestinal tract with the cells (turnover time of 2-3 days[18]), under unusual circumstances they may detach and transit through cells into other parts of the body or be inhaled through the lungs. In these cases, chronic accumulation similar to that of nanoparticles may take place if nanowires are not biodegradable. To determine their degradation timescale in biological solutions, nanowires were exposed to PBS, Survanta (also named beractant; a lung surfactant typically

given to neonates), and Mucin (Porcine Gastric Mucin, Type II Sigma, 2% in water, a gastrointestinal mucus layer model).

Devices were sonicated for 30 minutes in water to remove nanowires. After agitation by pipette, nanowires stayed in suspension, whereas the microspheres precipitated. Thus, the supernatent nanowire suspension was removed. Nanowires were incubated on a shaker plate at room temperature for up to 4 weeks, with solution changed three times a week. To change the solution, nanowire suspensions were centrifuged to the bottom of tubes at 14 krpm for 10 minutes; the supernatent was removed and new solution was added and suspended by pipette.

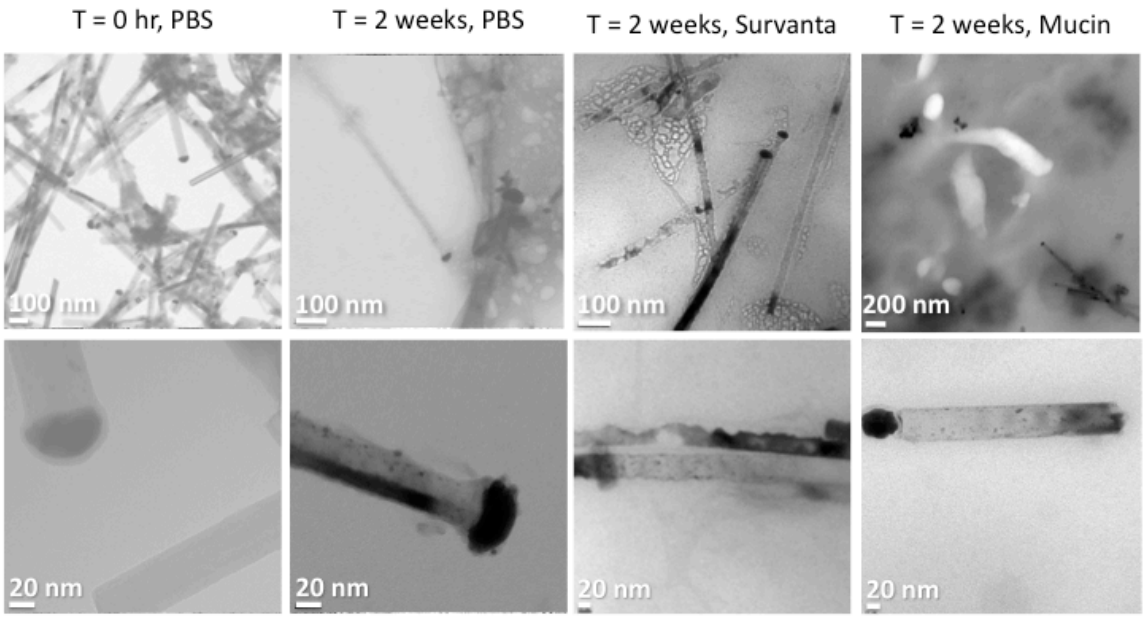

Figure 21: TEM images of nanowire degradation in PBS and Survanta

To quantify degradation, images were taken on a TEM (Figure 21, see Methods section) and analyzed using ImageJ. The actual areas and perimeters of nanowires were obtained by thresholding the images. Initial areas and perimeters were extrapolated from images by connecting the most external points of the nanowires into a box, and assuming these points constituted the original surface of the nanowires. The actual areas were compared to initial areas to obtain an estimate for surface area lost.

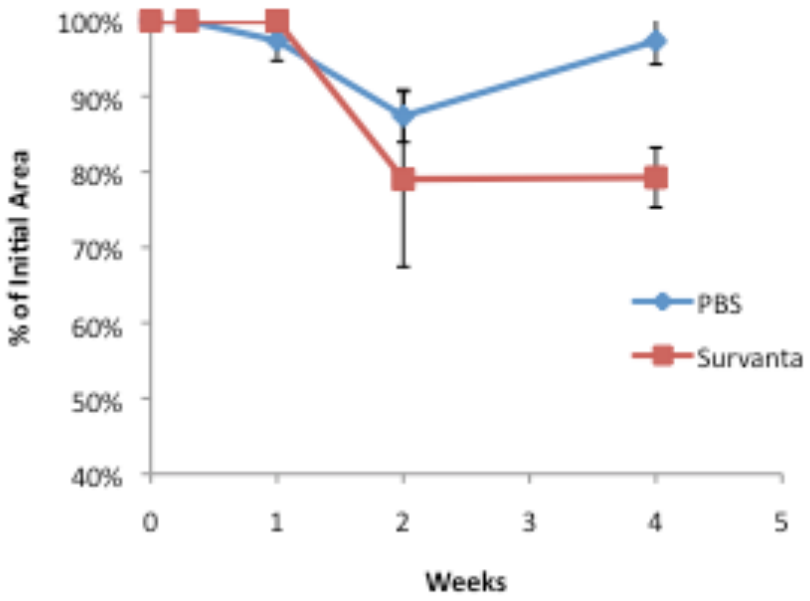

Figure 22: Nanowire surface area lost in physiological solution

Until roughly 1 week, very little degradation took place in any solution. At two weeks, some degradation was observed in PBS (85% of surface area remaining) Survanta (79% of surface area remaining - Figure 22). After four weeks, very few nanowires remained, and those that did were somewhat degraded (Figure 23). Thus, if nanowires were exposed to physiological solutions or inhaled, they would likely degrade within a matter of 2-4 weeks.

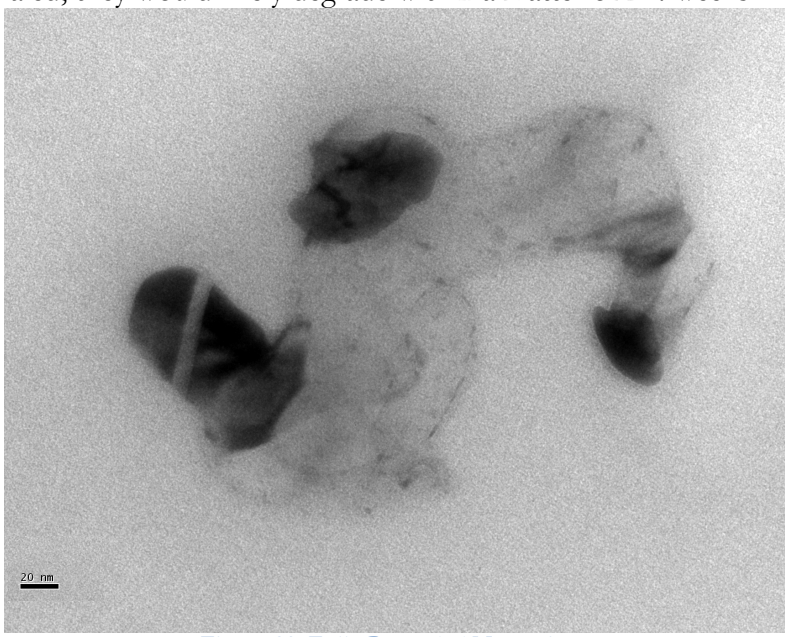

Figure 23: Fully Degraded Nanowires

Multiple Functionality Nanowire Modifications

Finally, different chemical modifications were made to improve targeting and allow for multiple functionalities using nanowires. Because each silicon nanowire has an attached

gold nanoparticle catalyst at the end, it is possible to spatially pattern the nanowires using silane chemistry and thiol chemistry. Figure 24b shows non-specific adsorption of fluorescein isothiocyanate (FITC) to all surfaces of the nanowire-coated bead. In Figure 24c, a polyethylene glycol (PEG)-modified silane (2-[Methoxy(polyethyleneoxy)propyl]trimethoxysilane, Gelest) was covalently attached to the silicon nanowires in toluene. Then, thiolated biotin (Nanocs, Inc) was added to the gold tips, and FITC-avidin was bound to the biotin. Figure 24c shows the fluorescent tips of nanowires without the nonspecific FITC binding to the wires (FITC is visible as punctate structures). Because there are two distinct surfaces, multiple functionalities may be attached to the nanowires, including targeting molecules, imaging agents, therapeutic molecules, or drug-loading scaffolds.

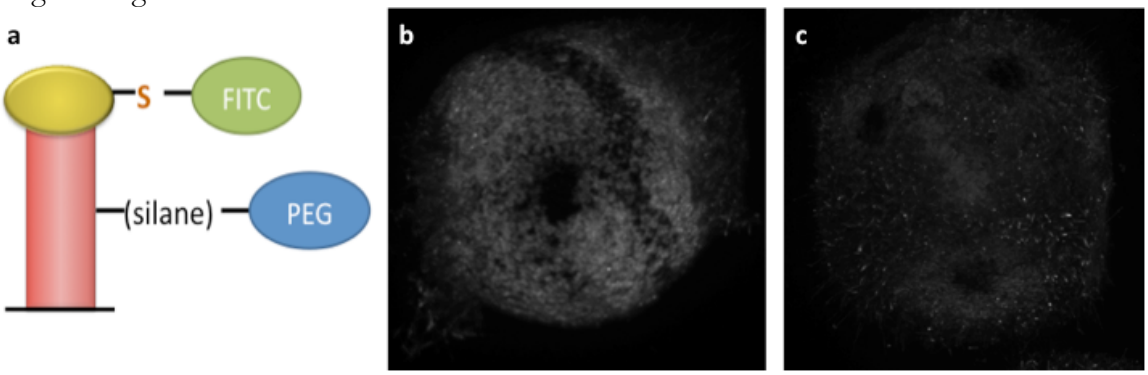

Figure 24: Multiple functionality nanowire modifications

Chapter 3: Methods

Cell Culture

Caco-2 cells are a heterogeneous cell line of human colon carcinoma epithelial cells that spontaneously differentiate and become morphologically and functionally similar to healthy enterocytes. Confluent monolayers of Caco-2 cells are widely used in pharmaceutical testing because they form tight junctions, become polarized, and express intestinal drug efflux transporters, thus enabling them to become a relatively accurate in vitro model of an epithelial mucosal membrane with a good correlation to in vivo results[65,66,67,68]. However, they do not generate mucus, so a mucin layer must be added to model drug diffusion through mucus and a cell layer.

The Caco-2 cell line (American Type Culture Collection (ATCC), Manassas, VA) was used at passages between 3 and 15. Cells were grown in culture medium of Eagle's minimum essential media (ATCC) with Earle's Balanced Salt Solution, 2.0 mM l-glutamine, 1.0 mM sodium pyruvate, 0.1 mM nonessential amino acids, 1.5 g/L sodium bicarbonate, 20% fetal bovine serum (Sigma), and 1% penicillin-streptomycin in a humidified 5% CO_2/95% air atmosphere at 37 °C. Cells were grown to confluence (5-15 days) using standard protocols before each experiment.

For flow testing, cells were seeded onto Type I Rat Tail Collagen-coated glass slides to improve confluency according to the following protocol: Slides were cleaned in oxygen plasma for 30 seconds. 1 mL of 1:67 dilution of collagen: 0.02 N acetic acid was added to each slide. After a 1 hour incubation at room temperature, slides were washed two times with sterile PBS and cells were added.

Caco-2 cell maturation

Caco-2 cells grow to confluency within a week and continue to mature and differentiate spontaneously up to 3 weeks after seeding[65]. This differentiation process includes the formation of tight junctions and apical microvilli. While initial microvilli-like structures appear on the surface of a few cells by day 3 (Figure 25), the majority of cells express few if any microvilli, making them a possible control for Caco-2 surface nanotopography.

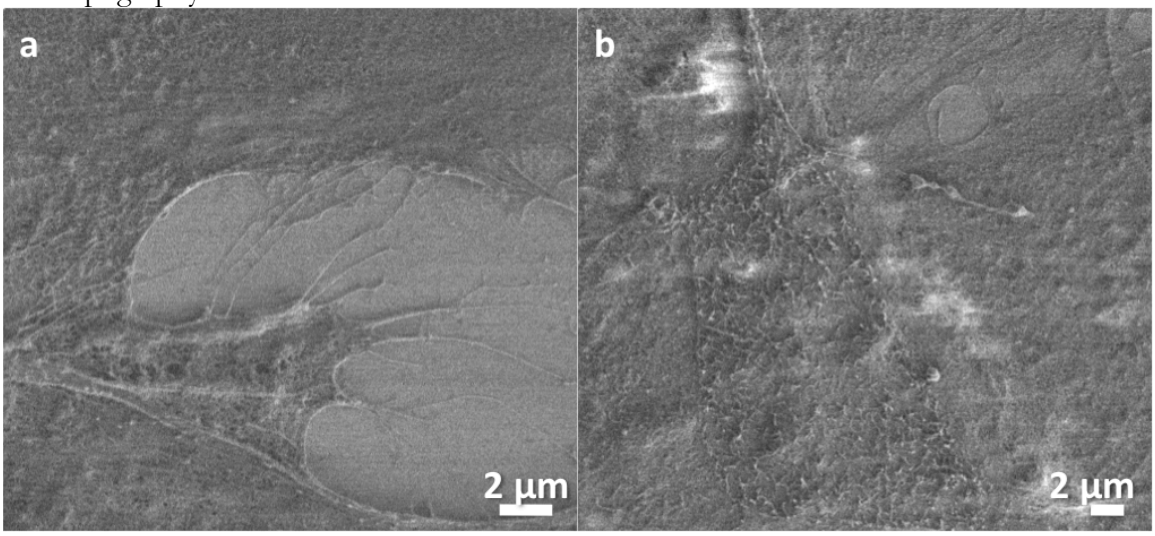

Figure 25: Caco-2 cells prior to confluency or maturity (Day 3)

Static adhesion

Control beads, nanowire-coated beads, and lectin-modified nanowire-coated beads were incubated with cells in 2% w/v mucin (Porcine Gastric Mucin, Type II, Sigma, pH 3.7) in Hanks Balanced Salt Solution (HBSS), a HBSS-HCl solution of pH 5.1 ± 1.0 (s.d), and 0.03% trypsin-EDTA in HBSS. After 30 minutes of shaking incubation, the cells were washed, and devices attached to cells and in the washes were counted. Percent adhesion was defined as the ratio of devices remaining on the cells to total devices exposed to cells.

Flow studies

To model the effects of shear on the adhesion to tissue, the devices were tested on a Caco-2 cell monolayer using a parallel plate flow chamber (Glycotech, Gaithersburg, MD - Figure 26). Cells were grown to confluency on a collagen-coated glass slide as described under cell culture. Devices were incubated on the cells for two hours prior to shear testing (for geometric optimization and chemical targeting experiments) or were incubated for less than five minutes (for all other flow experiments). Once the chamber was assembled, cell culture media flowed across the cells and devices in the geometric optimization experiments; all other experiments were done using 2% mucin. Shear was increased from roughly 0 to 200 dynes/cm^2 in a step-wise fashion, allowing the devices to come to a steady state before imaging (typically 10 minutes between shear increases).

The shear in the chamber was estimated by

$$\tau = \mu\gamma = \frac{6\mu Q}{a^2 b},$$

where τ is the wall shear stress (dynes/cm^2), γ is the shear rate (1/s), μ is the apparent viscosity (P), a is the channel height (cm), b is the channel width (cm), and Q is the volumetric flow rate (ml/s). Viscosity of the mucin solution was determined using an Ubbelohde viscometer. The flow chamber was typically imaged on a Nikon Eclipse TI-E motorized inverted microscope at 2x and stitched using NIS-Elements Advanced Research software. Devices were counted using Microsoft Excel-based, in-house software or Adobe Photoshop CS4. The detachment of the devices was quantified using a Kaplan-Meier product-limit estimate of the survival of the devices.

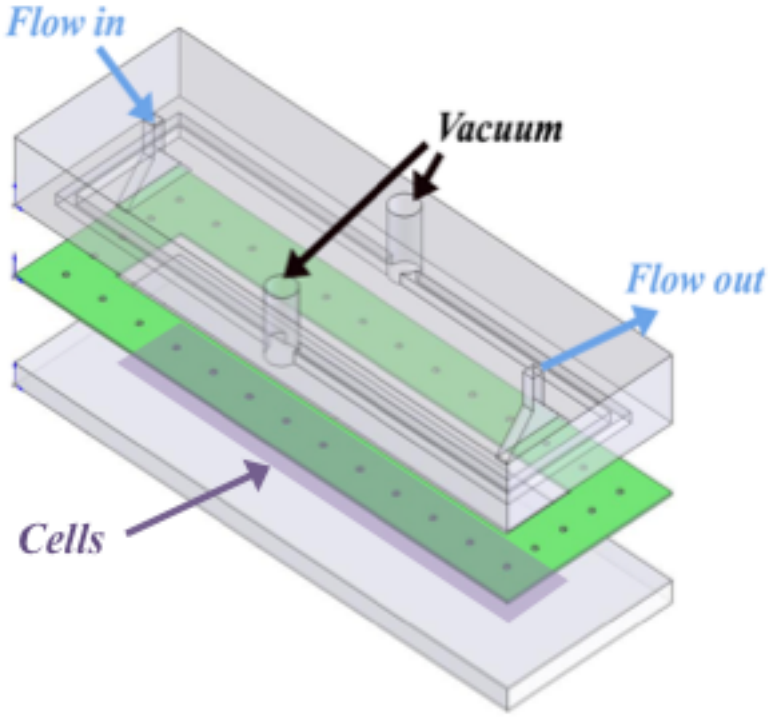

Figure 26: Schematic of a the parallel plate flow chamber

Limits to Shear Flow Experiments

In certain sets of experiments, the shear studies are complicated by temperature and cellular considerations. Because the physicochemical interactions of mucin change with response to temperature, the retention rates from the experiments done at 4°C are not directly comparable to those done on the immature and control cells, even though they were done at comparable shears. Because all actin polymerization is knocked out by cytochalasin D, rendering the cell shapeless and unsupported, these experiments are not directly comparable to the other flow experiments.

AFM

All atomic force microscope (AFM) measurements were conducted in the Zettl lab at UC Berkeley with the help of Benjamin Alemán. The following protocol was mainly developed by him for this project.

Adhesion measurements using an AFM (Asylum Research MFP-3D-BIO) were achieved by attaching test beads (nanowire-coated and control) to tipless AFM cantilevers (Mikromasch CSC-12 and NSC-12 Al backside coated tipless cantilevers - Figure 27). First, spring constant calibration of bare AFM cantilevers was performed on freshly cleaved mica using the thermal method[69,70,71]; typical cantilever spring constants ranged from 30-1000 pN/nm. Next, similar to Kappl *et al.*[72], micromanipulators were used under a stereoscope to place a small amount of epoxy (Varian Torr Seal) onto the end of bare cantilevers. A separate micromanipulator was then used to place test beads on the epoxy and devices were allowed to cure at 70° C for 2 hours. Optical microscopy was used to avoid contamination by biological debris in solution prior to adhesion testing.

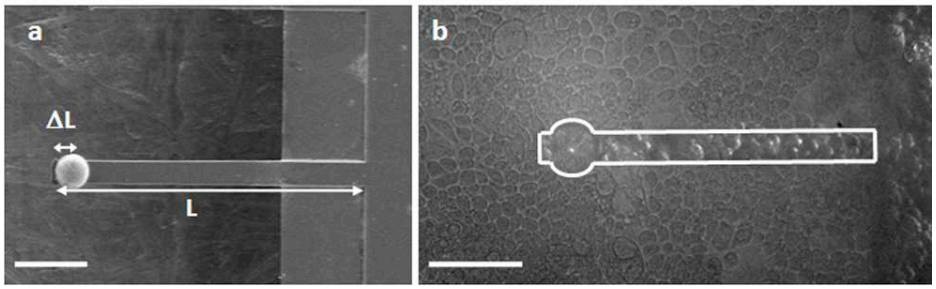

Figure 27: AFM cantilever system

Experimental limitations (e.g. probes should only contact cells once) led to several modifications of the spring constant. Off-end loading adjustments[73,74] were made to the bare cantilever spring constant, k_0, by a simple measurement of the position of the center of the bead to the end of the cantilever (see Figure X), ΔL, yielding the effective spring constant:

$$k_{eff} = k_0\left(\frac{L}{L-\Delta L}\right)^3 \quad (1)$$

The measured spring constant of control bead- modified cantilevers agreed well with (1). Once in liquid, the thermal power spectral density (thermal) was obtained and used to fit the inverse optical lever sensitivity and obtain k_{eff} as calculated using (1). In all AFM measurements, including initial calibration, laser diode spot size and position corrections were taken into account according to Proksh *et al.*[75] Final spring constant uncertainty would ultimately be roughly 20-30%.

Single contact adhesion force measurements on cells were performed by carefully lowering bead-modified cantilevers toward the surface of the cells using an AFM stage and head (Asylum Research MFP-3D-BIO) mounted on an inverted optical microscope (Nikon Eclipse TE2000-U). Special attention was required to avoid suspended debris near the cells. The cantilever was then brought into focus just above the cells and extended onto cells until it reached a trigger force of 5-100 nN. Retraction and extension speeds were typically between 0.2-2 μm/s. Control experiments were done using the same technique on flat tissue culture polystyrene surfaces and nanowire-coated beads. All experiments were conducted in phosphate buffer solution (PBS) at 37^{o} C and performed in an acoustic-isolation enclosure (Herzan) on an isolation table (Herzan TS-140), and all optical images of the experiment were taken using a CCD camera (CoolSnap ES, Roper Scientific) mounted on a side port of the optical microscope.

SEM

Cell Preparation

Cells were fixed with 3% gluteraldehyde (Polysciences) in a 0.1 M sodium cacodylate (Polysciences), 0.1 M sucrose in HBSS buffer for 2-3 days at room temperature. The fixative was replaced with the sodium cacodylate-sucrose buffer and incubated twice for 5 minutes. Samples were then dehydrated using a graded series of ethanol solutions, each for 10 minutes in the following order: 35%, 50%, 70%, 95%, 100%, 100%. The last ethanol solution was replaced with hexamethyldisilazane (HMDS, Polysciences) for 10 minutes and then left to dry. Prior to imaging, cells were typically sputter-coated with 3-15 nm of gold. Samples were stored in a desiccator until imaged.

Device Preparation

Beads, nanowire-coated beads, and AFM cantilever chips were situated directly on the conductive pads. For certain SEMs, the devices were sputter-coated with 3-6 nm of gold.

Imaging

Numerous SEMs were used to image samples in this dissertation, including a NovelX MySEM, a JEOL JSM-6500F field emission SEM, a Hitachi S-5000 SEM, a FEI Sirion (operating at 5 keV) and a Hitachi Model S-800 SEM.

Loading

Controlled Pore Glass Loading

The CPG particles were loaded by placing approximately 5-10 mg of devices in 500 μL of a loading solution and heating at 35°C for approximately 24 hours, after [56] (until dry – Figure 28). Loaded particles were washed with PBS in a filter flask to remove residual protein crystals. Bovine immunoglobulin G (IgG, 10 mg/mL, Biomeda), trypan blue (0.4% w/v in normal saline, Mediatech), and bovine pancreatic insulin (10 mg/mL. Sigma) were used as loading solutions. Bovine serum albumin (Sigma) was mixed with phosphate-

buffered saline (Fisher Scientific) to produce loading solutions at concentrations of 11.9 ± 3.6 mg/mL (s.d.).

Figure 28: Schematic of nanowire reservoir loading protocol

Microsphere Loading

Two experiments were conducted to understand the loading capabilities of three different batches of microspheres. Batch 0 consists of control microspheres with no nanowires, Batch 3 of microspheres with short nanowires attached and Batch 17 of microspheres with long nanowires attached. In the first experiment, microspheres from Batches 1, 3 and 17 were loaded with bovine serum albumin (BSA) at a concentration of 10 mg/ml in phosphate buffered saline (PBS). Elution was then observed over the course of six hours, with timepoints being taken at various intervals. In the second experiment, batch 17 microspheres were loaded with concentrations of 1 mg/ml, 10 mg/ml, 50 mg/ml and 100 mg/ml and elution was observed over the course of six hours (Figure 29). In both experiments, the eluted samples were measured for protein concentration using a BCA assay. All samples were made in triplicate.

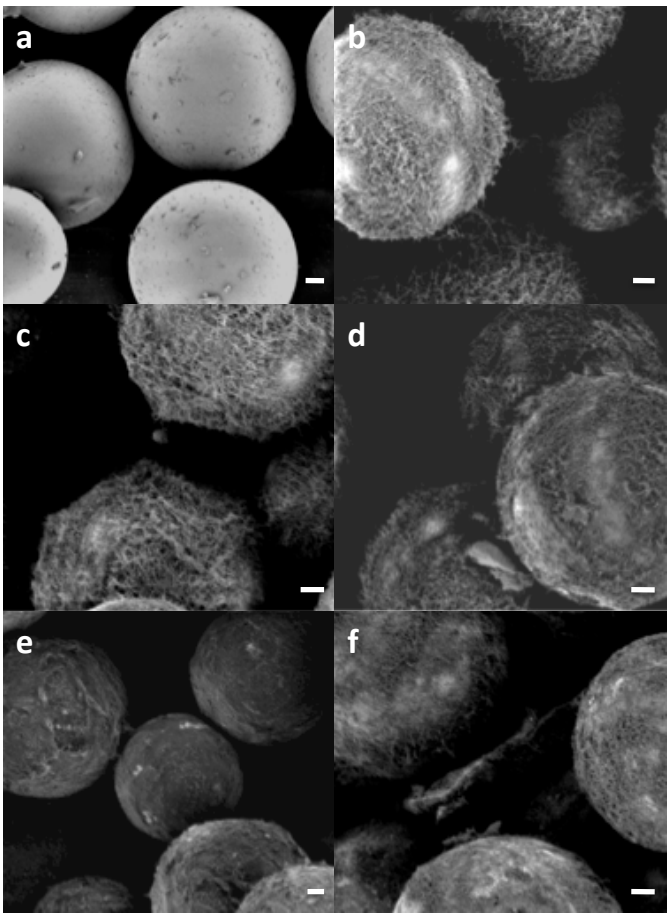

a) Unloaded control spheres. B) unloaded nanowire-coated spheres. C-f) 1, 10, 50, and 100 mg/ml loaded (respectively). Scale bar is 5 μm in all images.

Figure 29: Loaded and unloaded microspheres

Elution

The loaded CPG particles were suspended in 3 ml of PBS on a shaker plate for up to 10 days. However, due to instability of the drug molecules, only data points from 0 to 120 minutes were considered. At each time, 150 μL of solution was removed to a 96 well plate for quantification, and 150 μL of PBS was added to replace it.

The loaded microspheres were suspended in 3 ml of PBS for six hours. At approximately 0 hr, 40 min, 1 hr, 2h, 4 hr and 6 hr, 150 μl of the solution was removed after the suspension had been stirred and the microspheres were allowed to settle. The sample was placed in a 96 well plate and 150 μl of PBS was added to the suspension to replace the removed quantity.

For BSA, IgG, and insulin, the protein concentrations in the samples were analyzed using a micro and/or regular BCA assay and a spectrometer. The absorbance of the samples was read at a wavelength of 560 nm. Trypan blue was measured directly at an absorbance wavelength of 590 nm.

In vivo

Dosing and Observation

Gelatin capsules (about 21.7 x 7.5 mm) were filled with roughly 1 gram of devices, after [57]. The capsules were administered to healthy, female beagles (11-14 kg weight, after an overnight fast of 14 hours). Images were taken at 15 and 30 minutes post administration and then at 30 min intervals for the remainder of the experiment using a GE OEC 9800 Plus C-Arm fluoroscope. After 180 minutes, the experiment concluded and the dogs were fed. Throughout this time, the animals were observed for acute reactions and were allowed to maintain normal activity.

Imaging

In vivo imaging was done using fluoroscopy, which takes x-rays at a frame rate of 30 frames/seconds, allowing real-time positioning. In the video of Dog 4 (200 μm uncoated control particles) at 15 minutes, we can observe uncoated devices flowing through the intestine without any adhesion. However, in the supplementary videos of Dogs 1, 2, and 5 (with 300, 200, and 1000 μm particles, respectively), taken at 15 minutes, we observe nanowire-coated devices adhering to the stomach initially, and in Dog 1 continuing to adhere at 180 minutes, despite strong gastroduodenal contractile activity. In Dogs 1, 4, and 5, stomach and intestinal contractions can be seen at 15 minutes as particles are moving or expelled. Dog 2 does not display contractions at 15 minutes.

Actin remodeling and internalization

For actin staining, cells were fixed using 3.7% paraformaldehyde in PBS for 20 minutes. After a PBS wash, 0.5% Triton X-100 in PBS was incubated with cells for 10-15 minutes. Cells were washed, then incubated with 1% BSA in PBS for 30-60 minutes to block non-specific adsorption of stains. After a PBS wash, a 1:200 AlexaFluor 488 Phalloidin (Invitrogen): PBS solution was incubated on cells for 45-60 minutes at room temperature and covered with parafilm to prevent evaporation. Cells were washed and a 1:1000 dilution of Propidium Iodide (Invitrogen) in PBS was added for 5 minutes.

For internalization assays, cell monolayers were imaged live in PBS at 37°C. FITC – labeled devices were added to the cells, and after a 5 minute to 1 hour incubation, 100-200 microliters of 0.4% Trypan Blue solution was added. Confocal imaging was conducted 1 to 2 minutes afterwards, and brightfield imaging of the trypan blue stain was used to confirm that the cell monolayer was not otherwise compromised. A Nikon TE Spinning Disk inverted confocal microscope was used to take the images, and NIS Elements and ImageJ were used to reconstruct the images.

Toxicity

Using the CACO-2 cell line, cell viability five hours after the addition of the nanowire coated devices was determined using a trypan blue exclusion assay. Fluorescent staining for live and dead cells was done at varying times after the addition of the devices using CMFDA, which diffuses through membranes of live cells and binds to glutathione to make entire cells fluoresce green, and Ethidium Homodimer-1, a red stain which only passes through the compromised membranes of dead cells. Images were processed using ImageJ software in combination with a Matlab™ statistics package.

A 3-[4,5- dimethylthiazol-2-yl]-2,5-diphenyl tetrazolium bromide (MTT) assay (Sigma) was used to assess mitochondrial activity. Cells were grown in a 96 well plate. After confluency, devices were added and incubated on cells for 2 hours. Cells were washed with PBS, then incubated in phenol-red free and serum-free media with 10% of reconstituted MTT for 2 hours. After incubation, MTT solubilization solution was added and mixed with pipettes and on a shaker plate. A sample of the solution was transferred to a 96 well plate for spectrophotometric imaging at 570 nm (subtracting the background at 690 nm).

TEM

Dry nanowire samples were suspended in PBS for TEM image preparation. A 5-10 μL sample of the nanowire solution was pipetted onto a TEM grid and incubated at room temperature until the solution evaporated. Samples were imaged using a FEI Tecnai TEM.

Chapter 4: In vitro adhesion

Adhesion observations

From scanning electron microscopy (Figure 30), significant interdigitation of the nanowires and microvilli was visible at the cell-nanostructure interface, showing significant areas of contact between the cells and nanowires. Typical handling of the nanowire-coated devices in solution with pipettes often induced clumping of numerous devices. Devices immediately precipitate out of solution. Furthermore, after even momentary exposure to cells, the nanowire-coated microspheres became extremely difficult to remove, as compared with control microspheres, which could usually be removed with the cell culture media.

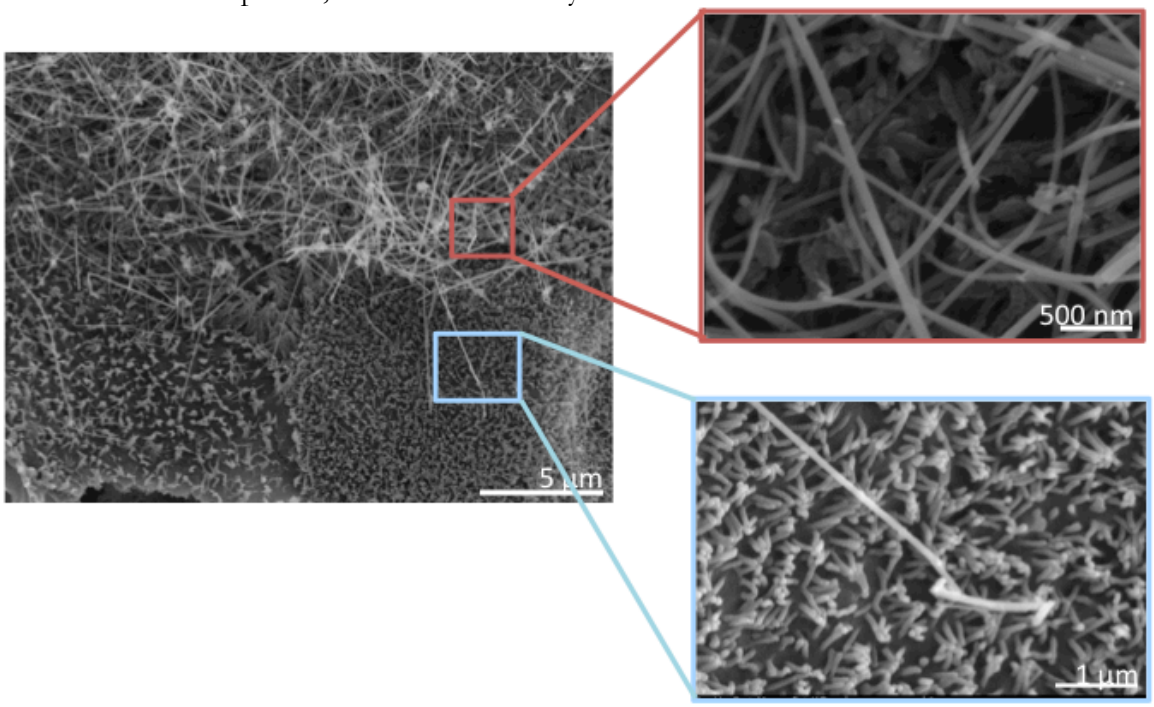

Figure 30: Nanowire interdigitation with surface microvilli

Initial static adhesion experiments indicated that nearly 100% of nanowire coated microspheres were retained within 40 minutes of contact with cells (Figure 31). Even at 120 minutes, only 40% of uncoated devices were retained.

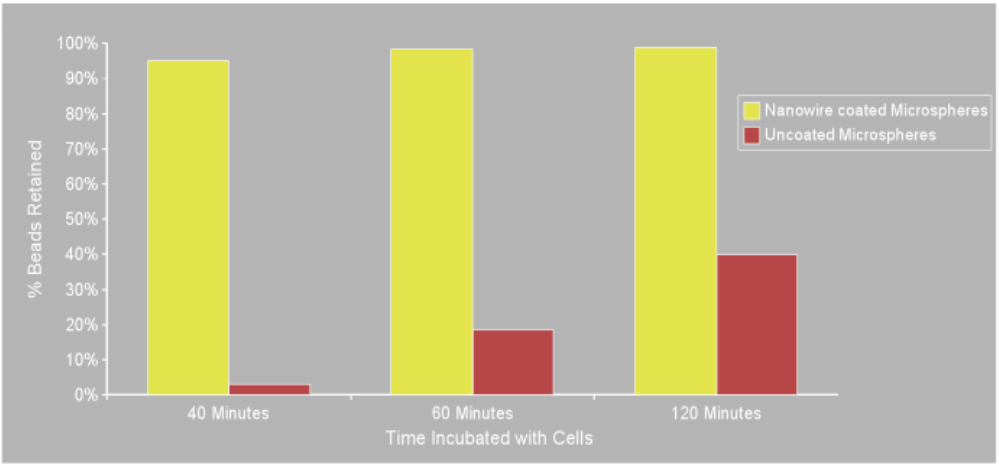

Figure 31: Static Adhesion at Varying Timepoints; Reproduced with permission from [1]

Static adhesion studies under different conditions

To isolate the effects of various factors within the mucosal environment which could lead to reduced adhesion, devices were incubated with cells while in the presence of either Hanks Balanced Salt Solution (HBSS), 2% w/v mucin, HBSS at pH 5.1 ± 1.0 (s.d.), or 0.03% trypsin (Figure 32). In all solutions, nanowire-coated beads adhered to cells at a frequency 5 times greater than control beads. Additionally, except in the mucin solution, the tomato lectin-modified, nanowire-coated devices adhered as well or slightly better than the nanowire-coated beads, indicating that these solutions have no significant effect on the targeting capabilities of tomato lectin[76]. The reduced adhesion of lectin modified, nanowire-coated devices in mucin suggests that unmodified nanowire-coated devices may have an advantage when exposed to mucus.

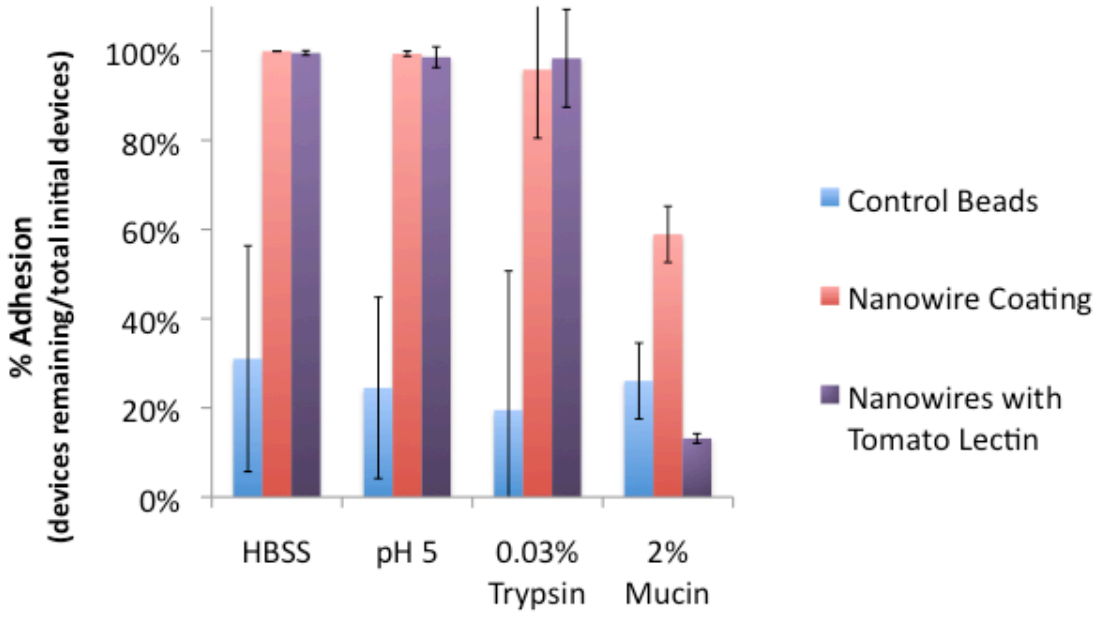

Figure 32: Static Adhesion in Physiologically Relevant Conditions

Flow studies in media

In order to characterize the effects of geometric and chemical modifications of the nanowires, three nanowire test geometries and a control group with no nanowires (See Table 3) were fabricated. A subset of the long nanowire group and the control group were chemically modified with tomato lectin, a well characterized mucoadhesive intestinal targeting molecule[33,77,78]. Each test geometry had nanowires with an average diameter of 60 nanometers, but with varying lengths and numbers of adhesive elements per surface area (coating densities). Within each geometry, the quality of surface area nanowire coverage varied bead by bead (expressed as percent surface area covered).

	No Nanowires (Control)	Long Nanowires	Medium Nanowires	Short Nanowires
Effective Average Microsphere Diameter (mm)	40.9 ± 6.0	47.6 ± 6.8	47.0 ± 3.4	46.8 ± 4.5
Average Nanowire Length (mm)	n/a	12.1 ± 6.3	4.2 ± 2.0	1.4 ± 0.6
Average Surface Area Coverage (%)	n/a	97.8 ± 2.1	85.2 ± 21.7	86.1 ± 17.6
Nanowire Coating Density	n/a	High	Medium to Low	Medium to Low
Median Survival Shear in Media (dynes/cm^2)	n/a	54.4	17.8	9.6

Table 3: Geometric Properties of Nanowire Groups

Shear flow studies conducted on nanowires with varying geometric properties indicated strong device retention rates (Figure 33), above 90%, for all geometries in shear less than 4 dynes/cm^2, with the long nanowires providing the greatest adhesion at higher shears (median survival shear of 54.40 dynes/cm^2). The median survival shears for the medium and short nanowires were 17.79 dynes/cm^2 and 9.54 dynes/cm^2, respectively. The median survival shear correlated to the length of nanowires, indicating a relationship

between nanowire length and adhesion under shear flow.

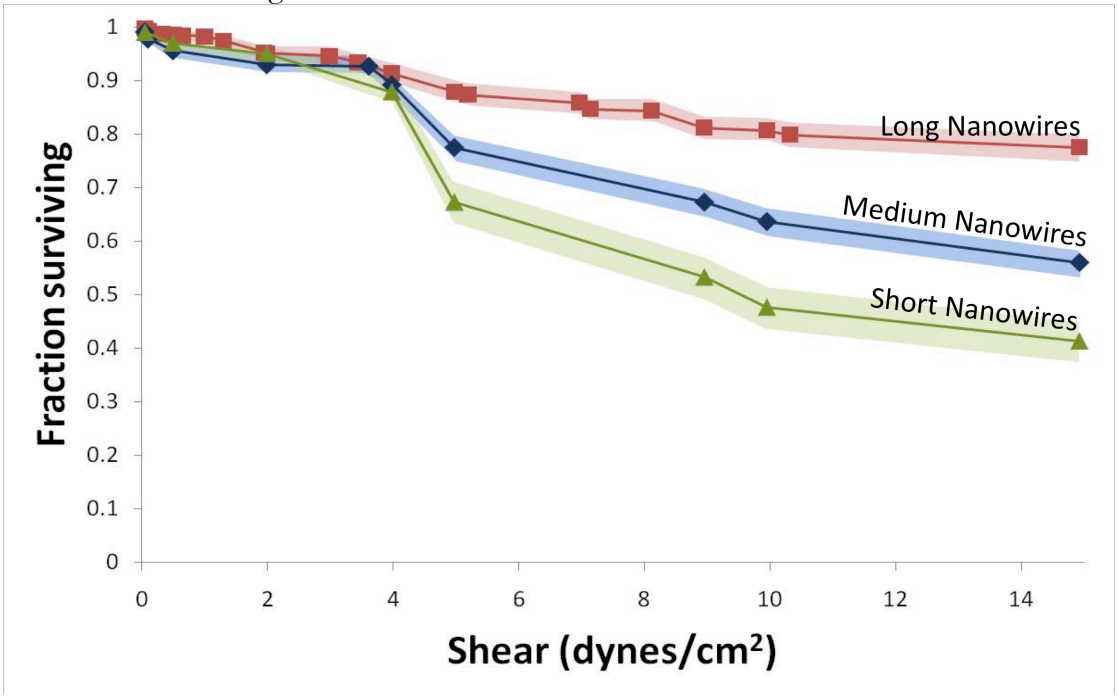

Figure 33: Geometric Effects on Device Retention in Shear in Cell Culture Media

Flow studies in mucin

Lectin-modified and unmodified devices incubated on a Caco-2 monolayer were exposed to mucin flow to determine the effect of chemical modification on adhesion under shear stress (Figure 34). Unmodified control beads and lectin-modified beads detached at the lowest shears, with median survival shears, the shear at which 50% of the devices had detached, of 2.35 dynes/cm^2 and 3.60 dynes/cm^2, respectively. Though lectin-modified nanowires decreased the level of bead detachment, unmodified nanowires showed the greatest retention (median survival shears of 5.70 dynes/cm^2 and 9.15 dynes/cm^2, respectively). Compared to unmodified nanowires, lectin modification enhanced detachment from cells under mucous flow, indicating that mucoadhesive chemistry may reduce overall mucosal tissue adhesion, compared to geometry-based adhesion. Because lectins bind to both cells and mucus, adding a mucin layer introduces competition between these elements for binding to the lectin-modified nanowires, which may explain the reduced adhesion.

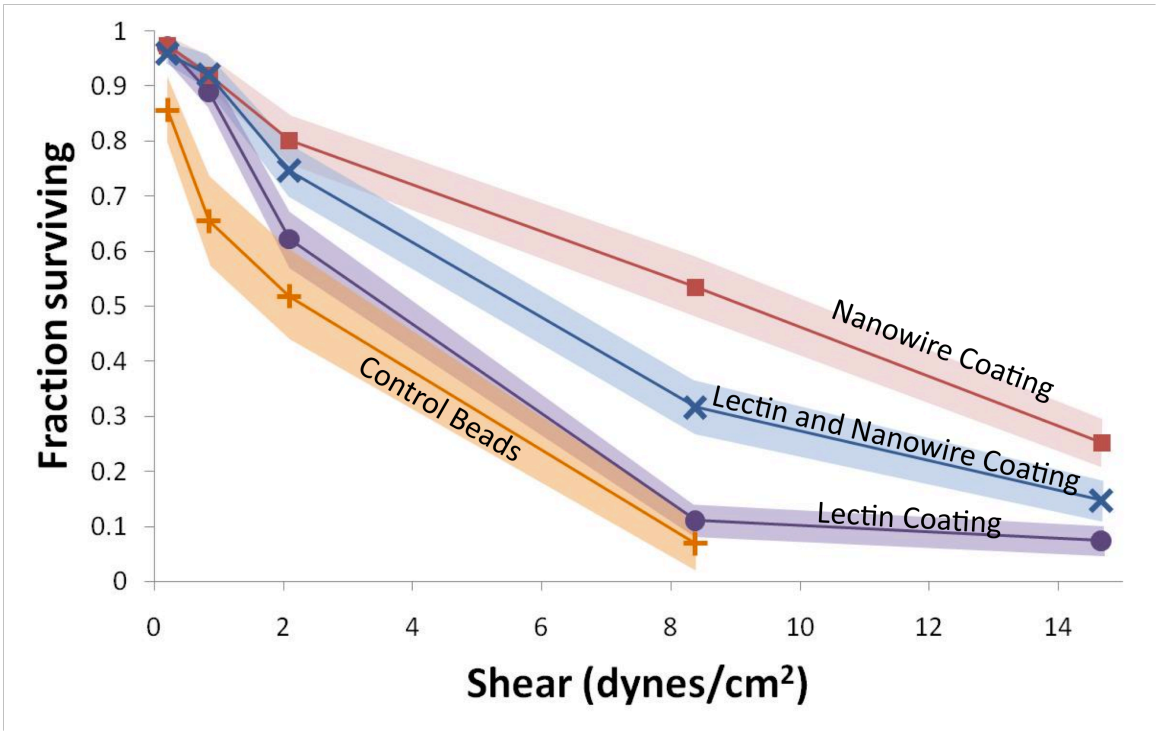

Figure 34: Retention of Devices under Increasing Shear in Mucin

Flow studies on different cell types

To determine if nanowire-mediated adhesion is applicable to other mucosal tissues, we conducted shear tests on a variety of cell types *in vitro*. The RPMI-2650 nasal cell line[79], forms large clusters on the microscale, but few active extrusions on the nanoscale (Figure 35c, scale bars are 10 μm). Caco-2 intestinal cells form a flat monolayer on the microscale, but have numerous apical microvilli (Figure 35b)[65]. Adult bovine aortic endothelial cells (BAEC, or ABAE) form a monolayer that is flat both on the micro- and nanoscale, and

since they are endothelial cells, they do not function as an absorptive interface with the external environment (Figure 35a)[80]. To measure adhesion, we added devices to a slide with the cells of interest, and then subjected it to flow of a model mucus layer consisting of 2% porcine gastric mucin (Sigma) in deionized water (pH 3.7).

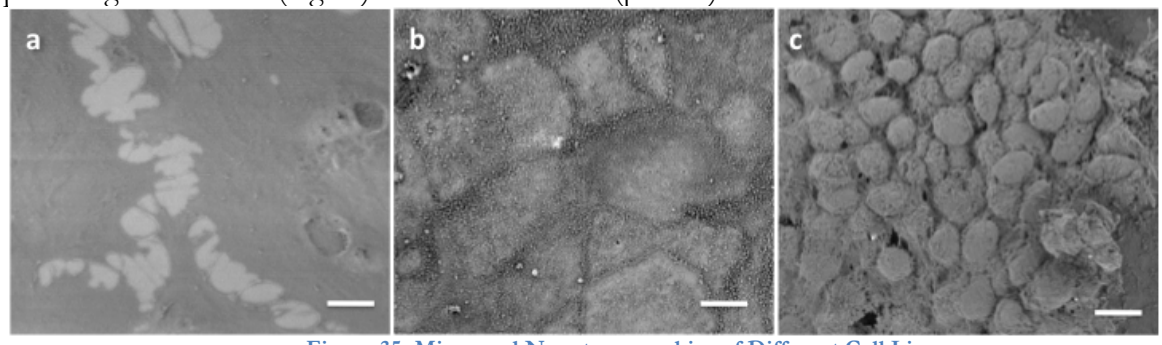

Figure 35: Micro and Nanotopographies of Different Cell Lines

When NEMPs were exposed to these three cell lines, there was significant improvement in retention at low and medium shears (Figure 36, nanowire-coated devices – black, control devices - white). Though the nanowire coating increases relative adhesion for all three cell types (4.9-fold for BAECs, 4.0-fold for Caco-2 cells, and 2.7-fold for RPMI-2650 cells over unmodified devices at a shear of 8.3 dynes/cm^2), the absolute adhesion of nanowires is highest in the micro- and nano-structured Caco-2 and RPMI-2650 cells. This data suggests that nanowires can improve adhesion to many cell types regardless of cell-specific attributes, though they may be most useful in cells with micro- and nanotopographical features.

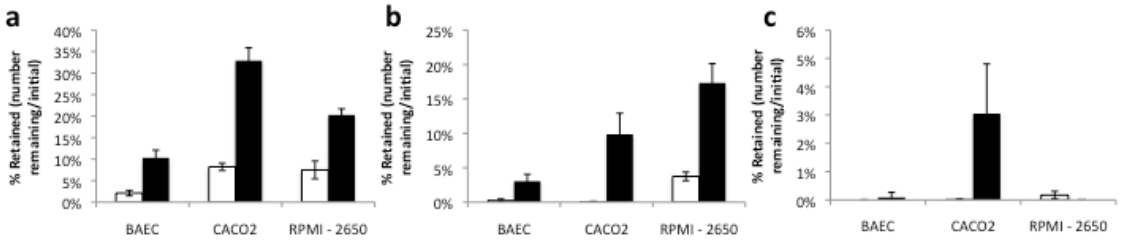

Figure 36: Retention of Devices on Various Cell Lines

Flow studies under different conditions

Nanoscale bioadhesive mechanisms remain poorly characterized. In dry environments, nanowires and other related nanostructures adhere primarily via van der Waals forces[36,81], demonstrating the strong effect of charge-related forces at the nanoscale. Longer nanowires improve bioadhesion over shorter wires, indicating a related effect due to nanowire geometry. Particle shape affects cellular internalization[82], and nanoparticles of similar end shape are endocytosed by macrophages[83], suggesting an effect due to cytoskeletal restructuring. In this experiment, we consider the role of nanowire charge as well as that of cellular morphology and remodeling.

Native silicon nanowires are negatively charged both at physiological pH and at the low pHs found in the GI tract (-16.5 mV at pH 7.5 +/- 0.1, and -11.2 mV at pH 3.6 +/-0.1, respectively). To test the effects of charge on adhesion, we modified the nanowires to have

different charges at low pHs using silane chemistry with amine modifications and FITC labeling (see Methods). This chemistry resulted in two groups with zeta potentials of 10.6 +/- 1.7 and -8.7 +/- 4.4 mV at pH 3.6 +/-0.1.

When exposed to Caco-2 intestinal cells under mucin, positively charged NEMPs adhered significantly better than negatively charged NEMPs at 16.6 dynes/cm^2 (the upper limits of a healthy intestinal shear) and better than negatively charged NEMPs, though not significantly, at 166.6 dynes/cm^2 (Figure 37). Thus, positive charge improves nanowire adhesion to Caco-2 cells, expanding previous reports of mechanisms of nanoparticle adhesion and internalization to include nanowires[84]. Neutral nanowire charge, from hydrophilic polyethylene glycol (PEG) modifications, reduces adhesion to roughly the same as uncoated MPs, demonstrating that charge is essential to nanowire adhesion. Similar to findings with nanoparticles, nanowire adhesion requires some charge, and is optimal when that charge is positive[85].

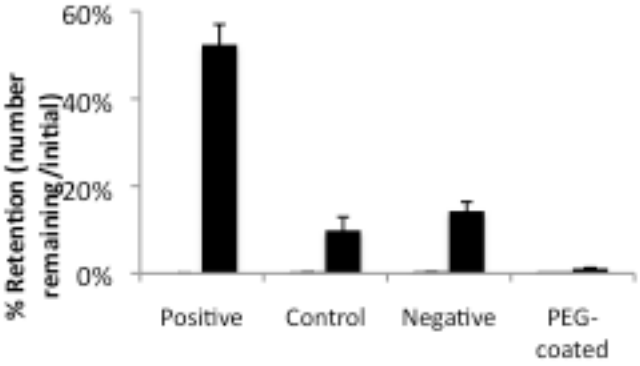

Figure 37: Effects of Charge on Device Retention

Nanotopographical cytoadhesion may also be modulated by microvilli covering the apical surface of mature gastrointestinal epithelial cells – either actively, via a remodeling in response to nanowire stimuli, or passively via a "Velcro-like," physical interdigitation. The actin cytoskeleton may be critical to these interactions, either by modulating cell structure underneath the microvilli or the structure of the microvilli themselves[86,87].

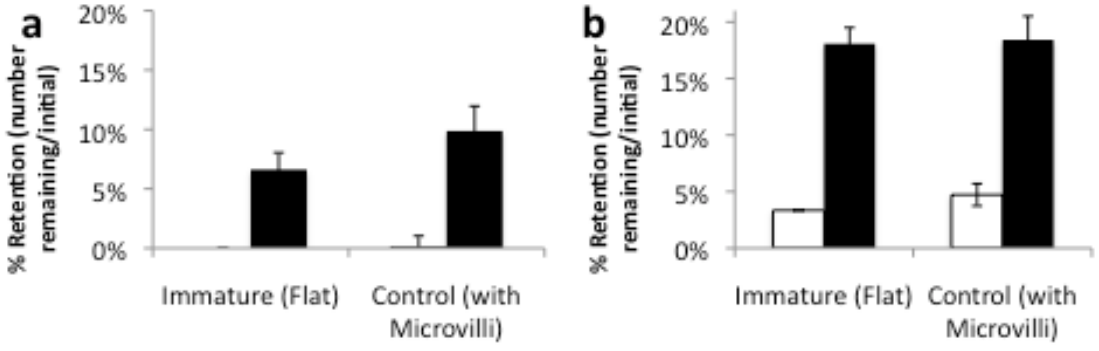

Figure 38: Effects of Microvilli Geometry and Activity on Device Retention

Adhesion to immature Caco-2 cells, which do not express significant quantities of microvilli, and on Caco-2 cells at 4 °C, which slows actin polymerization, effectively immobilizing the microvilli and preventing active internalization processes can be studied to determine the importance of microvilli in adhesion (Figure 38). In the immobilized state

(Figure 38b), both "flat" immature and microvilliated control cells exhibit similar retention of devices, suggesting that the microvilli are not acting in a "Velcro-like" fashion, despite greater adhesion by nanowire-coated beads. When the cells are maintained at an active temperature, microvilliated control cells do retain nanowires in greater quantities, though not significantly. Thus, while microvilli may be involved in adhesion to some degree, nanowires continue to adhere strongly even when microvilli interactions, both active and passive, are minimal.

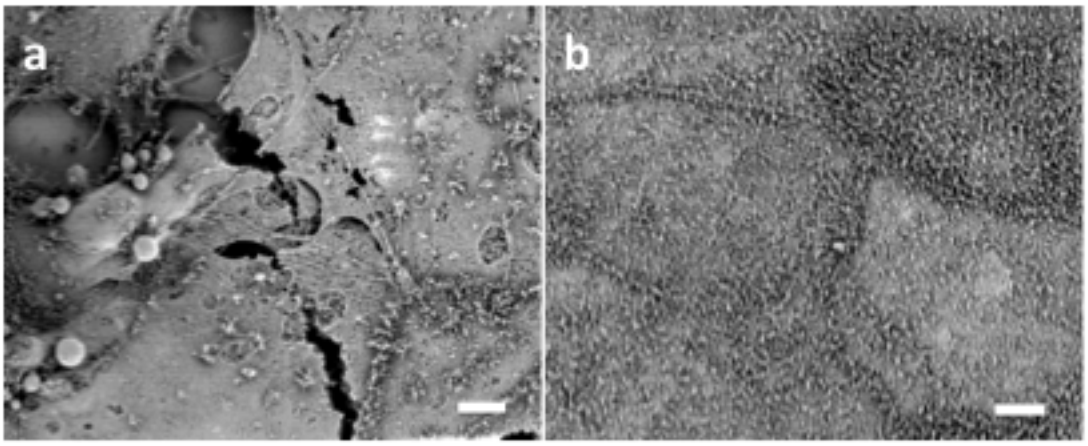

Figure 39: Effect of Cytochalasin D on Caco-2 Morphology

Although microvilli-specific interactions are minimal, the actin cytoskeleton may be involved with adhesion at a more general level. To knock out the cytoskeleton, cells were incubated for two hours with cytochalasin D, a fungal mycotoxin which transiently prevents actin polymerization in Caco-2 cells (Figure 39)[88,89]. A significant proportion of NEMPs were retained under flow in comparison to the rapid loss of MPs (Figure 40).

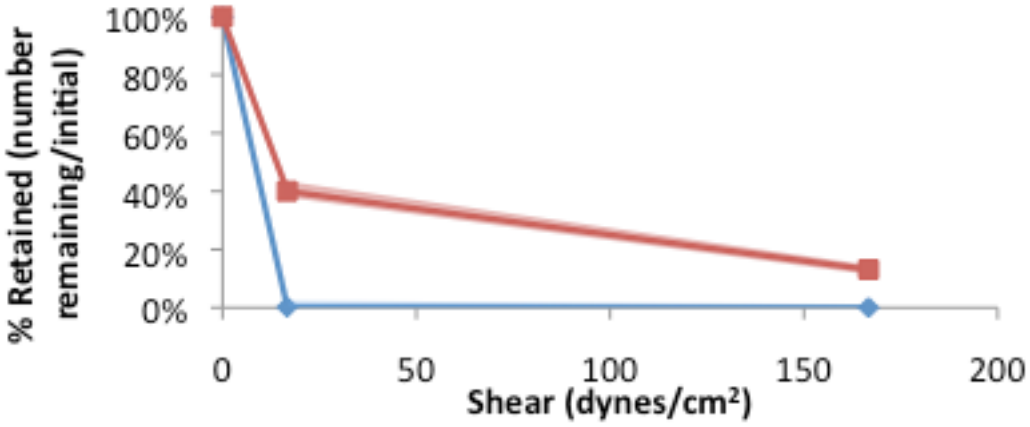

Figure 40: Effect of Cytochalasin D on Device Retention

Overall, deformation of cells increased the surface area in contact with devices, and if the devices had nanowires, this deformation increased adhesion. Thus, even in the most extreme cytoskeletal conditions, nanowires increase adhesion significantly.

Adhesion Mechanisms

Both cell-related and nanowire-related effects are involved in nanowire-mediated adhesion. Nanowires may be optimized either with chemistry, as in modification with positive charge, or geometry, as with longer nanowires. The characteristics of the underlying cell substrate affect adhesion as well, with cell type, contact surface area, and the actin cytoskeleton each affecting adhesion. As long as they are charged, nanowires significantly improve adhesion when compared to control devices. PEG-coated nanowires do not increase adhesion, likely because PEG is not charged and does not interact with cell surface proteins, thereby negating the charge and surface area enhancement by nanowires.

Pinpointing the particular roles played by various cellular features in nanowire-mediated adhesion is a complicated matter, as comparing the adhesion across experiments is difficult given the number of factors that can play a role in the efficacy of the nanowires. For example, shear flow experiments on normal and immature cells determined that microvilli do not significantly improve retention with or without an active actin cytoskeleton. However, these experiments could not be used to determine the effect of the actin cytoskeleton itself.

Similar experiments on cells treated and untreated with cytochalasin D demonstrated that actin polymerization does not significantly improve adhesion, although it is possible that the primary mechanism of adhesion differs in these cases and that actin in fact plays a critical role in the retention on healthy cells, even if it does not in the flaccid cytochalasin D-treated cells. Regardless of the mechanism, both types of cells showed sizeable deformation in response to the devices, thereby increasing the cell surface area in contact with the nanowires.

Additionally, nanowires on microspheres are not internalized by healthy Caco-2 cells, indicating that the adhesion stems from interactions that are mediated by the surface of the cells (see Chapter 7). It is possible that initial adhesion is charge-related and mediated by the surface, but over time, cells remodel internally in response to these interactions. Thus, numerous mechanisms may play a role in nanowire-mediated adhesion.

AFM studies

All atomic force microscope (AFM) measurements were conducted in the Zettl lab at UC Berkeley with the help of Benjamin Alemán. The following analysis was mainly documented by him for this project.

An AFM with devices affixed to cantilevers was used to quantitatively determine tensile adhesive forces. Typical curves from this system (Figure 41) indicated control beads produced an adhesion force of 1.80 ± 0.2 nN (s.e.m.) when contacting cells. When a nanowire-coated bead made contact with cells, forces upward of 100 nN were common (mean force: 172.0 ± 53.8 nN s.e.m.).

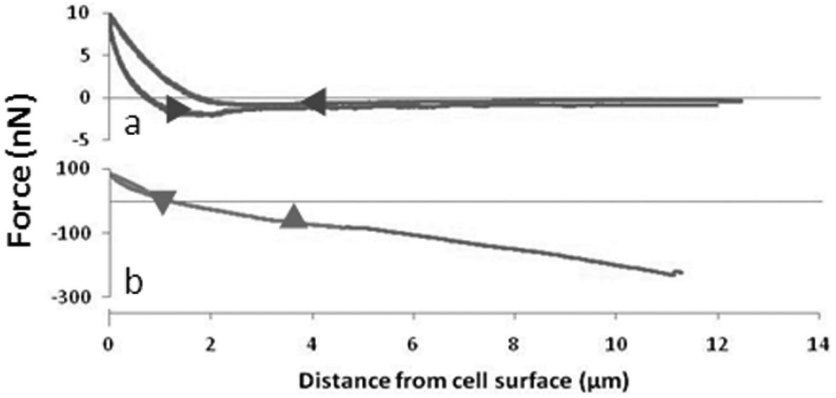

Figure 41: Typical AFM adhesion force curves

Using scanning electron microscopy after AFM experiments, length and surface area coverage of a given bead were quantified, to determine the relationship between nanowire geometry and maximal forces generated in the AFM experiments (Figure 42). At one extreme, short nanowires provided a smaller increase in surface area than longer nanowires, reducing available contact forces comparatively; at another extreme, long nanowires tended to fold over on themselves, creating a matted surface and reducing the overall available surface area compared to freestanding nanowires. Accordingly, within our AFM testing length range (0-3 μm nanowire length), the data suggest that it is possible to optimize adhesion by growing nanowires between 1 and 2 μm (Figure 42a). In addition to nanowire length, the quality of surface area coverage affected maximum forces achieved, with devices exhibiting reduced coverage, such as those that contain patches without nanowires, achieving lower maximum forces (Figure 42b). Based on surface area coverage and maximum force measurements, the force of adhesion of nanowire-coated devices was found to be 0.11 kPa; this estimation is a lower limit.

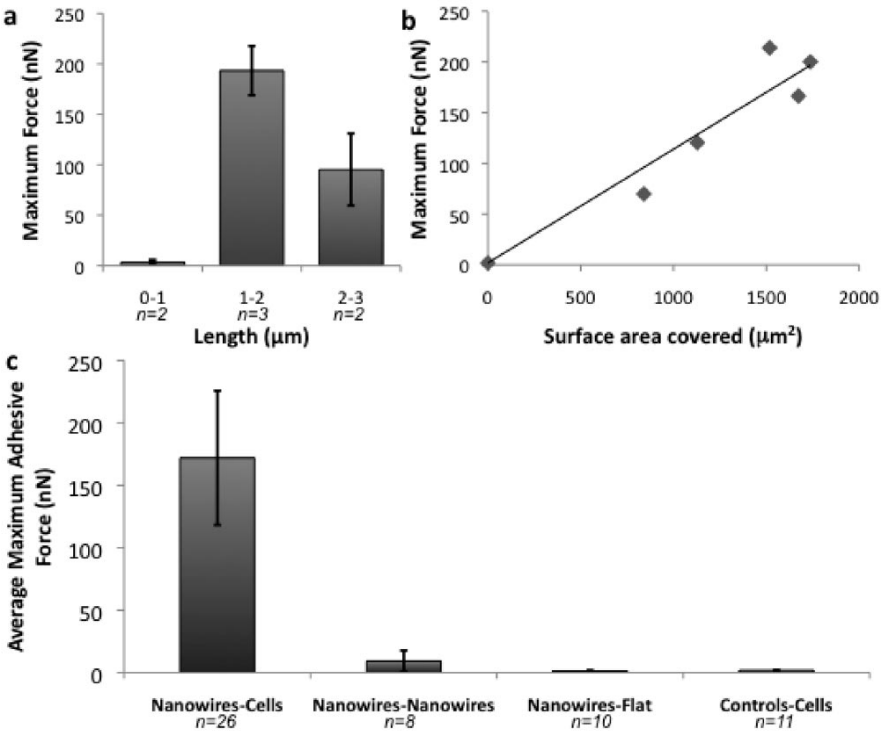

Figure 42: Geometric effects on maximum tensile force

In addition to nanowire geometry and chemistry, we considered physiologically relevant variations in the geometry and chemistry of the underlying cell surface. Because much of the documented dry nano-structure adhesion is due to van der Waals forces, which are dependent on the surface area in contact with the substrate, a nano-structured surface (such as a cell with microvilli or a nanowire-coated bead), would be expected to increase the adhesion over a flat surface. As expected, nanowire-coated beads brought into contact with flat polystyrene produced a mean force of adhesion of 1.30 ± 0.5 nN (s.e.m.); however, a nanowire-coated bead in contact with a nanowire substrate only increased the adhesion force to 9.3 ± 8.4 nN, still an order of magnitude less than the mean adhesion between nanowires and cells (Figure 42c). This minor increase suggests that forces beyond van der Waals forces may be responsible for a significant proportion of nanowire-cell adhesion.

Interpretation of Atomic Force Microscopy Data

Although AFM is an excellent tool for determining maximum lift-off forces, its data must be interpreted in a biological context. In many cases of the shear flow experiments, devices were observed to roll slightly until they reached a state of strong adhesion. However, when a device was confined to a specific position on the tip of an AFM cantilever, it lost five degrees of freedom, creating somewhat artificial values for some of the force trials.

Single Nanowire and Cluster Adhesion

One reason for poor contact of some devices in AFM trials may be that only one or a few nanowires were actually touching the cells. For nanowires, Euler buckling force is:[90,91]

$$F = \frac{\pi^2 EI}{L^2} = \frac{\pi^3 Ed^4}{64L^2},$$

when E is Young's modulus, d is the nanowire diameter, L is the nanowire length, and $I = \pi d^4 / 64$. Using 100 GPa as the Young's modulus for silicon, buckling forces range from 2.1 nN to 18.9 nN for nanowires with diameter of 50 nm. In many cases, the AFM triggered at 10 nN, which is within the range of forces necessary to force a nanowire to buckle. Cell penetration forces for similarly sized nanostructures range between 200 pN[92] and 1 nN[93]. Thus, it is possible, especially for long nanowires, that a single nanowire penetrated the cell monolayer and buckled upon hitting the underlying petri dish without the other nanowires establishing sufficient contact with the cells. A larger bundle of nanowires could, instead of penetrating the cell membrane, deform the membrane, make contact with the surface, and in that way limit cell-device contact. In the cases of poor contact (Figure 43a), adhesion averaged 3.51 ± 2.52 nN (s.d.). A similar amount of force was seen in devices where good contact was made, but single or clusters of nanowires detached as the cantilever retracted (Figure 43b). In these instances, forces of adhesion ranged from 1.7 to 17.7 nN, suggesting that different quantities of nanowires were detaching at each occasion. Based on these considerations, only nanowire trials with trigger points above 15 nN were used to calculate the data presented in this paper.

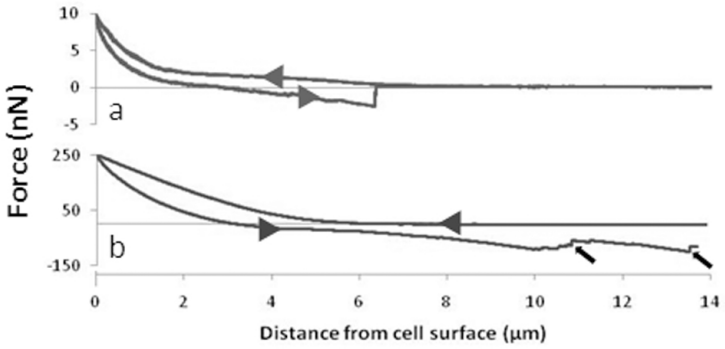

Figure 43: Single event AFM adhesion force curves

Chapter 5: Loading and elution

Controlled pore glass

Devices were loaded with trypan blue, bovine serum albumin (BSA), insulin, and immunoglobulin G (IgG) using an evaporation technique allowing surface tension and capillary action to draw drug into the pores between nanowires and/or onto the surface of the devices. A washing step was necessary in order to remove debris and drug not incorporated into the devices. Devices were imaged prior to elution experiments to determine the distribution of drug within the nanowires or on the surface (Figure 44a and b). At this stage, the nanowire-coated devices demonstrated minimal matting of the nanowires enmeshed in crystals.

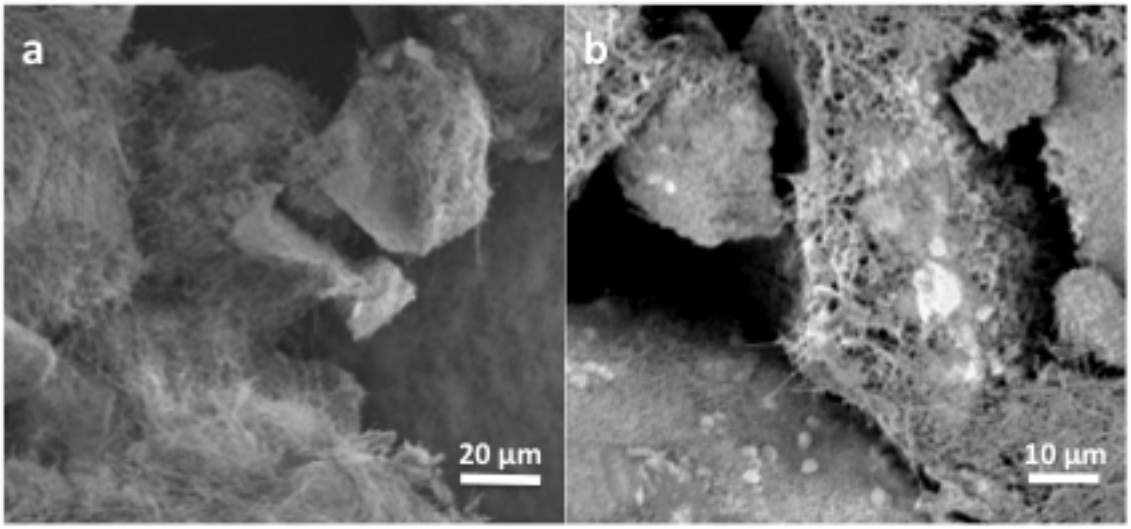

Figure 44: Loading of CPG particles - stock (a) and loaded (b)

Loaded CPG particles were then placed in solution and elution was measured over 120 minutes. The model molecules can be classified into different groups based on their elution characteristics. Larger molecules, including insulin and IgG, tended to have two phases of elution: an initial burst release of molecules very close to the surface and a longer term release as molecules captured at the base of the nanowires or in the pores elute (Figure 45 shows a typical curve for insulin - unmodified (gray) and nanowire-modified (black)). Smaller molecules like trypan blue showed a burst release. BSA was mainly characterized by a burst release with a very small secondary, long-term release. Overall, the amount of drug eluted from nanowire-coated particles (µg protein/ml solution/µl CPG) was greater for each molecule (Figure 45b- unmodified (gray) and nanowire-modified (black)). This finding, along with the two-step shape of the elution curves, suggests that the nanowires add an additional reservoir for drug, presumably at the base of the nanowires.

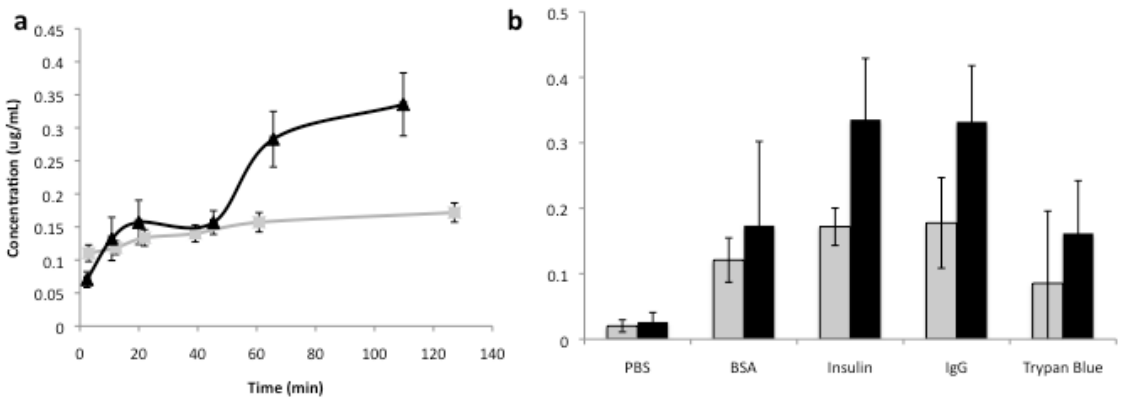

Figure 45: Elution profile for insulin in controlled pore glass particles (a) and total concentration of molecules eluted at 120 minutes (b)

Nanowires only

To test this hypothesis, microspheres without pores were loaded with BSA (Figure 46a – no nanowires - square, short nanowires - diamond, and long nanowires - triangle). Microspheres with longer nanowires held more drug than those with short or no nanowires. This suggests that longer nanowires create a larger reservoir at their base. Although the CPG particles could load some BSA even without nanowires (Figure 46b– nanowire-coated – black, uncoated - white), the nanowires significantly increase the loading capacity of the CPG. Furthermore, the lack of pores in the microspheres did not decrease loading in nanowire-coated devices, confirming that the nanowire are responsible for an additional drug reservoir.

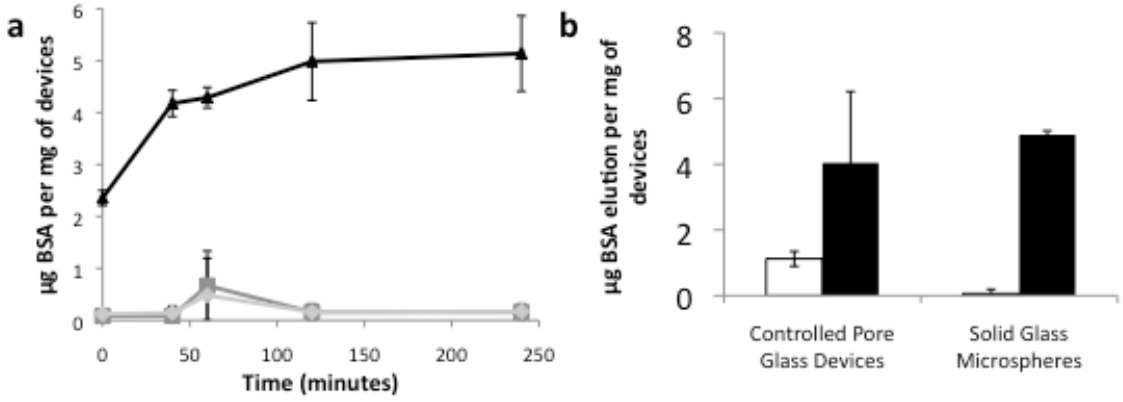

Figure 46: Elution from nanowire-coated spheres

Nanowire-coated microspheres were loaded at various concentrations of BSA to determine a maximum effective loading capacity (Figure 47- 10 mg/ml – circle, 50 mg/ml – diamond, 100 mg/ml – square). Although the nanowires are visible and mainly uncoated at 1 and 10 mg/ml, at 50 and 100 mg/ml loading solutions the wires become more matted, indicating saturation. When loaded devices are incubated in PBS, the spheres loaded with higher concentrations (50 and 100 mg/ml) elute roughly the same amount of BSA, significantly more than that eluted from the 10 mg/ml spheres. Thus, increasing loading

solution concentration increases the amount of drug loaded into the nanowire reservoir, though it saturates around 50 mg/ml.

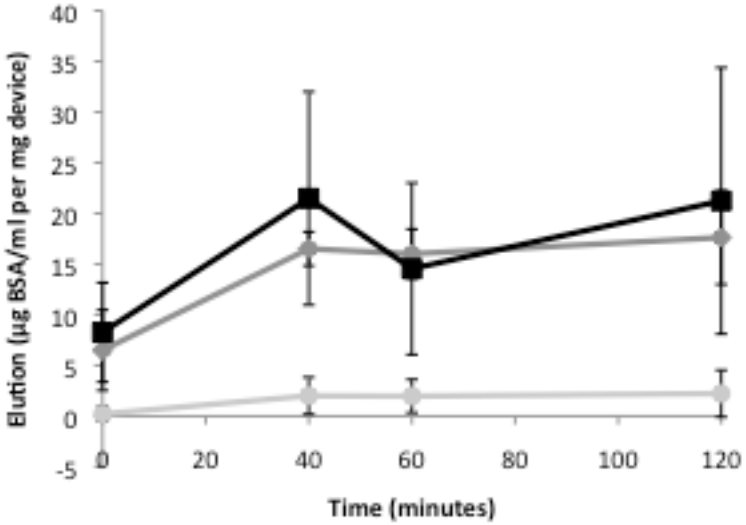

Figure 47: Elution from spheres with various loading concentrations

During loading, capillary forces pull molecules into the base of the nanowires similar to how drugs are loaded into nanotubes or pores[24,94,95,96]. Using this approach, therapeutics may be loaded into a reservoir formed by the base of the nanowires, leaving the exterior portion of the nanowires free to adhere to cells.

Adhesion after Loading

Because loading drug molecules into the nanowire reservoir could mask nanowires from cells, thereby reducing adhesion, the loaded devices were tested for adhesion strength under shear. Devices were introduced to cells in a mucous layer model (2% mucin), then subjected to increasing flow rates.

Loaded, nanowire-coated, CPG particles adhered significantly better than loaded, uncoated CPG particles (Figure 48a- nanowire-coated – gray square, uncoated control – black diamond). Nearly 60% of nanowire-coated CPG were retained at 167 dynes/cm^2. The CPG particles are non-spherical, so the orientation of the longer sides to the surface will reduce the particle flow profile[24,25]; a low shear helps particles situate optimally, increasing the surface area of devices in contact with cells, as is observed up to 16.7 dynes/cm^2 in this case.

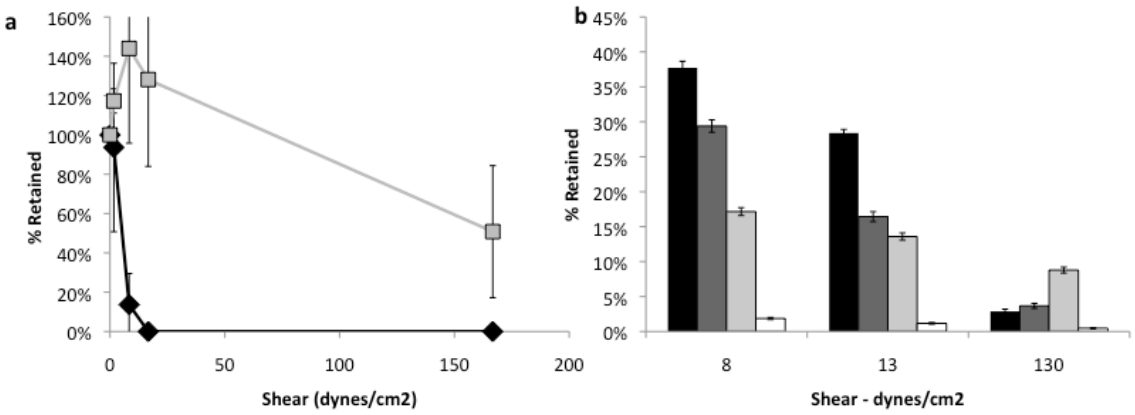

Figure 48: Adhesion of loaded particles

The levels of loading also affected adhesion (Figure 48b- unloaded – black, 10 mg/ml – dark gray, 50 mg/ml – light gray, 100 mg/ml – white), reducing adhesion significantly at physiological shears (up to 15 dynes/cm^2). A general trend confirmed that particles that were loaded in more concentrated solutions, leading to more matted and masked nanowires, did not adhere as well as those with less drug loading. Thus, there is a tradeoff between loading capacity and adhesive effects when the nanowires are used as a loading reservoir.

Chapter 6: In vivo imaging

Gastroretention Studies

A,b) Arrow indicates particles in stomach. c) small arrow indicates particles in proximal small intestine, large arrow indicates particles in distal small intestine. D,e) Arrow indicates particles in large intestine. f) corresponding position of uncoated, stainless steel particles at 15 minutes. Arrow indicates particles in distal small intestine.

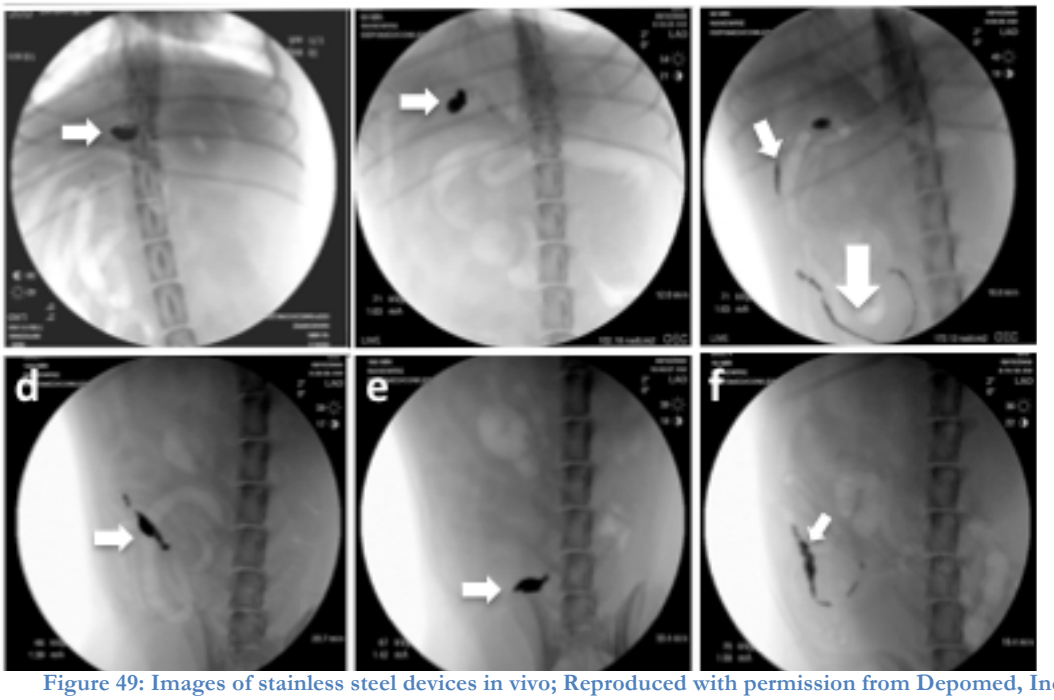

Figure 49: Images of stainless steel devices in vivo; Reproduced with permission from Depomed, Inc.

To determine the effectiveness of nanowire-mediated adhesion *in vivo*, we used a fluoroscope to track the stainless steel NEMPs and unmodified stainless steel microparticles (MPs). Devices were placed inside of a gelatin capsule (Capsugel, Peapack, NJ) and given to fasted, female beagles (for NEMPs: n=2 for 200-300 μm, n=1 for 500 μm, and n=1 for 1000 μm; for 200 μm MPs, n=1). The dogs were imaged at 30 minute intervals (Figure 49). The gelatin capsules dissolve in less than 10 minutes, so the initial imaging at 15 minutes mainly showed a distribution of devices in the stomach. Almost immediately, unmodified MPs were seen to transit into the intestine (Figure 50, C_d – distal colon; C_p – proximal colon; SI_d – distal small intestine; SI_p – proximal small intestine; D – duodenum; S – stomach). In contrast, 200-300 μm NEMPs were retained in the stomach up through 120 minutes, and slowly spread to the duodenum and upper small intestine. By 180 minutes, the NEMPs had accumulated mainly in the large intestine. Larger NEMPs of 500 and 1000 μm transited more quickly. Thus, in 200-300 μm NEMPs, the nanowire coatings alone were responsible for a significant increase in gastrointestinal adhesion over uncoated devices, increasing the

time that devices stayed in contact with the stomach by up to ten times.

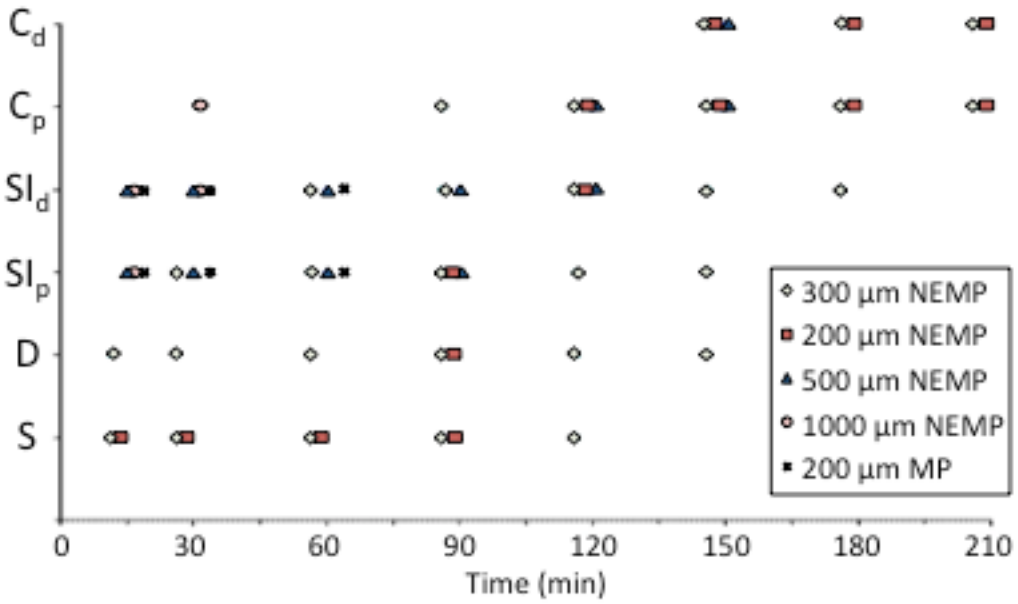

Figure 50: Transit of devices in vivo; Reproduced with permission from Depomed, Inc.

Expected Variation in Stomach Expulsion

During the fasted state, phase III of the migrating motor complex (MMC) cycle, which are the strongest contractions to occur in the normal physiological state and induce the greatest stomach and small intestine emptying rates (50% of total intestinal flow in the fasted state), occurs during a 10-20 minute segment in the stomach and doudenum out of every 80-100 minute cycle [97,98,99]. Additional transit occurs during phase II (the 20-30 minute segment preceding phase III), though these contractions are of smaller magnitude and may be propagated bidirectionally or be non-propagating. The remainder of the time is spent in phase I, a quiescent time during which minimal transit occurs. The introduction of the gelatin capsule and devices is not expected to trigger the fed state, so devices are expected to be in transit at least 30–50 minutes out of every 80-100 minute cycle. Because data is taken in real time, contraction may be assessed visually (phases II and III). In the dogs dosed with 300 µm NEMPs, 1000 µm NEMPs, and 200 µm MPs, contractions were indicated by moving particles during the first imaging timepoint after 15 minutes (supplementary videos of Dogs 1, 5, and 4, respectively). The dog dosed with 200 µm NEMPs did not show contractions until 45 to 60 minutes. Thus, based on the contraction stages, we can assume an offset of approximately 30-60 minutes, indicating that the observed difference in residence times (between 150 and 210 minutes) does in fact correlate to a roughly 10-fold increase due to nanowires.

Chapter 7: Cell response and remodeling

Confocal actin restructuring

To determine the extent of cytoskeletal involvement with nanowire adhesion, cells were incubated for two hours with cytochalasin D, a fungal mycotoxin which transiently prevents actin polymerization in Caco-2 cells (see Chapter 4)[88,89]. To resolve the nature of cytoskeletal changes underneath the NEMPs and MPs, confocal images were taken and reconstructed to view the x-z plane. Cytochalasin D-treated cells deformed under devices regardless of nanowires, suggesting a passive, weight-related deformation process (Figure 51a and c, scale bars are 5 μm). Control cells showed actin at their apical surface and only deformed under the influence of NEMPs, suggesting an active, actin-related deformation (Figure 51b and d, scale bars are 5 μm). Overall, deformation of cells increased the surface area in contact with devices, and if the devices had nanowires, this deformation increased adhesion.

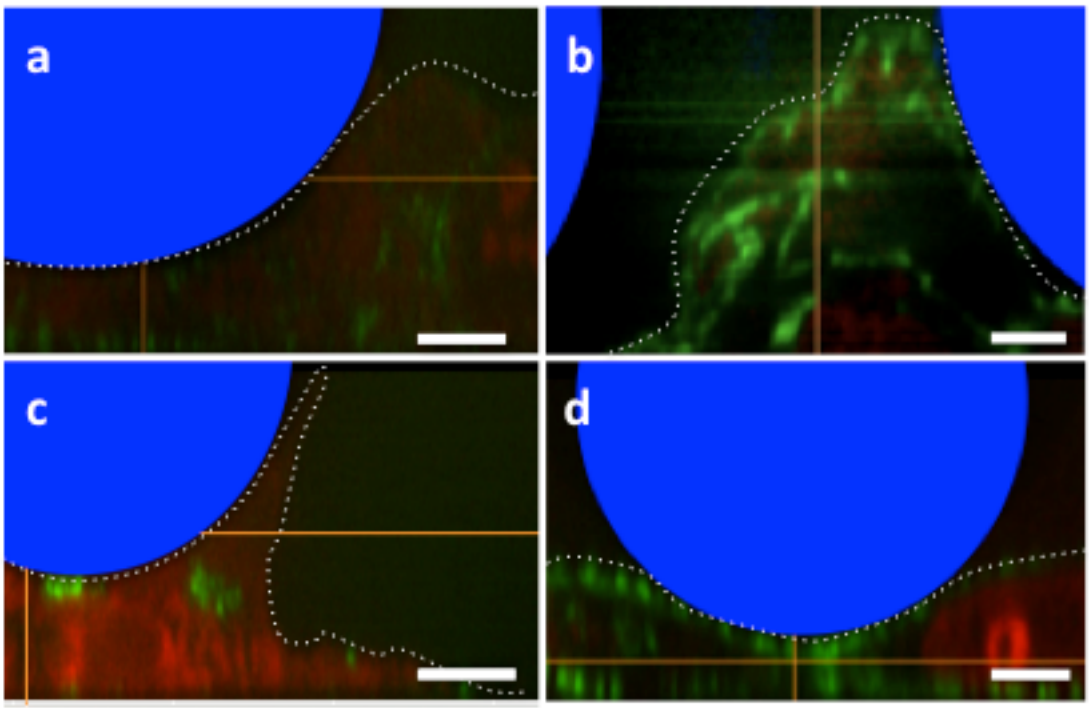

Figure 51: Confocal images of cytoskeletal response to microparticles

Internalization

Particle internalization is another major active cell process that affects nano-scale cytoadhesion, suggesting that it may play a role in mediating nanowire adhesion. To determine if the nanowires were being internalized, cells were exposed to FITC-modified devices for 30 minutes then imaged prior to and after fluorescence quenching by Trypan Blue (Figure 52). Because minimal fluorescence is observed after the quench, and Trypan

Blue does not enter healthy cells, it is clear that the nanowires are not being internalized. One additional possibility is that the nanowires are puncturing the cells, and thus Trypan Blue can enter these cells. However, brightfield imaging indicates that the cells themselves do not show Trypan Blue internalization.

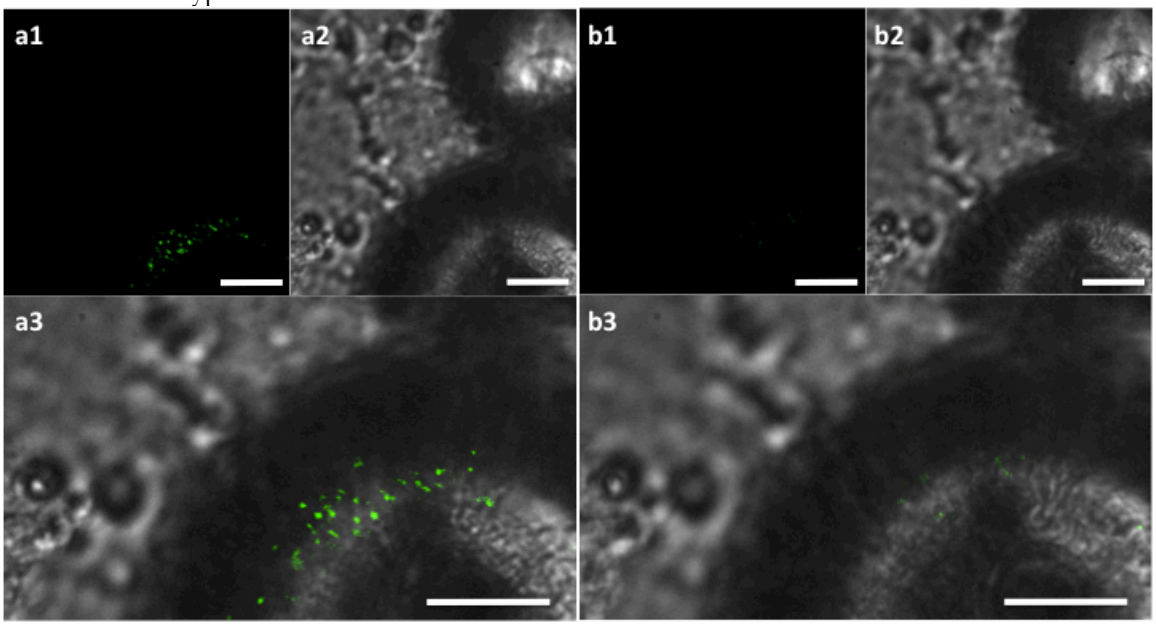

Figure 52: Particle internalization experiment images

Toxicity

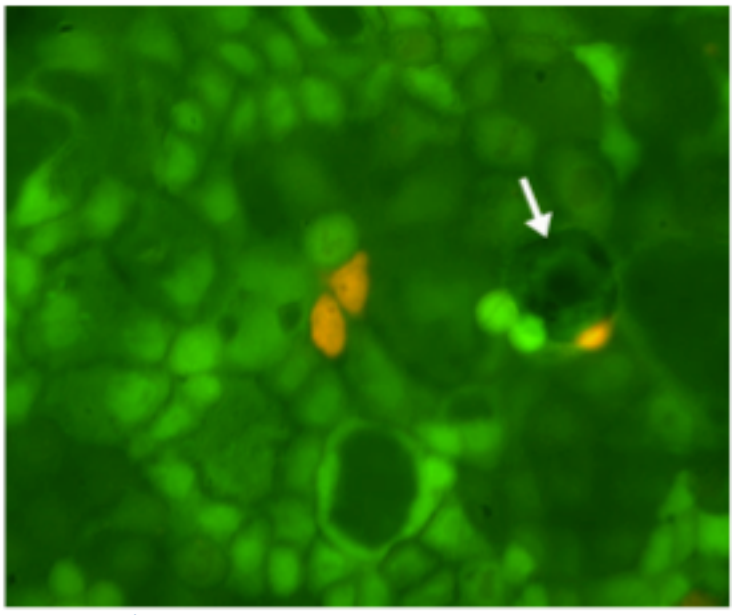

Figure 53: Live/Dead stain of cells after exposure to nanowire-coated devices

Both trypan blue and fluorescent staining indicated that the nanowire-coated microspheres have negligible deleterious effects on surrounding cells compared to

microspheres without nanowire coatings (Figure 53, arrow indicates a nanowire-coated microsphere; green stain – live cells, red stain - dead). The nanowire-coated microspheres performed similarly to the uncoated microspheres and the controls, indicating negligible toxicity as indicated by MTT assay (Figure 54; relative absorbance indicates level of mitochondrial activity). Cell toxicity studies were continued to 120 hours, with cell viability remaining above 97%.

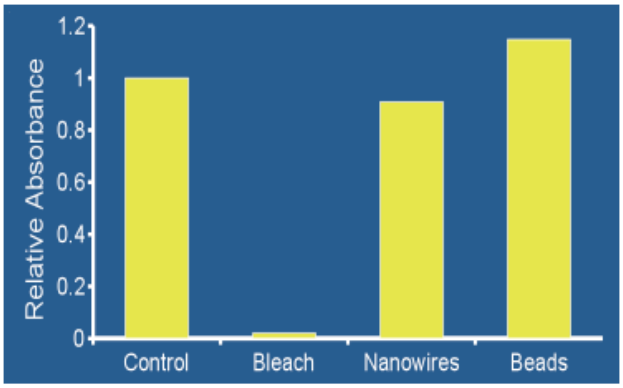

Figure 54: MTT assay after 2 hour incubation with devices

Chapter 8: Conclusions and Future Studies

Summary and Conclusions

The development of robust, conformal, and repeatable nanowire manufacturing processes has allowed study of the interaction of nanoengineered microparticles with the gastrointestinal mucosa. By using a vapor-liquid-solid technique, these nanowires may be grown on numerous different surfaces, such as silicon, glass, porous glass, and stainless steel. Because the nanowires are silicon, they may be chemically modified with a wide variety of proteins, fluorophores, and other molecules using well-established silane chemistry techniques. Furthermore, multiple regions, as defined by the silicon nanowire and the gold catalyst, are inherent in the growth technique and may be used to add spatially separate functionalities.

When tested for stability, nanowires perform well even in highly acidic conditions and can survive at least one week without disintegration in physiological solutions. Thus, nanowires are robust enough to undergo extensive surface chemical modification, but will not persist chronically in vivo even if they detach from microparticles.

Nanowire-coated microspheres interact with gastrointestinal cells at the nanoscale, interdigitating with surface microvilli. This increased surface area of contact produces substantial adhesive interactions that persist even after exposure to myriad harsh conditions which may be found in the gastrointestinal tract. Strong adhesion continues up to shears of 170 dynes/cm^2 (well into the disease state for the small intestines), and nanowires improve tensile adhesion at least 1000-fold over unmodified glass microspheres. Furthermore, particularly when exposed to a model mucus layer, nanowire-coated microspheres adhere to underlying cells better than comparable cytoadhesives. Nanowire coatings significantly improve adhesion to several different cell types, even those with minimal surface micro- and nanostructures, and continue to adhere to gastrointestinal cells even without microvilli or a functional cytoskeleton.

Shear flow studies suggest that several geometric aspects are most important to adhesion. On the microscale, tensile adhesion scales with the surface area of a device covered by nanowires. On the nanoscale, longer wires improve performance at least ten-fold over shorter wires (as measured by median survival shear), indicating a surface area-related adhesion phenomenon. Furthermore, positively charged surface modifications increase adhesion by more than five-fold over negatively charged surfaces. Modification with polyethylene glycol (PEG) reduces nanowire adhesion to that of flat controls, suggesting that charge (hydrophilicity) and the ensuing protein adsorption is critical to adhesion[100,101,102,103]. Although surface chemistry affects adhesion, the ability to adhere strongly at the macroscale is primarily produced by the increase in surface area due to the nanoengineered surface.

In addition to producing an adhesive force, the nanowires may be utilized as a drug-loading reservoir. Because long nanowires form a physically protected barrier against disruption at the surface of the underlying particle, medium to large molecules, such as insulin and immunoglobin G may be loaded and crystallized at the base of the nanowires. Ultimately, adhesion is sacrificed for loading capacity beyond a certain loading volume, but longer nanowires can improve both. Furthermore, loading into controlled pore glass devices (pores around 200 nm) instead of solid microspheres improves adhesion of loaded particles. Nonetheless, the loading volume of the nanowire reservoir is minimal in comparison to

other potential reservoirs, such as the interior of a hollow glass microsphere or a porous micropatch. Thus, while the nanowire reservoir provides a convenient proof of concept, ultimately, it is not likely to carry a high enough volume for therapeutic purposes.

Two separate in vivo models validate the in vitro shear flow test results. In beagles, nanowire coatings increase the gastric retention at least ten-fold. In mice, nanowire coated devices are still primarily in the stomach at five hours. Additionally, these studies were completed using microparticles of different materials, weights, and volumes, indicating the flexibility of nanowire-based adhesion onto a variety of biocompatible drug delivery devices.

In addition to the surface area-induced adhesion, longer term cell remodeling may be induced. After a 1-2 hours, actin restructuring is visible underneath and around nanowire-coated microspheres. However, internalization of the microsphere-bound nanowires does not take place. Overall, nanowires induce negligible toxic cellular responses, equivalent to those of the control up to at least 72 hours. In combination with previous research indicating a lack of inflammatory response[60], this lack of toxicity suggests that the nanowires are biocompatible and safe for use.

Goals for Oral Delivery

Nanowire coating success	Type	Objective
With enteric coating	Intestinal Location:	Duodenum
Yes	Protection:	Reduce enzymatic and pH degradation
Yes	Absorption:	Increase residence time (eg: increase device retention on or in cells)
Yes	Concentration gradient:	Increase in close proximity to cells
With appropriate microparticles	Volume:	Loading capacity high enough to obtain therapeutic efficacy in 1-3 pills (up to about 4.5 mL[21]) per day
Yes	Efficacy:	Demonstrated in vivo
Yes	Toxicity:	Nontoxic and noninflammatory

How do nanowires compare to the specified goals for oral drug delivery? Nanowires significantly increase residence time, even compared to well-studied cytoadhesives. Furthermore, they anchor microparticles in close proximity to cells, improving the concentration gradient at the cell surface. Because the nanowires are attached to microparticles, they can protect macromolecules from degradation, and potentially hold enough drug to be therapeutically viable. Held in an enteric capsule, they may be released directly into the small intestine, where they will adhere immediately, or they may be dosed into the stomach for gastric delivery, as demonstrated in vivo. Lastly, the nanowire coatings have been demonstrated to be nontoxic and non-inflammatory, and will degrade in a matter of weeks if accidentally ingested, preventing systemic accumulation. Thus, with addition to previously proven technologies, nanowire coatings have the potential to solve some of the

most difficult challenges in oral drug delivery by integrating the size and diffusive properties of the nanoscale with the loading capacity and biocompatibility of the microscale.

Future Studies

Because of their promise for improving oral drug delivery, nanowire research should proceed in several directions. To improve loading, nanowires should be grown on flat devices with appropriate reservoirs or onto devices with a hollow core. Flat micropatches offer improved shear resistance and greater surface area coverage, similar to that of the controlled pore glass devices. Alternately, polymer nanowires may provide similar surface area-related adhesive effects, allowing integration of the reservoir into the nanowires themselves and/or additional flexibility in device design.

Additional in vivo studies should consider pharmacokinetic and pharmacodynamic properties of several drugs when loaded into nanowire-coated devices. Also, the long-term inflammatory response to these devices must be investigated if they are to be used for chronic oral drug delivery. Further in vitro study on intracellular pathways and remodeling dynamics would be helpful in elucidating cellular responses to nanowires and highlighting the effects of nanoscale interactions for additional therapeutic purposes.

Additionally, nanowire coatings may be useful for delivering drugs to other mucosal surfaces, such as nasal, buccal, oral, ocular, and vaginal tissue. Because nanowires adhere strongly to numerous tissue types and are robust under many conditions, they may prove useful for biodegradable adhesive coatings for medical implants or tissue regeneration as well as drug delivery.

Nanowire coatings and nanoengineered surfaces provide a novel interface for interacting with cells at a previously unimaginable scale. Because of the ability to precisely engineer structures at this scale, we can now utilize geometric characteristics to influence many different aspects of bio-material interactions, from adhesion to cellular remodeling, with implications in myriad fields of science and medicine.

References

[1] Mendelsohn, A. D. *Static Adhesion of Nanowire-coated Devices - Unpublished Work* (2006).

[2] World Oral Drug Delivery Markets. (Kalorama Information, New York, 2009).

[3] in *Encyclopedia Britannica Online* (2010).

[4] Lee, J. W., Park, J. H. & Robinson, J. R. Bioadhesive-based dosage forms: The next generation. *J. Pharm. Sci.* **89**, 850 (2000).

[5] Freitas, R. A. in *Nanomedicine, Volume I: Basic Capabilities* Vol. 1 (Landes Bioscience, 1999).

[6] Freitas, R. A. in *Nanomedicine, Volume I: Basic Capabilities* Vol. 1 (Landes Bioscience, 1999).

[7] Smart, J. D. The basics and underlying mechanisms of mucoadhesion. *Adv. Drug Delivery Rev.* **57**, 1556 (2005).

[8] Degen, L. P. & Phillips, S. F. Variability of gastrointestinal transit in healthy women and men. *Gut*, 299-305 (1996).

[9] Camilleri, M. *et al.* Human gastric emptying and colonic filling of solids characterized by a new method. *AJP - Gastrointestinal and Liver Physiology* **257**, G284-290 (1989).

[10] Lehr, C. M. An estimate of turnover time of intestinal mucus gel layer in the rat in situ loop. *Int. J. Pharm.* **70**, 235 (1991).

[11] Brannon-Peppas, L. & Blanchette, J. O. Nanoparticle and targeted systems for cancer therapy. *Adv. Drug Delivery Rev.* **56**, 1649 (2004).

[12] Peppas, N. A. & Huang, Y. Nanoscale technology of mucoadhesive interactions. *Adv. Drug Delivery Rev.* **56**, 1675-1687 (2004).

[13] Cone, R. A. Barrier properties of mucus. *Advanced Drug Delivery Reviews* **61**, 75-85 (2009).

[14] Olmsted, S. S. *et al.* Diffusion of Macromolecules and Virus-Like Particles in Human Cervical Mucus. *Biophysical Journal* **81**, 1930-1937 (2001).

[15] Bhat, P. G., Flanagan, D. R. & Donovan, M. D. The limiting role of mucus in drug absorption: Drug permeation through mucus solution. *International Journal of Pharmaceutics* **126**, 179-187 (1995).

[16] Lai, S. K., Wang, Y.-Y. & Hanes, J. Mucus-penetrating nanoparticles for drug and gene delivery to mucosal tissues. *Advanced Drug Delivery Reviews* **61**, 158-171 (2009).

[17] Silverthorn, D. U. *Human Physiology: An Integrated Approach*. 2nd edn, (Benjamin-Cummings Publishing Company, 2000).

[18] Stevens, C. E. & Leblond, C. P. Renewal of the Mucous Cells in the gastric Mucosa of the Rat. *The Anatomical Record* **115**, 231-245 (1953).

[19] Riley, S. A. & Turnberg, L. A. in *Handbook of physiology* (ed D. Green) 977-1008 (Oxford Press, 1985).

[20] Madara, J. L. in *Handbook of physiology* (ed D. Green) 977-1008 (Oxford Press, 1985).

[21] Torpac. in http://www.erowid.org/archive/rhodium/pdf/gelcap.sizechart.pdf (ed Torpac Inc.) (2000).
[22] Eaimtrakarn, S. *et al.* Possibility of a patch system as a new oral delivery system. *International Journal of Pharmaceutics* **250**, 111-117 (2003).
[23] Foraker, A. B. *et al.* Microfabricated porous silicon particles enhance paracellular delivery of insulin across intestinal Caco-2 cell monolayers. *Pharm Res* **20**, 110-116 (2003).
[24] Tao, S. L. & Desai, T. A. Gastrointestinal patch systems for oral drug delivery. *Drug Discovery Today* **10**, 909-915 (2005).
[25] Tao, S. L. *Off-wafer fabrication of asymmetric, polymeric gastrointestinal micropatch systems: Characterization of caco-2 monolayer binding and compatibility* Ph.D. thesis, Boston University, (2006).
[26] Tao, S. L., Popat, K. C., Norman, J. J. & Desai, T. A. Surface modification of SU-8 for enhanced biofunctionality and nonfouling properties. *Langmuir* **24**, 2631-2636, doi:10.1021/la703066z (2008).
[27] Kumar, V. & Prud'homme, R. K. Thermodynamic limits on drug loading in nanoparticle cores. *Journal of Pharmaceutical Sciences* **97**, 4904-4914 (2008).
[28] Freitas, S., Merkle, H. P. & Gander, B. Microencapsulation by solvent extraction/evaporation: reviewing the state of the art of microsphere preparation process technology. *Journal of Controlled Release* **102**, 313-332 (2005).
[29] Teeguarden, J. G., Hinderliter, P. M., Orr, G., Thrall, B. D. & Pounds, J. G. Particokinetics In Vitro: Dosimetry Considerations for In Vitro Nanoparticle Toxicity Assessments. *Toxicological Sciences* **95**, 300-312 (2007).
[30] Sanvicens, N. & Marco, M. P. Multifunctional nanoparticles - properties and prospects for their use in human medicine. *Trends in Biotechnology* **26**, 425-433 (2008).
[31] Cheng, H. & Bjerknes, M. Cell production in mouse intestinal epithelium measured by stathmokinetic flow cytometry and coulter particle counting. *Anat. Rec.* **207**, 427 (1995).
[32] Naisbett, B. & Woodley, J. The Potential Use Of Tomato Lectin For Oral-Drug Delivery.3. Bioadhesion In-Vivo. *Int. J. Pharm.* **114**, 227 (1995).
[33] Bies, C., Lehr, C.-M. & Woodley, J. F. Lectin-mediated drug targeting: history and applications. *Adv. Drug Delivery Rev.* **56**, 425 (2004).
[34] Arzt, E., Gorb, S. & Spolenak, R. From micro to nano contacts in biological attachment devices. *Proceedings of the National Academy of Sciences of the United States of America* **100**, 10603-10606 (2003).
[35] Sun, W., Neuzil, P., Kustandi, T. S., Oh, S. & Samper, V. D. The nature of the gecko lizard adhesive force. *Biophys. J.* **89**, L14 (2005).
[36] Autumn, K. Evidence for van der Waals adhesion in gecko setae. *Proc. Nat. Acad. Sci. U.S.A.* **99**, 12252 (2002).
[37] Autumn, K. Adhesive force of a single gecko foot-hair. *Nature* **405**, 681 (2000).
[38] Huber, G. Resolving the nanoscale adhesion of individual gecko spatula by atomic force microscopy. *Biol. Lett.* **1**, 2 (2005).
[39] Lee, J., Majidi, C., Schubert, B. & Fearing, R. S. Sliding induced adhesion of stiff polymer microfiber arrays: 1. Macroscale behavior. *J. R. Soc. Interface* **5**, 835 (2008).

[40] Kim, S. & Sitti, M. Biologically inspired polymer microfibers with spatulate tips as repeatable fibrillar adhesives. *Appl. Phys. Lett.* **89**, 26911 (2006).
[41] Yurdumakan, B., Raravikar, N. R., Ajayan, P. M. & Dhinojwala, A. Synthetic gecko foot-hairs from multiwalled carbon nanotubes. *Chem. Commun.*, 3799 (2005).
[42] Campo, A. d. & Arzt, E. Design parameters and current fabrication approaches for developing bioinspired dry adhesives. *Macromo. Biosci.* **7**, 118 (2007).
[43] Peressadko, A. & Gorb, S. N. When less is more: Experimental evidence for tenacity enhancement by division of contact area. *J. Adhes.* **80**, 247 (2004).
[44] Lee, H., Lee, B. P. & Messersmith, P. B. A reversible wet/dry adhesive inspired by mussels and geckos. *Nature* **448**, 338 (2007).
[45] Mahdavi, A. A biodegradable and biocompatible gecko-inspired tissue adhesive. *Proc. Nat. Acad. Sci. U.S.A.* **105**, 2307 (2008).
[46] Spolenak, R., Gorb, S. & Arzt, E. Adhesion design maps for bio-inspired attachment systems. *Acta Biomater.* **1**, 5 (2005).
[47] Spolenak, R., Gorb, S., Gao, H. J. & Arzt, E. Effects of contact shape on the scaling of biological attachments. *Proc. R. Soc. London, Ser. A.* **461**, 305 (2005).
[48] Mygind, N. & Dahl, R. Anatomy, physiology, and function of the nasal cavities in health and disease. *Adv. Drug Delivery Rev.* **29**, 3 (1998).
[49] Alberts, B. *et al. Molecular Biology of the Cell*. 4th edn, (Garland Science, 2002).
[50] Tortora, G. J. & Anagnostakos, N. P. *Principles of Anatomy and Physiology*. 44 (Canfield Press, 1975).
[51] DeSesso, J. M. & Williams, A. L. Chapter 21 Contrasting the Gastrointestinal Tracts of Mammals: Factors that Influence Absorption. *Annu. Rep. Med. Chem.*. **43**, 353 (2008).
[52] Fischer, K. E. *et al.* Biomimetic Nanowire Coatings for Next Generation Adhesive Drug Delivery Systems. *Nano Letters* **9**, 716-720 (2009).
[53] Fischer, K. E., Bunger, M. D., Daniels, R. H., Li, E. M. & Desai, T. A. Nanowires for Improved Tissue Adhesion and Cellular Remodeling. *Proceedings of the 2009 Controlled Release Society Meeting* (2009).
[54] Fischer, K. E. *et al.* Silicon Nanowires for Improved Intestinal Bioadhesion. *Proceedings of the 2007 Controlled Release Society Meeting* (2007).
[55] Fischer, K. E., Tao, S., Daniels, H., Li, E. & Desai, T. in *Electron Devices Meeting, 2008. IEDM 2008. IEEE International.* 1-4.
[56] Fischer, K. E. *et al.* Loading and Elution of Cytoadhesive Nanoengineered Microdevices. *In preparation* (2010).
[57] Fischer, K. E. *et al.* Hierarchical Nanoengineered Surfaces for Enhanced Cytoadhesion and Drug Delivery. *Submitted to PNAS* (2010).
[58] Fischer, K. *et al.* in *First Global Congress of NanoEngineering for Medicine and Biology.* (ASME).
[59] Ainslie, K. M., Tao, S. L., Popat, K. C. & Desai, T. A. In vitro Immunogenicity of Silicon-Based Micro- and Nanostructured Surfaces. *ACS Nano* **2**, 1076-1084 (2008).
[60] Ainslie, K. M. *et al.* In vitro inflammatory response of nanostructured titania, silicon oxide, and polycaprolactone. *J. Biomed. Mater. Res. A* (2008).

[61] Cui, Y., Lauhon, L. J., Gudiksen, M. S., Wang, J. F. & Lieber, C. M. Diameter-controlled synthesis of single-crystal silicon nanowires. *Appl. Phys. Lett.* **78**, 2214 (2001).

[62] Duan, X. F. & Lieber, C. M. General synthesis of compound semiconductor nanowires. *Adv. Mater.* **12**, 298 (2000).

[63] Sultzbaugh, K. J. & Speaker, T. J. A method to attach lectins to the surface of spermine alginate microcapsules based on the avidin biotin interaction. *J. Microencapsulation* **13**, 363 (1996).

[64] Papra, A., Gadegaard, N. & Larsen, N. B. Characterization of Ultrathin Poly(ethylene glycol) Monolayers on Silicon Substrates. *Langmuir* **17**, 1457-1460, doi:10.1021/la000609d (2001).

[65] Pinto, M. *et al.* Enterocyte-Like Differentiation and Polarization of the Human-Colon Carcinoma Cell-Line Caco-2 in Culture. *Biol. Cell* **47**, 323 (1983).

[66] Artursson, P., Palm, K. & Luthman, K. Caco-2 monolayers in experimental and theoretical predictions of drug transport. *AdV. Drug DeliVery Rev.* **46**, 27-43 (2001).

[67] Hidalgo, I. J., Raub, T. J. & Borchardt, R. T. Characterization of the human colon carcinoma cell line (Caco-2) as a model system for intestinal epithelial permeability. *Gastroenterology* **96**, 736-749 (1989).

[68] Artursson, P. & Karlsson, J. Correlation between oral drug absorption in humans and apparent drug permeability coefficients in human intestinal epithelial (Caco-2) cells. *Biochemical and Biophysical Research Communications* **175**, 880-885 (1991).

[69] Butt, H. J. & Jaschke, M. Calculation Of Thermal Noise In Atomic-Force Microscopy. *Nanotechnology* **6**, 1 (1995).

[70] Hutter, J. L. & Bechhoefer, J. Calibration Of Atomic-Force Microscope Tips. *Rev. Sci. Instrum.* **64**, 1868 (1993).

[71] Salapaka, M. V., Bergh, H. S., Lai, J., Majumdar, A. & McFarland, E. Multi-mode noise analysis of cantilevers for scanning probe microscopy. *J. App. Phys.* **81**, 2480 (1997).

[72] Kappl, M. & Butt, H. J. The colloidal probe technique and its application to adhesion force measurements. *Part. Part. Syst. Charact.* **19**, 129 (2002).

[73] Sader, J. E., Larson, I., Mulvaney, P. & White, L. R. Method For The Calibration Of Atomic-Force Microscope Cantilevers. *Rev. Sci. Instrum.* **66**, 3789 (1995).

[74] Cleveland, J. P., Manne, S., Bocek, D. & Hansma, P. K. A Nondestructive Method For Determining The Spring Constant Of Cantilevers For Scanning Force Microscopy. *Rev. Sci. Instrum.* **64**, 403 (1993).

[75] Proksch, R., Schaffer, T. E., Cleveland, J. P., Callahan, R. C. & Viani, M. B. Finite optical spot size and position corrections in thermal spring constant calibration. *Nanotechnology* **15**, 1344 (2004).

[76] Kilpatrick, D. C., Pusztai, A., Grant, G., Graham, C. & Ewen, S. W. B. Tomato Lectin Resists Digestion In The Mammalian Alimentary Canal And Binds To Intestinal Villi Without Deleterious Effects. *FEBS Lett.* **185**, 299 (1985).

[77] Lehr, C. M. Bioadhesion By Means Of Specific Binding Of Tomato Lectin. *Pharm. Res.* **9**, 547 (1992).

[78] Gabor, F. & Wirth, M. Lectin-mediated drug delivery: fundamentals and perspectives. *STP Pharma. Sci.* **13**, 3 (2003).
[79] Werner, U. & Kissel, T. In-vitro Cell Culture Models of the Nasal Epithelium: A Comparative Histochemical Investigation of Their Suitability for Drug Transport Studies. *Pharmaceutical Research* **13**, 978-988 (1996).
[80] Gospodarowicz, D., Moran, J., Braun, D. & Birdwell, C. Clonal growth of bovine vascular endothelial cells: fibroblast growth factor as a survival agent. *Proceedings of the National Academy of Sciences of the United States of America* **73**, 4120-4124 (1976).
[81] Autumn, K., Dittmore, A., Santos, D., Spenko, M. & Cutkosky, M. Frictional adhesion: a new angle on gecko attachment. *J. Exp. Biol.* **209**, 3569 (2006).
[82] Gratton, S. E. A. *et al.* The effect of particle design on cellular internalization pathways. *Proceedings of the National Academy of Sciences* **105**, 11613-11618, doi:10.1073/pnas.0801763105 (2008).
[83] Champion, J. & Mitragotri, S. Shape Induced Inhibition of Phagocytosis of Polymer Particles. *Pharmaceutical Research* **26**, 244-249 (2009).
[84] Li, S.-D. & Huang, L. Pharmacokinetics and Biodistribution of Nanoparticles. *Molecular Pharmaceutics* **5**, 496-504 (2008).
[85] Verma, A. & Stellacci, F. Effect of Surface Properties on Nanoparticle-Cell Interactions. *Small* **6**, 12-21.
[86] Weinbaum, S., Guo, P. & You, L. A new view of mechanotransduction and strain amplification in cells with microvilli and cell processes. *Biorheology* **38**, 119-142 (2001).
[87] Gorelik, J. *et al.* Dynamic assembly of surface structures in living cells. *Proceedings of the National Academy of Sciences of the United States of America* **100**, 5819-5822, doi:10.1073/pnas.1030502100 (2003).
[88] Sampath, P. & Pollard, T. D. Effects of cytochalasin, phalloidin and pH on the elongation of actin filaments. *Biochemistry* **30**, 1973-1980 (2002).
[89] Fu, Y.-Y., Sibley, E. & Tang, S.-C. Transient cytochalasin-D treatment induces apically administered rAAV2 across tight junctions for transduction of enterocytes. *J Gen Virol* **89**, 3004-3008, doi:10.1099/vir.0.2008/001446-0 (2008).
[90] Jensen, K., Mickelson, W., Kis, A. & Zettl, A. Buckling and kinking force measurements on individual multiwalled carbon nanotubes. *Phys. Rev. B: Condens. Matter* **76** (2007).
[91] Timoshenko, S. & Gere, J. *Theory of Elastic Stability*. (McGraw-Hill, 1961).
[92] Obataya, I., Nakamura, C., Han, S., Nakamura, N. & Miyake, J. Nanoscale operation of a living cell using an atomic force microscope with a nanoneedle. *Nano Lett.* **5**, 27 (2005).
[93] Vakarelski, I. U., Brown, S. C., Higashitani, K. & Moudgil, B. M. Penetration of living cell membranes with fortified carbon nanotube tips. *Langmuir* **23**, 10893 (2007).
[94] Anglin, E. J., Cheng, L., Freeman, W. R. & Sailor, M. J. Porous silicon in drug delivery devices and materials. *Advanced Drug Delivery Reviews* **60**, 1266-1277 (2008).

[95] Salonen, J. *et al.* Mesoporous silicon microparticles for oral drug delivery: Loading and release of five model drugs. *Journal of Controlled Release* **108**, 362-374 (2005).

[96] Salonen, J., Kaukonen, A. M., Hirvonen, J. & Lehto, V.-P. Mesoporous silicon in drug delivery applications. *Journal of Pharmaceutical Sciences* **97**, 632-653 (2008).

[97] Johnson, L. R. *Physiology of the gastrointestinal tract, Volume 2*. 4 edn, Vol. 2 944-946 (Academic Press, 2006).

[98] Mochiki, E. *et al.* Pyloric Relaxation Regulated Via Intramural Neural Pathway of the Antrum. *Digestive Diseases and Sciences* **46**, 2307-2313 (2001).

[99] Sarna, S. K. Cyclic Motor Activity; Migrating Motor Complex: 1985. *Gastroenterology* **89**, 894-913 (1985).

[100] Arnold, M. *et al.* Activation of Integrin Function by Nanopatterned Adhesive Interfaces. *ChemPhysChem* **5**, 383-388 (2004).

[101] Norris, D. A., Puri, N. & Sinko, P. J. The effect of physical barriers and properties on the oral absorption of particulates. *AdV. Drug DeliVery Rev.* **34**, 135 (1998).

[102] Norris, D. A. & Sinko, P. J. Effect of size, surface charge, and hydrophobicity on the translocation of polystyrene microspheres through gastrointestinal mucin. *Journal of Applied Polymer Science* **63**, 1481-1492, doi:10.1002/(sici)1097-4628(19970314)63:11<1481::aid-app10>3.0.co;2-5 (1997).

[103] Jung, T. *et al.* Biodegradable nanoparticles for oral delivery of peptides: is there a role for polymers to affect mucosal uptake? *European Journal of Pharmaceutics and Biopharmaceutics* **50**, 147-160 (2000).

Appendix 1: Notes from Qualifying Exam Calculations

Note: I thought these might be useful for others who encounter similar calculations. I did not have time to type them up, so I have compiled photographs of my original hand-written calculations. I did the majority of these calculations in preparation for my qualifying exam in May of 2007. These photographs are available from Professor Tejal Desai.

Appendix 2: Protocols

The specific protocols I used to conduct these studies are included below. In certain cases (such as surface modification of the silicon wires), I modified the protocols slightly to achieve different goals for different experiments.

MTT Assay

Kayte Fischer, 7/28/10
Based on protocol sheet provided in MTT kit

Summary:
This assay tests the mitochondrial activity of cells after exposure to some experimental protocol as they cleave a tetrazolium salt to make it turn into a purple precipitate. This typically takes 2-4 hours. There should be less than 10^6 cells/cm^2. If this is not possible, during the incubation period monitor plate every 30 minutes until any purple crystals appear (then add solubilization solution). This protocol can be done on the bench top if the cells are appropriate to BSL I.

Materials:
MTT kit (in Brangelina)
Serum-free media, PBS, or HBSS
Bleach or 70% Ethanol
96 well plate

Methods:

- Prepare MTT solution by adding 10% MTT to the serum-free media (or PBS/HBSS). Suggested volumes below.
- Remove media, then add MTT solution.
- Incubate on the gyratory shaker plate in the non-sterile incubator in the hallway for 2-4 hours, until purple crystals begin to precipitate out of solution.
- Add MTT solubilization solution as suggested volumes below.
- Dissolve crystals:
    - Place plate on gyratory shaker at room temperature for 3-10 minutes and/or
    - Vigorously pipette up and down to help break up precipitate.
- Transfer 100 µL of the solutions to a 96 well plate to read on the plate reader.
- Read absorbance at 570 nm and subtract background read at 690.

Plate type	***Volume of solution***	***Volume of MTT***	***Volume MTT solubil. soln.***
96 well plates	95 ul/well	9.5 ul/well	95 ul/well
24 well plates	480 ul/well	48 ul/well	480 ul/well
6 well plates	1430 ul/well (1.43 ml/well)	143 ul/well	1430 ul/well (1.43 ml/well)

Controls:
Positive: Live cells exposed to no experimental protocols
Negative: Dead cells (kill for 15 minutes in a 5% bleach solution in water or 70% Ethanol)
MTT assay (to ensure no contamination of the MTT solution): Just MTT solution + solubilization solution

Live/Dead Staining for coverslips, etc

Kayte Fischer
7/23/10

Materials:

- CellTracker Green (CMFDA) – Invitrogen (CellTracker Blue can also be used)
- Propidium Iodide
- FBS-free media
- PBS

Methods (for membranes/slides in a 96 well plate or 24-well transwell):

- Dilute CellTracker Green to 10 µM in FBS-free media.
- Aspirate media from wells, and wash one time with PBS.
- Add 100 µL CellTracker Green solution to cells.
- Incubate in the incubator for 30 minutes to 48 hr.
- Add 0.1 µL of Propidium Iodide per well.
- Incubate in the incubator for 5-7minutes.
- Remove staining solution and wash 1x with PBS.
- Add 100 µL of a 3.7% paraformaldehyde (or formaldehyde) solution to each well
- Incubate at room temperature for 15 minutes.

*At this point, the cells can be removed from the tissue culture room and moved to benchtop. Make sure to have a special container for the paraformaldehyde disposal. This must be disposed of as hazardous waste.

- Remove coverslips/membranes/transwell bottoms from the wells and mount on a coverslip in VectaShield.

Methods for larger wells:

For plates with wells larger than those described above, multiply the above volumes by:

Plate type:	Multiplier
48 wells	2
24 wells	3
12 wells	8
6 wells	10
35 mm	10
Rectangular wells	10
6-well transwells	10

Alexa Fluor 680 – Functional Protocol

Kayte Fischer, 2/8/10

Materials:
Isopropyl Alcohol (IPA)
Alexa Fluor 680 succinimidyl ester (aliquoted to 10 mg/ml in anhydrous DMF)
Aminopropyltriethoxysilane (APTES)

Methods:

- Mix IPA and APTES, then add Alexa Fluor 680, according to the proportions below.
- Incubate overnight at room temperature on shaker plate in foil.
- Weigh devices in 0.65 mL conical tubes.
- Plasma treat devices in tubes for 30 s.
- Add solution immediately.
- Incubate at room temperature for at least 3-4 hr (up to overnight).
- Filter dry/rinse with IPA for 10 minutes or more (depending on quantity).
- Vacuum dry at room temperature overnight.
- For nanowires: sonicate for 30 minutes in water.

Proportions per mouse:

IPA	1000 µL
APTES	100 µL
Alexa Fluor 680	50 µL
Devices	50 mg

Surface Modification of Silicon NANOWIRES – with FITC

Kayte Fischer, Ganesh Nagaraj 8-18-09

Materials:

- Hydrochloric acid, 8 M (50%, with water)
- 2-propanol, flammables cabinet
- Hydrogen peroxide (H_2O_2, 30%), in cold room
- Ammonia (in the form of ammonium hydroxide, 25%)
- FITC (in Harry)

Procedure:

Removal of Nanowires:

- Combine a scoop of nanowire-coated beads, 10-12 mL di water in a 15 mL centrifuge tube.
- Suspend in sonicator with tape, and sonicate for 30 minutes.
- Vortex/invert the tube, and then wait 1 minute for the beads to settle.
- Remove the supernatent and put into another tube.
- Centrifuge this tube for 7 minutes at 3.2 krpm.
- Remove the supernatent, leaving a nanowire pellet. Usually, aspirate to the top of the visible streak, about 1.5 mL remaining.
- Mix with a pipette and transfer to a microcentrifuge tube.

Hydroxylation of silicon surfaces:

- Add substances so that you have 1:1:5 ammonia:H_2O_2:deionized water solution (a good amount is: 3 ml ammonia, 3 ml H_2O_2, and 15 ml water, but can be done at .3 ml and 1.5 ml with smaller beakers) at 80 C for 5 minutes (until boiling).
- Mix with pipette.
- Centrifuge for 5 minutes at 14 krpm (removing~100-200 µl if necessary to close the cap).
- Remove supernatent and replace with water.
- Repeat centrifugation and washing.
- Add 1:1:6 HCl:H_2O_2:di water solution (a good amount is: 3 ml HCl, 3 ml H_2O_2, 18 mL di water, but can be done at .3 and 1.8 ml in small beakers) at 80 C for 5 minutes.
- Mix with pipette.
- Centrifuge for 5 minutes at 14 krpm (removing~100-200 µl if necessary to close the cap).
- Remove supernatent and replace with water.
- Repeat centrifugation and washing.

NH2 functionalization:

- Resuspend samples in 5 ml 2-propanol (or .5 ml for smaller beakers) **NOTE: Do not use glass containers for this step!**
- Add 45 ml (or 4.5 ml) 2-propanol, and 1 ml (or .1 ml) APTES
- Cover and leave for 90 minutes at room temperature on a shaker plate
- Centrifuge for 5 minutes at 14 krpm (removing~100-200 µl if necessary to close the

cap).

- Remove supernatent.
- Leave in a vacuum oven to dry out overnight

FITCattachment:

- Place dry particles in an excess solution of FITC (50 μg) and 4 mL water.
- Leave on shaker plate at 30 rpm overnight (or at least 3 hrs) at room temperature.

Live Cell Hoechst Staining Protocol

Kayte Fischer, 9/22/09 (based on Invitrogen spec sheet)

- Wash with warm PBS.
- Add Hoechst stain for 30 minutes.
- Wash 3x with PBS.

To make solution:
Hoechst: 1:2000 dilution in PBS (BLUE - 461nm)

Collagen Coating Protocol

Kayte Fischer, 7/10/09
Based on BD Biosciences Product Spec sheet for Rat Tail Collagen, Type I

Materials

Acetic Acid (glacial, from in corrosives cabinet)
dI water in tissue culture hood
Type I Rat Tail Collagen (in tissue culture refrigerator, top left shelf)

Preparation

Make 0.02 N Acetic acid solution in water.

- An easy ratio is 20 uL of acetic acid into 17.5 mL of water.
- This can be kept in the fridge for a couple weeks if there is extra.

Make Collagen solution.

- 1:67 dilution of collagen in 0.02 N acetic acid for a collagen solution of ~3.35 mg/mL.
- An easy ratio is to add 250 uL of collagen to the 17.5 ml of acetic acid solution made above.
- This can be kept in the fridge for a couple weeks if there is extra.

Methods

- Plasma clean the slides for 30 seconds.
- Take slides to the tissue culture hood, put into 4 well rectangular plate.
- Add 1 mL of collagen solution to each slide, being careful to only add it on top of the slide (not the rest of the well).
- Incubate plate with slides at room temperature in the tissue culture hood for 1 hr, rotating it 180 degrees every 20 minutes or so.
- Remove remaining solution from slides.
- Rinse 2x with sterile PBS.
- Add cells as per cell seeding protocol.

Preparation of Samples for SEM

(based on Corning Transwell Prep Protocol)
Kayte Fischer, 6/17/09

Reagents
Sodium cacodylate (Polysciences Cat. # 01131)
3% Glutaraldehyde E.M. grade (Polysciences)
Sucrose, reagent grade
Ethanol, 95% and 100%
Hexamethyldisilazane (HMDS) (Polysciences Cat. # 00692)
Hank's Balanced Salt Solution (HBSS)

Protocol

1. Rinse the sample by adding HBSS (37°C). The rinse should be added slowly and then aspirated. Repeat.

2. Replace the HBSS with a primary fixative (3% glutaraldehyde in 0.1M sodium cacodylate, pH 7.4, containing 0.1M sucrose) to adjust the osmolarity to approximately 300mOsm. The fixative is added for at least 45 minutes at room temperature. *(We usually leave it in fixative for 2-3 days.)* **This procedure should be conducted in a fume hood.**

3. Remove the primary fixative and add the cacodylate-sucrose buffer (0.1 M sodium cacodylate, 0.1 M sucrose, pH 7.4) for 5 minutes at room temperature. Remove the buffer and repeat this rinse procedure for an additional 5 minutes.

4. At this point, the samples may be refrigerated in the cacodylate-sucrose buffers. If prolonged storage is necessary, rinse the cultures with fresh cacodylate-sucrose buffer after 48 hours.

5. Remove the cacodylate-sucrose buffer and dehydrate the insert by gently adding solutions of ethanol in a graded series of concentration as follows:

35% Ethanol -10 minutes
50% Ethanol -10 minutes
70% Ethanol -10 minutes
95% Ethanol -10 minutes
100% Ethanol -10 minutes
100% Ethanol -10 minutes

Note: Do not let the sample dry out at any time during the procedure.

6. Replace the last 100% ethanol solution with HMDS or quickly transfer the sample to a container with enough HMDS to cover the insert. **This step should be done in a fume hood.**

b) Leave the insert in HMDS for 10 minutes.
c) Air-dry in the hood for 20 to 30 minutes.

Note: Store in a desiccator if the sample is not to be mounted immediately.

7. Sputter coat the samples with 200 Angstroms of Gold-Palladium and examine. *(We don't always do this, since we have an ESEM that has a low voltage beam. For most SEMs, it is necessary.)*

Trypan Blue Quench Protocol (Internalization)

Kayte Fischer, 6/15/09
Based on Desimone 2008, PNAS

Timeframe: 15 min to 4 hr
They quantified with FACS
Trypan blue solution: 0.4% in PBS

- Add FITC particles to cells in a PBS suspension
- Confocal image
- Add 20 µl trypan blue solution
- Confocal image

Control: Image fluorescent particles, then fluorescent particles + TB

Surface Modification of Silicon

Kayte Fischer, 1/16/07
(adapted from Sarah)

Materials:

- Hydrochloric acid, 8 M (50%, with water)
- 2-propanol, flammables cabinet
- Hydrogen peroxide (H_2O_2, 30%), in cold room
- Ammonia (in the form of ammonium hydroxide, 25%)
- N-Hydroxysulfosuccinimide (NHSS, or HOSu), in desiccator
- Carbodiimide hydrochloride (EDC, or EDAC), in freezer
- Avidin, in Sarah's box in the freezer in lab
- 3-aminopropyltrixethoxy silane (APTES), in desiccator
- Tomato lectin (biotin labeled), in Sarah's box in the freezer

Procedure:

Hydroxylation of silicon surfaces:

- Put silicon pieces in 1:1:5 ammonia:H_2O_2:deionized water solution (a good amount is: 3 ml ammonia, 3 ml H_2O_2, and 15 ml water, but can be done at .3 ml and 1.5 ml with smaller beakers) at 80 C for 5 minutes (until boiling).
- Rinse 3x with di water
- Add 1:1:6 HCl:H_2O_2:di water solution (a good amount is: 3 ml HCl, 3 ml H_2O_2, 18 mL di water, but can be done at .3 and 1.8 ml in small beakers) at 80 C for 5 minutes.
- Rinse 3x with di water.
- Centrifuge at 1200 rpm or let particles settle, discard supernatent.

NH2 functionalization:

- Resuspend samples in 5 ml 2-propanol (or .5 ml for smaller beakers) **NOTE: Do not use glass containers for this step!**
- Add 45 ml (or 4.5 ml) 2-propanol, and 1 ml (or .1 ml) APTES
- Cover and leave for 90 minutes at room temperature
- Transfer to a vacuum filter unit, washing with IPA
- Leave vacuum on to dry it out overnight

Avidin attachment (from Sultzbaugh et al)

- Place dry particles in a solution of 0.06 M EDC, 0.04 M NHSS, and 1.5 µM avidin in di water in a teflon vial with a cap.
- Shake solution at 30 rpm overnight (or up to a few days), at room temperature
- Rinse 3x with di water.

Lectin conjugation:

- In teflon vial, add 200 µg (excess) biotin-labeled lectin and 6 ml di water to samples.

- Leave on shaker plate at 30 rpm overnight (at least 3 hrs), at room temperature.

  Notes:
  EDC -> weight: 191.71 g/mol, for 0.06 M, in 5 ml di water, need 0.0575 g
  NHSS -> weight: 115.09 g/mol, for 0.04 M, in 5 ml di water, need .0230 g
  Avidin -> use 500 µg for 5 ml di water (that gives 1.5 µM)

Phalloidin Staining Protocol

Kayte Fischer, 10/8/08 (Based on Rahul's recommendations)

- Wash with warm PBS.
- Fix cells in 3.7% paraformaldehyde (in PBS) for 10-20 minutes at room temperature.
- Wash 3x with PBS.
- Extract with a solution of 0.5% Triton X-100 (in PBS) for 10-15 min.
- Wash 3x with PBS.
- Pre-incubate cells with 1% BSA (in PBS) for 30-60 minutes.
- Wash with PBS.
- Put phalloidin stain on cells for 45-60 minutes at room temperature (covered to prevent evaporation).
- Add parafilm to the tops of the slides if additional surface area coverage is needed (reduces surface tension/forces spreading).
- Wash 3x with PBS.
  (IF want to visualize nucleus:)
- Add Hoechst stain for 5-7 minutes.
- Wash 3x with PBS.
  (IF want to visualize cytoplasm:)
- Add Propidium Iodide stain for no more than 5 minutes.
- Wash 3x with PBS.

- Air dry, then mount.

To make solutions:

AlexaFluor Phalloidin stain (amount per coverslip) (GREEN – 488 nm):
1 µL stock solution
200 µL in PBS

Additional stains:
Propidium Iodide: 1:1000 dilution in PBS (RED – 568 nm)
Hoechst: 1:2000 dilution in PBS (BLUE - 461 nm)

Note: This whole protocol can be done bench-top.

Static Adhesion Protocol

Kayte Fischer, 7/22/08

Materials:

- Plated cells
- Media (or other fluids if desired)
- Devices
- Extra 24 well plate

Methods (for 24 wells in a 96 well plate, can be modified for other setups; using 7 different batches of nanowire (nw) coated beads + a control):

With 24 wells, and 8 experimental groups, we have 4 wells per group. Each well takes ~200 ul of media.

- Before starting, warm media to 37 C in water bath.
- For each experimental group, prepare 800 ul of media + devices.
- Remove the media from each well.
- Replace with 200 ul of the appropriate media+device solution. Make sure to resuspend the devices before EACH dispensation.
- Put in incubator for 30 minutes. Return media to water bath.
- Do 3 rinses, each time transferring the media (and any loose devices) in each well to the corresponding well in the extra 24 well plate. Make sure to change pipette tips between experimental groups to prevent contamination. If you see devices stuck to the tip, try taking in extra media to clean the tip.
- Using a tissue culture scope and cell counter, count the devices remaining on the cells. Count the devices in the washes.

Data Analysis:

We seek to know the % remaining for each well, which is:

% remaining = devices counted on the cells/total devices introduced to the cells

which is simply:

% remaining= devices counted on the cells/(devices counted on the cells + devices counted in the washes)

CMFDA/EthD-1 (Live/Dead fixing) Assay

Sarah Tao, Kayte Fischer 6/27/06

- Perform experiment (or at least kill some cells with 70% EtOH for 20 min).
- Remove media and rinse with HBSS or PBS.
- Add solutions with probes to cover coverslips in wells.
- Cover with foil.
- Incubate for 45 min at 37 C.
- Rinse once then replace with HBSS.
- Incubate for 30 min at 37 C.
- Rinse cells then fix in 3.7% paraformaldehyde for 15 minutes at room temperature.
- Rinse cells in HBSS or PBS.
- Mount with Vectashield.

To make solutions:

CMFDA – GREEN, alive, in cytoplasm, make 10 mM stock from 1 vial + 10.76 uL DMSO

5 uM	Add .5 uL/mL of HBSS
2.5 uM	Add .25 uL/mL of HBSS
10 uM	Add 1.0 uL/mL of HBSS

EthD-1 (Ethidium Homodimer 1) RED, dead, in nucleus only – comes in 2 mM stock

.5 uM	Add .25 uL/mL of HBSS
5 uM	Add 2.5 uL/mL of HBSS
2.5 uM	Add 1.25 uL/mL of HBSS
10 uM	Add 5.0 uL/mL of HBSS

Loading Bovine Serum Albumin (BSA) and Other Molecules Into Controlled Pore Glass

Ganesh Nagaraj and Kayte Fischer
Tejal A. Desai Lab
Written 7/23/09; revised 9/25/09

Materials:

Devices - ~50 um diameter controlled-pore glass (CPG) particles with 200 nm diameter pores

5 mg Bovine Serum Albumin (BSA) per replicate - located in top shelf of FRED

1 polyethylene vial per replicate

1 filter flask set up per replicate (10 um filter paper)

1x PBS squirt bottle

Instructions:

Decide how many replicates you need (we usually have 3).

Clean one polyethylene vial per replicate with ethanol and a paper towel and allow it to dry.

Add 0.5 mL of PBS to each polyethylene vial.

Add 4-6 mg of BSA to each vial. Record the exact amounts added.

Gently swirl containers to dissolve the BSA crystals.

Add a desired amount of CPG to each vial (we usually add 1/3 to 1/2 of a small spatula, or roughly 5 mg).

Place vials on a hot plate set to 35^0 C (no more than 37^0 C) until the particles are completely dry (they should look like white powder). Usually, this takes at least one day and night of drying. While the particles dry, keep them lightly covered with foil to prevent dust from entering the vials.

For each polyethylene vial, turn the vial sideways and squirt PBS onto the particles, causing them to be dislodged and fall into a filter flask. Use as little PBS as possible to remove all visible BSA and CPG from the vials.

Rinse the CPG particles with PBS by squirting directly onto all areas where particles are visible, again using minimal PBS. Check that you have used the same amount of PBS to rinse all replicates by comparing the volume of fluid in the filter flask.

Wait at least 20 minutes, or until you think all the particles are dry. If there are large clumps of CPG, it may be beneficial to wait longer.

For loading other molecules:

Molecule	Loading solution
Trypan Blue	500 uL stock, 0.4% w/v in normal saline on cell culture shelf
IgG	500 uL stock, Biomeda Corp. bovine IgG (concentration measured to be 10.3 mg/mL)
Insulin	500 uL stock, Sigma bovine pancreatic insulin (10mg/mL)
PBS	500 uL 1x PBS

Degradation Study Protocol

Aishwarya Jayagopal, Ganesh Nagaraj, Kayte Fischer - 09/16/09

Summary

Total # of Samples: 108
# of Samples per Batch: 36
    # of Solutions per Batch: 3
    # of Timepoints per Batch: 4
# of Samples per Solution: 36
# of Samples per Timepoint: 27

Materials

- 15 mL of Batch 2, 11 and 15 Nanowires
- 12 mL Survanta
- 12 mL Mucin
- 12 mL PBS
- 36 Orange Centrifuge Tubes
- 36 Green Centrifuge Tubes
- 36 Yellow Centrifuge Tubes
- 3 15 mL tubes for sonication

Method

A. Preparation of Samples
    1. Sonicate 15 mL of Batch 2 Nanowires for 30 minutes
    2. While they are being sonicated, label 36 centrifuge tubes as with: Batch #, Solution, Time and Sample #
        i) Orange = Batch 2
        ii) Green = Batch 11
        iii) Yellow = Batch 15
    3. Once sonication is complete, mix the solution by pipette
    4. Wait for 1-2 minutes to allow beads to settle to the bottom.
    5. Transfer 300 uL of the supernatant to each centrifuge tube.
    6. First centrifuge all 12 tubes labeled "Survanta".
    7. Once centrifuging is complete, remove supernatant and leave only the nanowire pellet on the bottom.
    8. Add 300 uL of Survanta to all 12 tubes labeled survanta. Pipet up and down to thoroughly mix the nanowires
    9. Centrifuge all tubes labeled "Mucin" and remove supernatant. Then, add 300 uL of Mucin to all 12 tubes labeled Mucin. Pipet up and down to thoroughly mix the nanowires
    10. Centrifuge all tubes labeled "PBS" and remove supernatant. Add 300 uL of PBS to all 12 tubes labeled PBS. Pipet up and down to thoroughly mix the nanowires
    11. Repeat these steps for Batches 11 and 15.
B. Sample Preparation for TEM

1. Separate all 27 tubes labeled "0 hr" to use in this step.
2. Place all tubes in the vacuum oven and allow to dry overnight.
3. Resuspend nanowires in 10 μL water and put 5 μL onto a TEM grid.
4. Allow to dry for 10 minutes, then wick away remaining water using a KimWipe.

PEGylation of silicon

Yushan Kim 12/16/09
Adapted from Papra 2001 & Rachel Lowe

Materials

- Ammonium hydroxide (25% in corrosive cabinet under hood)
- Hydrochloric acid, 8 M (50% in corrosive cabinet under hood)
- Hydrogen peroxide (H_2O_2, 20% in cold room)
- Ethanol (yellow flammables cabinet)
- Toluene (gray flammables cabinet)
- PEG silane (dessicator, Gelest 2-[Methoxy(polyethyleneoxy)propyl]trimethoxysilane)

Procedure

Hydroxylation of silicon surfaces:

- Mix following in a small beaker, then add particles, then heat at 80C for 5 min
  - 0.3 mL ammonium hydroxide
  - 0.3 mL H_2O_2
  - 1.5 DI water
- Rinse 3x with DI water
- Mix following in a small beaker, then add particles, then heat at 80C for 5 min
  - 0.3 mL HCl
  - 0.3 mL H_2O_2
  - 1.8 DI water
- Rinse 3x with DI water.
- Vacuum filter to dry particles. Add 10 mL EtOH to facilitate drying. Dry for at least 30 min. (Water inhibits the PEG-silane from attaching)

Grafting surface with PEG silane

- Mix following solution in a plastic vial, add dry particles, and put on plate shaker for at least 2 hours (Papra 2001 says 18 hours, Rachel has shown 2 hours is the same result)
  - 3 mL toluene – use glass pipettors only!
  - 44.1 uL PEG silane
- Remove toluene solution from vial, then rinse:
  - Once in toluene
  - Twice in EtOH
  - Twice in DI water
  - Immerse in water, and pulse on vortex (to remove nongrafted material)
- Dry on vacuum filter. Rinse out in EtOH to dry faster.

Thiol functionalization of gold catalyst

Yushan Kim, 12.16.09

Please note that thiol and avidin concentration and adsorption time are not fully optimized; these are probably more concentrated than necessary.

Materials

- Thiol-PEG-Biotin (HS-PEG-Biotin) MW 3400, from Nanocs
  - Aliquot concentration: 10 mM [9.62 mg in 283 uL water] – 30 uL aliquots
- Avidin-FITC
  - Aliquot concentration: 1.0 mg/mL in water – 200 uL aliquots
- Ethanol

Procedure

Thiol-Biotin attachment

- Prepare 500 μM concentration thiol-PEG-biotin in EtOH in plastic vial
  - For smaller volumes, can use 10 μL of thiol-PEG-biotin stock into 570 μL of EtOH
- Add small amount (spatula tip full) of nanowire-coated particles into solution
- Leave in solution for at least 30 minutes, then remove solution and rinse 3x with EtOH. (Rinsing step is more efficient when done in vial rather than on filter.)
- Filter dry for at least 30 minutes.

Avidin attachment

- Prepare 100 μg/mL avidin-FITC in EtOH.
  - For smaller volumes, can use 10 μL of avidin-FITC stock into 490 μL of EtOH.
- Add thiol-biotin-functionalized particles.
- Place on plate shaker for 30 minutes, then remove solution and rinse 3x with EtOH.
- Filter dry for at least 30 minutes.

Shear Flow Protocol

Kayte Fischer, 7/28/10

Summary:
This technique allows one to quantify the adhesion of particulates under given levels of shear. Under microfluidic conditions as found in the flow chamber, flow is laminar, which allows the shear at a given flow rate to be determined by that flow rate, flow chamber dimensions, and viscosity.

Materials:
Slide with cells growing on it (suggest using the protocol for collagen coating slides prior to cell growth for a good monolayer)
Shear flow chamber top, gasket
Syringe pump, syringes (suggest 60 ml syringes, and a few extra 5-10 ml syringes)
Vacuum chamber
Lint-free q-tips
70% Ethanol
Experimental particulates
Solution to flow over devices (eg: cell culture media, 2% mucin, etc; suggest > 250 mL for longer experiments)
Hot plate, stir bar, glass beaker
Tubing, should already be attached to the flow chamber top (for multiple syringes, you will need a tube splitter)
Microscope for imaging flow (suggest 6D microscope at NIC or one with an automatic stage)

Preparation:
Heat flow solution in glass beaker to 37°C, while stirring.
Put syringes in syringe pump and attach to tube splitter if necessary.
I usually fill the syringes slightly in order to avoid the plunger sticking to the syringe tip. If you fill the syringes a bit, you can also use them to fill the line attaching them to the flow chamber.
Otherwise, use the 5-10 ml syringe to fill the line attaching the syringe pump to the flow chamber and attach to the syringe pump, being careful not to get bubbles in the line or connections.
Using the 5-10 ml syringe, fill the line attaching the flow chamber to the reservoir with flow media (the beaker on the hot plate).

Methods:
Chamber assembly:
Put gasket onto the top of the flow chamber, making sure to align the protrusions with the indentations on the chamber. Use q-tip or kimwipe to remove bubbles and wrinkles.
Suspend devices in 200 μL of mucin and drop onto various places on slide with cells growing on it (not where the gasket will be).[1]
Turn on the vacuum and get the vacuum line to be accessible.

[1] Note: This may not be necessary if devices will stay suspended in solution, as with most polymer devices. Silicon and silica, however, must be introduced this way.

Assemble chamber by putting the top part (with gasket) onto the bottom part. I suggest doing this with the top part at an angle at first to prevent bubbles.
Make sure the top and slide are aligned, then quickly attach vacuum line to the vacuum lines in the chamber. Press the top and bottom together to ensure a good seal.

Flow and Imaging:
Image areas of interest before starting flow.
Before starting the syringe pump, make sure that the line into the reservoir is open (ie: not attached to a syringe).
Start the syringe pump, and let flow for ~10 minutes (or until equilibriated).
Image areas of interest.
Repeat the flowing and imaging, with increasing flow rates until complete.

Disassembly:
Stop the syringe pump.
Put flow chamber in a dish or other container.
Disconnect the syringe pump from the flow chamber, and remove flow media from pump. (Back into the reservoir is not a bad idea if your particles don't' stay in suspension.)
At this point, if more studies will be done immediately, simply remove the slide and wipe the chamber with a KimWipe. Proceed to chamber assembly.

If studies are concluded, remove the slide and wipe with a KimWipe.
Put the flow lines connected to the chamber in the dish as well. Proceed to clean using vacuum, ethanol, and/or PBS.

Calculations, Calibration, etc:
The shear at the walls (ie: where the cells are) can be calculated as:

$$\tau = \mu\gamma = \frac{6\mu Q}{a^2 b},$$

where τ is the wall shear stress (dynes/cm^2), γ is the shear rate (1/s), μ is the apparent viscosity (P), a is the channel height (cm), b is the channel width (cm), and Q is the volumetric flow rate (ml/s).

To accurately gauge the flow rate, Q, I suggest calibrating the setup with a graduated cylinder. A depends on the gasket, and b is 1 cm. the viscosity can be found in literature, online, or measured using a viscometer. I analyzed my images by eye with counting software, but I challenge you to make a computer do all of it.

Generic Cell Seeding Protocol

Kayte Fischer 10/10/08

	CACO-2	3T3	RPMI 2650	HeLa	BAEC	RAW
Remove media						
Rinse cells with sterile PBS or 0.25% (w/v) Trypsin-0.03% (w/v)						
Add Trypsin	2 mL	2 mL	5 mL	2 mL	2 mL	NO TRYPSIN:
Incubate	10 min	1 min	3 min	3-5 min	3-5 min	USE
Quench with	5 mL	5 mL	5 mL	8 mL	8 mL	SCRAPER
Triturate						
If passing:	1:10	50 uL	1:5	1:10	1:10	1:3 or 1:6
Passing frequency:	1 wk	1 wk	1 wk	1 wk	2-3 days	As needed
If seeding: centrifuge at 1000 rpm for 3-5 min, keeping some cells out to count						
Count cells using hemacytometer						
Reconstitute pellet according to following chart (# cells/well, unless otherwise noted)						
96 wells	5e4	25 uL		20 µL		1.6e4
48 wells	6e4	50 uL				
24 wells	7.5e4	100 uL		80 uL	2e4	
12 wells	1.5e5	100 uL		150 uL		2e6
6 wells	3e5	150 uL	3e6		4e4	
Rect slide	3e5	200 uL				
Rect slide accel	4e5	400 uL		1:5	8e4	
25 mm petri	3.5e5	200 uL				
25 mm petri accel	4e5	400 uL				
Per cm^2						5e5

Handy little formula for getting the right number of cells/well:

n = number of cells in hemocytometer (round to nearest 10's place)
x = number of cells/well $*10^4$ (ie: for a 24 well plate of CACO-2, x=7.5)

Reconstitute the pellet with **n/10 mL**
Put **x*10 µL** in each well
Fill the rest with media

If passaging at the same time, each flask should get ***n/100 mL*** *of the reconstituted solution.*

General Cell Media Needs

Kayte Fischer 10/10/08

	CACO-2	3T3	RPMI 2650	HeLa	RAW	BAEC
Base	EMEM with Earle's BSS (500 mL)	DMEM High glucose	MEM with Earle's BSS (500 mL)	MEM with Earle's BSS (500 mL)	DMEM High glucose	DMEM Low glucose (1 mg/ml)
Pen-strep	1 % (5 mL)	1 % (5 mL)	1 % (5 mL)	1 % (5 mL)	1 % (5 mL)	1 % (5 mL)
FBS	20% (100 mL)	10% (50 mL)	10 % (50 mL)	10 % (50 mL)	10 % (50 mL)	10 % (50 mL)
Sodium Pyruvate	1 % (5 mL)	0 % (0 mL)	0 % (0 mL)	0 % (0 mL)	0 % (0 mL)	0 % (0 mL)

Cell Culture Facility Product List:

EMEM with Earle's BSS – CCFAC001
Pen-strep – CCFGG001 (aliquoted in freezer)
Sodium Pyruvate – CCFGE001 (aliquoted in freezer)
FBS – aliquoted in freezer
DMEM Low Glucose (1 mg/ml) DME H-16 – CCFAA001
DMEM High Glucose (4.5 mg/ml) – CCFDA003 (I think)